The mode of prion infection of neuronal cells with extracellular PrP amyloids

A thesis submitted in partial fulfilment of the requirements for the degree of Doctor of Philosophy from University College London

Hazim Arief Bin Halim

MRC Prion unit at UCL, Institute of Prion Diseases,

University College London

2023

Declaration

I, Hazim Arief Bin Halim, confirm that the work presented in this thesis is my own. Where information has been derived from other sources, I confirm that this has been indicated in the thesis.

Acknowledgement

I would like to express my deepest gratitude to my PhD supervisor, Peter Kloehn, for his unwavering support and guidance throughout my doctoral journey. Despite the challenges we faced, including the transition to a new project midway through my studies, Peter's mentorship has been instrumental in shaping me into the scientist I am today. I am truly fortunate to have been under his supervision. I am also immensely grateful to my secondary supervisor, Parmjit Jat, for his invaluable assistance and tremendous support.

In addition, I would like to extend my highest appreciation to my dedicated teammates in the Kloehn Lab. Juan Ribes, with his wealth of experience, provided close supervision in the lab. I would also like to thank Mitali Patel, who consistently offered her assistance and support no matter the circumstances. Antonio Beretta, despite our intense discussions on experimental methods, provided valuable perspectives and challenged my ideas in a constructive manner.

I extend my thanks to the principal investigators and senior investigators, namely Jan Bieschke, Azadeh Khalili (Azy), Graham Jackson, Iryna Benilova, and Emmanuel Risse who provided me with valuable insights throughout my PhD studies.

To my fellow PhD students, your support and words of encouragement have meant the world to me. I extend my deepest thanks to Julia Ravey, Ines Whitworth, Athanasios Dimitriadis (Thanos), Emma Jones, Yuanzi Sun, Catherine Turnbull, Kezia Jack, Elizabeth Hill, Tom Murphy, and Tom

Trainer. Your presence in the lab, especially on weekends, made it feel more bearable in this challenging journey.

I would also like to acknowledge the lab technicians in the department who consistently provided excellent assistance, including Adam Wenborn, Mark Batchelor, Daljit Sangar, and Aline Marinho.

To my friends outside the department, particularly Raif Norisam, Hazim Hanif, Azim Rahman, Badri Kudos, Nadjmi Azamin, Qaisy Jaslenda, Danial Daud, Balqis Azhar, Azfar Azizi, Wai Lun, Fadzli Irwan, Hairi Halimi and many others, I am deeply grateful for the tremendous moral support you lot have provided me during challenging times.

To my loving and caring mother, Mak, who answered my calls every single day despite the significant time difference, thank you. Your sacrifices and unwavering support are truly admirable. To my soulmate, Izatul Ashikin, who has been by my side emotionally throughout our long-distance relationship since 31st of December, 2019, thank you for patiently waiting for over three years. I am now proud to have you as my wife, and I have no intention of being apart from you.

Lastly, I would like to express my heartfelt appreciation to my late father, Abah. Thank you for always pushing me to reach my full potential and succeed in life. While Mak provided the safety net, you served as my motivator. Stepping out of my comfort zone was not always easy, but with your push and Mak's monumental support, I have been able to go far in this life.

Abstract

Prion diseases, also referred to as transmissible spongiform encephalopathies (TSEs), are fatal and incurable neurodegenerative disorders. Extracellular prion plaques, composed of disease-associated PrP (PrP^{D}), are found across human and mammalian brain tissues, and interact with the extracellular matrix (ECM). However, it is not known whether matrix-bound prions are released upon ECM remodelling, a process involving degradation of the bioscaffold by proteinases. In turn, prions released from the ECM will potentially infect cells within its vicinity. To investigate the implication of ECM remodelling in prion infection, we developed a decellularised ECM (dECM) model derived from prion-infected iS7 cells to mimic infectious extracellular scaffolding *in vivo*, and introduced reporter cells with perturbed matrix-degrading function. The dECM was generated via osmolysis of infected iS7 cells, and immunopositive against PrP aggregates as well as resident ECM proteins such as Collagen IV and CSPG4. The infectivity of dECM was equivalent to prion infection with 3.3×10^{-5} of 10% (w/v) RML brain homogenate. Mice inoculated with dECM-infected S7 cell lysates succumbed to scrapie sickness at 171 days post inoculation, only 10 days later than an equivalent amount of persistently prion-infected cells. Furthermore, we demonstrated that following 24 hours of contact with infectious dECM, ECM-bound prion aggregates were mobilised and internalised into 40% of reporter N2a-*Prnp*$^{-/-}$ cells.

To investigate the influence of ECM remodelling in prion infection, we treated uninfected S7 cells seeded onto infectious dECM with siRNA complexes designed to target genes associated with matrix degradation. The

knockdown of peptidase-encoding genes; *Adam19*, *Adamts4*, or *Mmp11*, led to a decrease of infection by over 30%. We also examined whether disruption of V-ATPase, a proton pump involved in maturing matrix-degrading enzymes, modulates extracellular infection. Interestingly, the gene knockdown of *Atp6ap1*, which involves in the synthesis of V-ATPase complex, reduced infection by 45%, and the silencing of both *Atp6ap1* and *Mmp11* blocked infection by 60%. Furthermore, pharmacological inhibition of V-ATPase using bafilomycin A1 resulted in an approximate 80% block in infection. Thus, this body of work demonstrates that the disruption of prion-embedded matrices promotes infection. This shows that the ECM degradation in prion diseases plays a key role in modulating infection, and targeting the bioscaffold-degrading mechanism will abrogate infection stemming from prion-embedded ECM. We also attempted to develop disease-specific antibodies using subtractive immunisation. This advanced immunisation strategy favours the generation of antibodies against poorly immunogenic epitopes. Unfortunately, since *Prnp* null mice had shown severe complications following immunisations using antigens including PrP peptides and prion-infected exosomes, this project was discontinued.

Impact statement

The work presented in this doctorate thesis is significant in expanding our understanding of extracellular matrix (ECM) remodelling in transmissible spongiform encephalitis (TSEs). TSEs, or also known as prion diseases, is a group of fatal neurodegenerative disorders caused by accumulation of abnormal PrP aggregates in the central nervous system. It is well established that aberrant PrP assemblies are present in the ECM, where they interact with certain ECM resident proteins. However, there is currently limited knowledge on the effect of ECM remodelling in prion diseases. During ECM remodelling, which involves degradation of the bioscaffold by proteinases, matrix components embedded within the scaffold are released and interact with nearby cells.

Given that prions are sequestered in the extracellular scaffold, this thesis addresses the role of ECM remodelling in promoting prion infection. Using cell-derived scaffolds, this study demonstrates that prion-infected ECM is highly infectious upon contact with prion-susceptible reporter cells. Wild type mice that were intracerebrally inoculated with infected reporter cells succumbed to rapid neurodegeneration. We also showed that prions embedded in the decellularised ECM (dECM) can be internalised by cells, and endocytosed prions are cleaved to form truncated isoforms intracellularly. This implies that prion aggregates that are sequestered within biomatrices can be mobilised and infect cells.

Using transient gene silencing of candidate genes, we identified secreted proteases involved in mobilising infectious prions sequestered in acellular

scaffolds. Adam19, Adamts4, and Mmp11 were found to play a role in mobilising infectious proteins from the dECM. Furthermore, V-ATPases were also found to be involved in releasing infection from the bioscaffold. Interestingly, previous studies have shown that V-ATPases play a role in activating endopeptidases which, upon secretion lead to ECM degradation and remodelling.

The findings of this thesis may have implications for the development of new treatments for prion diseases. The study provides evidence that targeting ECM-degrading proteases may curb prion infection by mobilising prions from the extracellular bioscaffold. Therefore, identification of proteases that are associated with prion infection offers a potential avenue for the development of new therapeutic interventions.

Table of Contents

List of Figures

List of Tables

List of Acronyms and Abbreviations

Aβ	Amyloid beta
AD	Alzheimer's disease
ADAM	A disintegrin and metalloproteinase, human protein
Adam	A disintegrin and metalloproteinase, mouse protein
ADAM	Human gene encoding for ADAM
Adam	Mouse gene encoding for Adam
ADAMTS	A disintegrin and metalloproteinase with thrombospondin motifs, human protein
Adamts	A disintegrin and metalloproteinase with thrombospondin motifs, mouse protein
Adamts	Mouse gene encoding for Adamts
ALS	Amyotrophic Lateral Sclerosis
AFM	Atomic Force Microscopy
ARRIVE	Animal Research: Reporting of *In Vivo* Experiment
ATP	Adenosine Triphosphate
BafA1	Bafilomycin A1
BSE	Bovine spongiform encephalopathy
BSF	Biological Services Facility
BCA	Bicinchoninic acid assay
CAD5	Murine catecholaminergic neuroblastoma cells

cDNA	Complementary deoxyribonucleic acid
CSPG	Chondroitin sulfate proteoglycan
dECM	Decellularised extracellular matrix
DAPI	4’,6-diamidino-2-phenylindole
DMEM	Dulbecco’s Modified Medium Eagle
DMSO	Dimethyl sulfoxide
DNA	Deoxyribonucleic acid
DPBS	Dulbecco’s Phosphate Buffered Saline
ECM	Extracellular matrix
EDTA	Ethylene diamine tetra-acetic acid
ELISA	Enzyme-linked immunosorbent assay
ELISPOT	Enzyme Linked Immunospot Assay
EMT	Endothelial-mesenchymal transition
EV	Extracellular vesicle
FBS	Fetal Bovine Serum
GAG	Glycosaminoglycan
gCJD	Genetic Creutzfeldt Jakob Disease
GdnHCl	Guanidine hydrochloride
GTC	Guanidinium thiocyanate
GSS	Gerstmann–Sträussler–Scheinker syndrome

Hpn	Mouse gene encoding for hepsin
Htra2	Mouse gene encoding for serine protease Htra2
HS	Heparan sulfate
HSPG	Heparan sulfate proteoglycan
iCJD	Iatrogenic CJD
Intr.	Intracellular
IPD	Inherited prion disease
iS7	N2a-PK1 prion susceptible subclone chronically infected with RML
KD	Knockdown
MBV	Matrix-bound vesicle
MMP	Matrix metalloproteinase, human protein
Mmp	Matrix metalloproteinase, mouse protein
Mmp	Mouse gene encoding for Mmp
MRC	Medical Research Council
N2a-*Prnp*$^{-/-}$	*Prnp* knockout N2a-PK1 cells
NFT	Neurofibrillary tangle
PBS	Phosphate-buffered saline
PBST	Phosphate-buffered saline with Tween-20
PD	Parkinson’s disease
PFA	Paraformaldehyde

PK	Proteinase K
Prnp	Prion protein gene, mouse
PRNP	Prion protein gene, human
PrP^{C}	Cellular prion protein
PrP^{D}	Disease-associated prion protein
PrP^{Sc}	Disease-related, PK-resistant form of the prion protein
PVDF	Polyvinylidene fluoride
RML	Rocky Mountain Laboratory prion
RT	Room temperature
RT-qPCR	Reverse transcription-quantitative polymerase chain reaction
RNA	Ribonucleic acid
S7	N2a-PK1 prion susceptible subclone 7 cells
SCA	Scrapie Cell Assay
SCEPA	Scrapie Cell Assay in End Point Format
sCJD	Sporadic Creutzfeldt-Jakob disease
SDS	Sodium dodecyl sulfate
siRNA	Small interfering ribonucleic acid
SP	Senile plaque
TBST	Tris-buffered saline with tween-20
TME	Transmissible mink encephalopathy

TSE	Transmissible spongiform encephalopathy
UCL	University College London
V-ATPase	Vacuolar H^+-ATPase
v/v	Volume per volume
vCJD	Variant Creutzfeldt-Jakob disease
VPSPR	Variably protease-sensitive prionopathy
w/v	Weight per volume

1. Introduction

Prion diseases, also known as transmissible spongiform encephalopathies (TSEs), are a group of rare and fatal neurodegenerative disorders caused by abnormal infectious proteins called prions. TSEs affect between 1 to 1.5 people per million per annum worldwide with varying distributions between countries (Tee et al., 2018). The causative agent, known as prions, are misfolded conformers of PrP^{C}, a physiological protein found in most mammalian cells. The ‘’protein-only hypothesis’’ puts forth the notion that prions act as seeding templates by converting PrP^{C} to aberrant conformers (Prusiner, 1982). In most cases, prion diseases are confirmed by the presence of PrP^{Sc} deposits, abnormal PrP aggregates that are partially resistant to proteinase K (PK).

Prion diseases were first described in sheep in the 18th century and dubbed ‘scrapie’ due to the compulsive scraping or scratching behaviour of affected sheep (Stockman, 1913). Interestingly, the sheep did not display any scabs upon examination, suggesting it may not be a form of skin disease. However, histopathological examinations revealed a distinctive neuronal vacuolation in scrapie-sick sheep (Zlotnik, 1958).

In the 1920s, Spielmeyer introduced the term Creutzfeldt-Jakob disease (CJD) to describe an emerging neurodegenerative disease documented by neurologists Hans Gerhard Creutzfeldt and Alfons Maria Jakob (J. H. Wolf & Foley, 2005). Since CJD is a rare disease, limited efforts were undertaken to elucidate its underlying mechanisms and interest quickly waned until the emergence of kuru, an endemic in Papua New Guinea that affected people

in the Fore linguistic group beginning in the late 1950s. Kuru spread through local mortuary rites by consumption of deceased kinfolk (Alpers, 2008). Neuropathological examinations of kuru patients showed distinctive spongiosis similar to that of scrapie, which led to the idea that both diseases belong to the same neurodegenerative group (Hadlow, 1959). The notion of disease transmission and propagation was upheld when kuru-infected brain suspension was injected into chimpanzees which subsequently developed kuru-like symptoms (Beck et al., 1966), and later on acquiring similar results from using CJD biopsy material as inoculum (Gibbs et al., 1968).

The three major categories in human prion diseases are sporadic, genetic or familial, and acquired. Human prion diseases include Creutzfeldt-Jakob disease (CJD), variant CJD (vCJD), fatal familial insomnia (FFI), Gertsmann-Sctraussler-Scheinker diseases (GSS), and kuru. Animals, namely mammals, could also contract such disease: scrapie for sheep and goats, transmissible mink encephalopathies (TME) in minks, chronic wasting disease (CWD) in cervids, and bovine spongiform encephalopathies (BSE) for cows.

1.1.1 Sporadic

As the name implies, sporadic prion diseases have no known cause and emerge spontaneously. It was hypothesized that sporadic prion diseases could arise from rare stochastic events of PrP^{C} misfolding or random somatic mutations in the *PRNP* gene leading to the formation of pathogenic prion seed (J. G. Safar, 2012). The most common form of sporadic prion disease

is sporadic CJD (sCJD), which accounts for approximately 85% of human prion diseases (Ladogana et al., 2005). The average onset of sCJD is between 55 to 75 years old (Brown et al., 1986), while isolated cases inpatients younger than 20 years of age have been reported (Murray et al., 2008). Patients developing sCJD commonly present rapid progressive dementia along with neurologic symptoms such as ataxia, visual impairment, and myoclonus, albeit symptoms can vary widely between patients (Sharma et al., 2009). Another example of sporadic prion disease is sporadic fatal insomnia (sFI), which is considered a phenocopy of FFI. sFI is a fatal disorder and even rarer than its genetic counterpart. It is characterised by substantial neuronal loss and relatively high PrP^{Sc} deposits in the thalamolimbic system which is involved in sleep regulation and other circardian functions (Montagna et al., 2003; Parchi et al., 2000).

Variably protease-sensitive prionopathy (VPSPr) is a rather unique form of sporadic or other prion diseases for that matter, as the disease hallmark is the presence of PK-sensitive abnormal PrP (Gambetti et al., 2008; Zou et al., 2010), as opposed to the majority of prion diseases, characterized by PK-resistant PrP. Interestingly, VPSPr shows differences in genetic susceptibility to disease, when compared to sCJD. In the general population, codon 129 of the PRNP gene is either MM or VV homozygous, or MV heterozygous. The three codon 129 genotypes of VPSPr were found to be MM 11%, MV 24%, and VV 65% (Notari et al., 2018). This is in contrast to sCJD since VV homozygous appears to be protective whereby MM homozygous is deemed as a risk factor (MM 68%, MV 16%, VV 16%) (S. J. Collins et al., 2006).

CREUTZFELDT-JAKOB DISEASE IN THE UK (By Calendar Year)

REFERRALS OF SUSPECT CJD		DEATHS OF DEFINITE AND PROBABLE CJD					
Year	Referrals	Year	Sporadic[1]	Iatrogenic	Genetic[2]	vCJD	**Total Deaths**
1990	[53]†	1990	28	5	0	-	**33**
1991	75	1991	31	1	4	-	**36**
1992	96	1992	45	2	6	-	**53**
1993	79	1993	36	4	7	-	**47**
1994	119	1994	53	1	9	-	**63**
1995	87	1995	35	4	5	3	**47**
1996	132	1996	40	4	6	10	**60**
1997	163	1997	59	6	7	10	**82**
1998	155	1998	64	3	5	18	**90**
1999	170	1999	62	6	2	15	**85**
2000	178	2000	48	1	3	28	**80**
2001	179	2001	58	4	6	20	**88**
2002	164	2002	73	0	5	17	**95**
2003	163	2003	79	5	7	18	**109**
2004	114	2004	50	2	6	9	**67**
2005	124	2005	67	4	13	5	**89**
2006	112	2006	68	1	9	5	**83**
2007	119	2007	63	2	11	5	**81**
2008	150	2008	84	5	6	2	**97**
2009	153	2009	78	2	8	3	**91**
2010	150	2010	85	3	6	3	**97**
2011	158	2011	91	4	14	5	**114**
2012	127	2012	92	5	12	0	**109**
2013	152	2013	108	2	10	1	**121**
2014	130	2014	100	3	13	0	**116**
2015	140	2015	105	0	4	0	**109**
2016	148	2016	118	1	6	1	**126**
2017	159	2017	122	0	12	0	**134**
2018	167	2018	137	2	12	0	**151**
2019	147	2019	128	1	7	0	**136**
2020	172	2020	135	1	8	0	**144**
2021	179	2021	132	0	6	0	**138**
2022	118	2022	90	0	2	0	**92**
Total Referrals	**4532**	**Total Deaths**	**2564**	**84**	**237**	**178**	**3063**

Table 1.1: Creutzfeldt Jakob disease cases in the UK. † Referral figure from 1990 is from 1 May onwards. 1 In addition to 20 vPSPr documented from 1997 to 2020. 2 Constitutes all forms of genetic prion diseases, including GSS. Source: National CJD Research and Surveillance Unit (NCJDRSU) website www.cjd.ed.ac.uk – updated 05/09/2022.

1.1.2 Acquired prion diseases

Acquired or iatrogenic prion disease is a form of TSE with a known source of infection, typically through means of surgical intervention, transfusion of biocomponents such as blood or growth hormones, and consumption of infected material. One of the first known acquired human prion disease is kuru, which was rampant in the eastern highlands of Papua New Guinea in the late 1950s. Kuru peaked between 1957 to 1961 with approximately 1000 fatalities (Alpers, 2008). This fatal disease was spread through the transumption of the deceased that succumbed to kuru. It affects mainly woman and children of both sexes. Typically, women of the Fore linguistic group were tasked to dismember the corpse and feast on the remains, of which were fed to young children below the age of 7. Men rarely partook the body, and refrained completely from eating the brain (Alpers, 2008).

Iatrogenic CJD is a form of acquired CJD that is based on transmission of prions from contaminated surgical instruments or tissue grafts. The first documented case was reported in 1974 when a donor received a corneal graft from a CJD patient (Duffy et al., 1974). The most prevalent causes of iCJD include human growth hormones (hGH) and dura mater grafts obtained from human cadavers. According to a comprehensive review in 2012, a total of 469 worldwide cases of iCJD were documented (Brown et al., 2012). Additionally, in the UK alone, 84 fatalities related to iCJD were reported between 1990 and 2022 (**Table 1.1**).

vCJD is an acquired prion disease in the sense that it was transmitted through the ingestion of bovine spongiform encephalopathies (BSE) infected

cattle (Asante et al., 2002; Bruce et al., 1997; Hill et al., 1997; Will et al., 1996). This disease emerged from 1995 onwards in the United Kingdom (Will et al., 1996). Until 2016, all vCJD cases arose from individuals with codon 129 MM homozygosity. However, in 2016, one case with 129 MV heterozygosity was reported, suggesting that more vCJD cases from the 129 MV heterozygous population may succumb to vCJD (Mok et al., 2017).

1.1.3 Genetic prion diseases

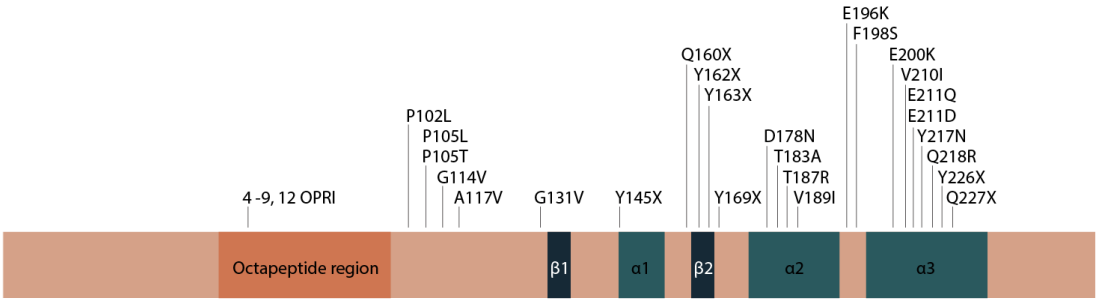

Figure 1.1: Disease-causing autosomal dominant mutations in human prion disease. OPRI = octapeptide insertion. Figure modified from (Mead et al., 2019). For a detailed PrP^{C} structure, refer to **Figure 1.2**.

Genetic or inherited prion disease (IPD) account for up to 15% of prion disease. IPDs are characterised by inheritance of a highly penetrant autosomal dominant *PRNP* mutation. IPD include genetic CJD (gCJD), FFI, and GSS. The earliest onset age of IPD was at 13 years old with P105T mutation (Rogaeva et al., 2006), whereas the oldest was at 94 years of age with 4-OPRI mutation (Kaski et al., 2011). GCJD, which is the most prevalent IPD, tend to develop relatively earlier in life (40 – 45 years age onset) compared to sCJD (55 - 75 years age onset) (Brown et al., 1986). While

there are several mutations linked to gCJD, the most common mutation is E200K (Begué et al., 2011; Kovacs et al., 2011).

GSS can be distinguished from other IPDs by non-glycosylated PrP^{Sc} fragments with relatively low molecular weight that varies between 6 and 8 kDa, depending on the specific *PRNP* mutation (Colucci et al., 2006; Parchi et al., 1998; Piccardo et al., 2001; Tagliavini et al., 1991, 2001). Some of the *PRNP* gene mutations that are associated with GSS include codons 102, 105, 117, 131, 145, 187, 198, and 217 (Liberski, 2012).

FFI is a genetic disorder with a missense mutation of D178N in the *PRNP* gene (Gambetti et al., 1995). It differentiates itself from most prion diseases as the lesions are mainly confined to the thalamus, which controls the sleeping cycles, among other functions (Montagna et al., 2003). Hence, causing a debilitating condition where a patient is not able sleep.

1.2 The prion protein

The human prion protein (PrP^{C}) is encoded by exon 2 of the *PRNP* gene located on the short arm of chromosome 20 (Kretzschmar et al., 1986; Liao et al., 1986; Robakis et al., 1986; Soldevila et al., 2006; Sparkes et al., 1986). The biosynthesis pathway of PrP^{C} starts from mRNA translation on the endoplasmic reticulum (ER)-attached ribosomes. Mature PrP^{C} consists of two major structural regions: a flexible unstructured N-terminal domain, comprising amino acid residues (AA) 23-127 (in mouse) and 23-120 (in human) following the signal peptide cleavage site, and the structured C-

terminal region comprising AA 128- 230 (in mouse) and AA 121-231 (in human) (McDonald et al., 2019; Riek et al., 1996; Zahn et al., 2000).

Following translocation in the endoplasmic reticulum, the signal peptides of N- (residues 1 - 22) and C- (residues 232 – 253) terminal of a fully translated PrP molecule is removed, followed by the attachment of a glycophosphatidylinositol (GPI) anchor to the extreme end of the C-terminus. One, two, or no N-linked glycans are also added at residues 181 and/or 197 for human PrP sequence, or 180 and/or 196 for its murine counterpart (Bolton et al., 1985; Stahl et al., 1987, 1993; E. Turk et al., 1988). Structurally, PrP^C contains 3 α-helical regions, and 2 β-pleated sheets. The octapeptide repeats is situated in the N-terminus at position 51 to 91 (refer to **Figure 1.2**)

PrP^C is a substrate to a variety of proteases and undergoes different types of cleavages with each having distinct physiological consequences. Four key cleavage events have been described, namely the α-, β-, and γ-cleavages, and its membrane-proximate shedding. In healthy tissues, cleavage of PrP^C in the vicinity of K109/H110 (in mouse) (McDonald et al., 2014) and K110/H111 (in human) (Linsenmeier et al., 2017), termed α-cleavage, separates the N- and C-terminal halves, resulting in released N1 (~11kDa) and membrane-anchored C1 (~18kDa). β-cleavage occurs between site 89/90, releasing the N2 (~9kDA) and C2 (~20kDA) fragments (Altmeppen et al., 2012; S. G. Chen et al., 1995; Jiménez-Huete et al., 1998; Mangé et al., 2004). Interestingly, PK digestion of aberrant PrP conformers generate a similar fragment size as C2 since the cleavage site is approximately at residue 90. For γ-cleavage, the exact site is unknown, however, the size of

the released fragments N3 (~20kDa) and C3 (~5kDa) suggests the cleavage site to occur within residues 170 to 200 (Haigh & Collins, 2016; V. Lewis et al., 2016). Shed PrP is produced when the extreme C-terminal end of PrP is cleaved, releasing a sizeable fraction of PrP into the extracellular space whilst maintaining a small number of residues on cell surface. ADAM10 and ADAM9 are the main known peptidases involved in shedding PrP molecules *in vitro* and *in vivo* (Altmeppen et al., 2011; McDonald & Millhauser, 2014; D. R. Taylor et al., 2009). Further analysis revealed the proteolytic site to release shed PrP is between residues 228 and 229 (D. R. Taylor et al., 2009).

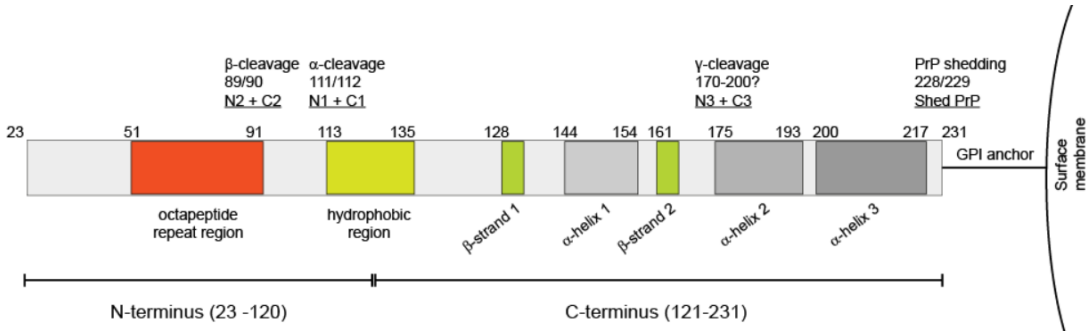

Figure 1.2: Human PrP^C and its known cleavage events. Mature PrP^C spans from residues 23-231. The N-terminal (1-22 aa) and C-terminal signal peptides (232 -253 aa) peptides are removed, followed by the attachment of a GPI anchor to the C terminus. The unstructured N-terminus encompasses residues 23 – 120 whereas the C-terminus covers the remaining region (residues 121-231). Identified cleavage sites include α (between 111/112), β (between 89/90), and γ (exact site undetermined, plausible within 170 to 200). Cleavage results in soluble (N1, N2, N3, shed PrP) and membrane-anchored (C1, C2, C3) PrP fragments. Image modified from **(Kovač & Šerbec, 2022)**.

1.2.1 Function of PrP^C

Although the role of PrP^C is widely established in prion diseases, the main function of PrP^C remains an enigma. However, there are studies providing clues to the functions of PrP using gene perturbation techniques such as gene silencing and gene overexpression *in vitro* and *in vivo*. PrP^C is highly conserved between mammals, suggesting an important role in maintaining physiological processes (Wopfner et al., 1999). It has been shown that it plays a role in mediating neurite outgrowth and synaptic function (Kanaani et al., 2005; Re et al., 2006). Another interesting facet of PrP^C is its association with myelination. PrP^C is expressed in the CNS in copious amounts. It can be found along the axons and in presynaptic terminals that are involved in anterograde and retrograde axonal transport (Borchelt et al., 1994; Herms et al., 1999; Mironov et al., 2003; Moya et al., 2004; Salès et al., 1998, 2002). Deletion of the α-cleavage region causes extensive demyelination effects in the spinal cord and cerebellar white matter in animals (Baumann et al., 2007; Radovanovic et al., 2005). The α-cleavage of axonal PrP serves as a criticial step in promoting myelination events in the peripheral nervous system (PNS) (Bremer et al., 2010). Mice that are devoid of whole PrP molecule developed chronic demyelinating neuropathy (Küffer et al., 2016).

1.2.2 Disease-associated PrP (PrP^D)

The term prion was first introduced in 1982 by Stanley Prusiner (Prusiner, 1982). Prions are referred to as abnormal infectious proteins that cause prion diseases. On the other hand, PrP^{Sc}, operationally defined as Proteinase K

(PK)-resistant PrP is an aberrant PrP molecule that can be detected in prion-infected samples following limited proteolysis with PK (Bolton et al., 1982). Structural analysis of purified PrP^{Sc} revealed substantial amounts of β-pleated sheet contents (43% β-sheet, 30% α-helix) when compared to PrP^{C} isolates (3% β-sheet, 42% α-helix) (K. M. Pan et al., 1993). While proteinase K digests a significant portion of the N-terminus of PrP^{Sc}, other proteinases such as pronase and trypsin leave the N-terminus intact (D'Castro et al., 2010; McKinley et al., 1991; Yam et al., 2010). While PK treatment is typically used in immunohistochemistry and immunoblotting to discern PrP^{Sc} from PrP^{C}, we experienced difficulties in treating cell cultures with PK as fixed cells were detached following limited proteolysis. We thus used guanidine thiocyanate (GTC), a potent denaturing agent, to detect abnormal PrP accumulations that are only present in infected cells (Taraboulos et al., 1990; Veith et al., 2009). Hence, we adopted the term disease-associated PrP (PrP^{D}) to denote aggregated PrP in prion-infected cells in the absence of PK digestion.

Studies using *in vitro* cultures as well as histopathological slices showed that aberrant PrP aggregates are detected both intra- and extracellularly (Jeffrey & González, 2007; Marbiah et al., 2014; Rouvinski et al., 2014; Tanaka et al., 2016). Interestingly, intracellular PrP^{D} differs to that of their extracellular counterparts as it is truncated at the N-terminus. Immunostaining using antibodies against the N-terminus does not stain intracellular aggregates, with immunofluorescence being visible at the boundary of cells (Rouvinski et al., 2014; Tanaka et al., 2016). However, the main endogenous protease responsible for this cleavage in aberrant PrP assemblies is not known.

Indeed, the presence of prions in the extracellular milieu is seen as a concern in decellularisation of whole organs (Singh et al., 2022). The presence of PrP^D deposition in the ECM or pericellular spaces suggests that prions, similar to growth factors and nanovesicles (Huleihel et al., 2016; G. S. Schultz & Wysocki, 2009), are sequestered extracellularly and may be released upon bioscaffold remodelling.

1.2.3 The protein only hypothesis

The protein only hypothesis suggests how a protein self-replicates without nucleic acid through the recruitment and conversion of normal PrP into abnormal PrP assemblies. Due to the prolonged incubation period of prion diseases, the causative agent was initially speculated to be a slow virus (Sigurdsson, 1954). In 1967, John Griffith, who was a biophysicist, proposed the thermodynamics model of self-templating proteins (Griffith, 1967). The idea was understandably controversial during its introduction as it challenges the central dogma of DNA not being the only biological substance to self-replicate under certain conditions. In 1982, Prusiner showed that despite treating prion-infected samples with several nuclei acid deactivation procedures, scrapie agents remained intact (Prusiner, 1982). When methods known to destroy proteins were applied, infectivity was effectively abolished, elevating the protein-only hypothesis to new heights (Bolton et al., 1982; Prusiner, 1982).

Following the discovery of the gene encoding PrP^C (Basler et al., 1986; Oesch et al., 1985), the protein-only hypothesis was yet again put to a test. If

PrP^C is a definite pre-requisite material for infectious prion formation, then animals that lack PrP^C must not contract prion disease. In 1993, Büeler and colleagues demonstrated that mice devoid of PrP^C were resistant to prion infection, whereas heterozygous *Prnp*$^{+/-}$ mice were partially resistant, relative to wild type mice (Büeler et al., 1993). Given the compelling arguments supporting the protein-only hypothesis, including the presence of highly-penetrant genetic prion diseases (discussed in **Section 1.13**), prion researchers have widely accepted the idea of a self-templating infectious protein.

1.3 Intercellular PrP^D spread

As mentioned, PrP^D assemblies are infectious particles that are capable of propagating by templating normal prion proteins into the misfolded, disease-associated conformation. Understanding the intercellular transfer of prions is critical in the development of therapeutic agents. Aberrant PrP assemblies can infect neighbouring cells through cell-to-cell contact (Kanu et al., 2002), exosome infection (Cheng et al., 2018), and tunnelling nanotubes (Schiff et al., 2008; Zhu et al., 2015)**.** According to the protein only hypothesis, pathogenic PrP seeds recruit and convert normal PrP^C into its rogue form. In the context of intercellular PrP^D transfer, it involves both nascent PrP^D formation and internalisation of native prions from infectious source.

1.3.1 Infection by cell-to-cell contact

Infection via physical cell-to-cell contact was highly anticipated since PrP^C, the substrate for PrP^D aggregates, has been shown to be anchored on surface membrane in early studies (Caughey et al., 1989; Stahl et al., 1987). Indeed, PrP^D was observed on neuronal plasma membrane and sites of cell-to-cell contact in infected mouse brain microsections (Godsave et al., 2013). Numerous studies have set up different experimental approach to probe for infectivity via direct cell contact, of which involved the usage of conjugated form of PrP or utilising transfected cells devoid of PrP. In the case of co-culturing uninfected astrocytes with infected Cad5 cells, PrP^D was detected in astrocytes, suggesting intercellular contact is sufficient to propagate PrP^D (Victoria et al., 2016). However, the study does not address whether the observed intracellular PrP^D aggregates in astrocytes were nascent or originated from the infected donor cell. To address whether surface bound PrP conversion into its aberrant form occurs *in situ*, Goold and colleagues generated a susceptible cell line that expresses Myc tagged PrP (Goold et al., 2011). This allows the distinction between newly formed Myc-PrP^D aggregates and inoculum without Myc residues. Interestingly, this study showed that PrP conversion occurs rapidly, within a minute after infection and the main site of conversion was the plasma membrane. This infers that PrP^D can directly convert surface-bound PrP on cells into abnormal conformers, which suggests that infected cells could transform PrP^C on healthy cells into prions upon physical contact.

1.3.2 Extracellular vesicles

According to the International Society for Extracellular Vesicles (ISEV), the nomenclature “extracellular vesicle” refers to the “generic term for particles naturally released from the cell that are delimited by a lipid bilayer and cannot replicate” (Théry et al., 2018). EVs are secreted from most, if not all, cell types into the bodily fluids (Robbins & Morelli, 2014). The two main subpopulation of EVs are microvesicles and exosomes. Microvesicles, also known as ectosomes, are formed through the outward budding of the plasma membrane. This vesicle would generally have a size of 100 nm to 1000 nm. On the other hand, exosomes are nanovesicles that ranges from 30 to 100 nm. Exosomes are constitutively formed from the early sorting endosomes (ESE), and subsequently assembled into the late sorting endosomes (LSE). LSEs then form multivesicular bodies (MVB) that expels its contents as exosomes after fusing with the cell membrane (Zhang et al., 2020).

EVs have been extracted from numerous biological fluids including blood (serum/plasma) (Caby et al., 2005; Lässer et al., 2011), saliva (Michael et al., 2010; Palanisamy et al., 2010), cerebrospinal fluid (Street et al., 2012; Vella et al., 2008), milk (Admyre et al., 2007; Lässer et al., 2011), urine (Pisitkun et al., 2004), semen (Poliakov et al., 2009), nasal, ascites, bronchoalveolar, and amniotic fluids (Harding et al., 1984; B. T. Pan et al., 1985), and bile (Masyuk et al., 2010).

PrP^{C}, which is mainly expressed on the membrane, can be internalised either by clathrin-coated vesicles or caveolae (Campana et al., 2005; Harris, 2003). Studies using the Chinese hamster ovary (CHO) cell line

demonstrated that PrP^C is concentrated in caveolar-structures bound at the cell surface and present in the intracellular endocytic caveolae as well (Peters et al., 2003). Endocytosed PrP^C are shown to transit through the early and late endosomes (Peters et al., 2003), which is consistent with the steady state localisation of PrP^C in endocytic MVBs present in hippocampal neurons as well (Mironov et al., 2003). In a gene perturbation study using neuroblastoma cells, PrP^C conversion into its aberrant form was observed in MVB (Yim et al., 2015). Indeed, isolated EVs of prion-infected cells contain both PrP^C and PrP^{Sc} (Bellingham et al., 2012; Coleman et al., 2012; Vella et al., 2007). As extracellular vesicles are ubiquitously present in bodily fluids and can be taken up by various cells via endocytosis, one can speculate that prion-infectious exosomes can spread and infect cells throughout the body.

1.3.3 Tunnelling nanotubes

Tunneling nanotube (TNT) was first reported in 2004 by Rustom and colleagues, which was seen as an elongated structure interconnecting single cells (Rustom et al., 2004). TNTs are made of actin rod enclosed in a lipid bilayer. TNTs are observed in a variety of cell cultures (Dubey & Ben-Yehuda, 2011; Gurke et al., 2008; Lou et al., 2012; Önfelt et al., 2006; Rupp et al., 2011; Sowinski et al., 2008) and shown to transfer a range of cellular components (Gurke et al., 2008; Rustom et al., 2004). TNTs have also been observed *in vivo* in blastocyst formation and neurulation in mice (Pyrgaki et al., 2010; Salas-Vidal & Lomelí, 2004). Interestingly, TNTs have been implicated in the transfer and spread of bacteria and viruses (Önfelt et al., 2006; Sowinski et al., 2008) as well as intercellular trafficking of aberrant rogue proteins such as prions and misfolded huntingtin involved in prion diseases and Huntington's disease (Costanzo et al., 2013; Gousset et al., 2009), respectively.

In 2009, Gousset and colleagues demonstrated that PrP^{C} was trafficked to nearby cells through TNTs. In the same study, PrP^{D} was also detected in these protruding structures under denaturing conditions (Gousset et al., 2009). Interestingly, PrP^{D} was also seen encapsulated in endocytic vesicles of infected cells and transferred to neighbouring recipient cells through TNTs (Zhu et al., 2015). At the moment, evidence for tunnelling nanotubes in prion diseases are limited, albeit this phenomenon is also observed in other neurodegenerative diseases such as Huntington's disease (Costanzo et al., 2013), Alzheimer's disease (Abounit, Wu, et al., 2016; Tardivel et al., 2016), and Parkinson's disease (Abounit, Bousset, et al., 2016).

1.4 Subcellular localisation of PrP^D

The cellular prion protein (PrP^C) is found predominantly on the outer leaflet of the plasma membrane in the central nervous system. Although PrP^C is normally found anchored to the surface membrane, abnormal PrP aggregates are found both intra- and extracellularly. This phenotype can be observed both in infected immortalised cell lines and primary cultures (Marbiah et al., 2014; Philiastides et al., 2019; Rouvinski et al., 2014; Tanaka et al., 2016). In 2014, Rouvinski and colleagues reported the presence of 'strings and webs' PrP aggregates decorating the periphery cellular membrane (Rouvinski et al., 2014). This phenotype can be detected using an anti-PrP antibody against the N-terminus, signifying the manifestation of full length PrP^D on the outer membrane. By using the same antibody, virtually no intracellular signals were detected, but appear positive when an antibody against the PrP core was used instead. This implies that intracellular PrP^D is N-terminally cleaved, leaving a truncated form of abnormal PrP. However, this study was entirely based on an immortalised cell line. A more biologically relevant model, primary neurons, showed the same phenotype. Tanaka and colleagues demonstrated that primary neurons or susceptible N2a cells infected with the 22L strain exhibited similar disease-associated intracellular staining (Tanaka et al., 2016). In this study, primary neurons showed truncated intracellular PrP^D granules, which was also seen in infected immortalised cell culture. Immunofluorescence using 8D5, an anti-PrP antibody targeting the N-terminus, showed membrane positivity but was negative intracellularly. Interestingly, infected primary neurons exerted full length fibrillar PrP aggregates from the cell periphary, which corroborated the

findings from Rouvinski and colleagues as explained earlier (Rouvinski et al., 2014).

Later in this thesis, we show that fibrillary protrusions were indeed observed in chronically infected N2a-PK1 cells. Interestingly, extracellular fibrillar PrP^D was also found in infected astrocytes extracted from cortico-hippocampal tissue (Philiastides et al., 2019). As the elongated PrP assemblies extend to the extracellular space, a follow up question is to understand the interactions of the infectious microscopic structures with its surroundings, namely the extracellular matrix (ECM) scaffold.

1.4.1 The extracellular matrix (ECM)

The extracellular matrix (ECM) consists of a highly structured network of cross-linked proteins and polysaccharides. The extracellular scaffold is located within most, if not all tissues and organs. It provides not only physical architectural support, but is also involved in biochemical cues that are essential for tissue morphogenesis, differentiation, and homeostasis (Daley et al., 2008).

The ECM is composed of proteoglycans and fibrous proteins such as collagen, fibronectin, elastins, and laminins. Proteoglycans permeate most of the interstitial space within the tissue (Frantz et al., 2010). In mammals, collagen is one of the major components of the ECM and makes up to 30% of the total protein mass in the body (Ricard-Blum, 2011). An important role of the ECM is to support cell adhesion, which is pivotal for the formation of organs. Cell adhesion to the ECM can occur through the formation of focal

adhesions, an intricate internetwork of aggregated cellular integrins and the extracellular substrate (Kanchanawong & Calderwood, 2022).

The extracellular bioscaffold is also imperative in wound healing. Upon the formation of fibrin clot during vascular damage, monocytes are stimulated to infiltrate the damaged ECM. The ECM-degraded products and cytokines differentiate monocytes into macrophages (Laurens et al., 2006). In turn, macrophages secrete growth factors, matrix metalloproteases (MMPs), and cytokines that promote angiogenesis and stimulate fibroblast migration and proliferation, and subsequently activate myofibroblasts that secretes more relevant ECM-resident proteins (G. S. Schultz & Wysocki, 2009). As the neo-ECM matures, superfluous cells are eliminated through apoptosis (Ren et al., 2022). Another fascinating facet of the ECM is the presence of growth factors and nanovesicles entrapped in the scaffold. These substances are released upon proteolytic degradation of ECM, which is explained in detail in **Section 1.4.3**. One of the known effects of ECM dysfunction is the development of the tumor microenvironment. This relates to the stiffness of the ECM which enhances cancer cell proliferation (Alonso-Nocelo et al., 2018), followed by ECM degradation which enables metastasis (McKenzie et al., 2018).

1.4.2 Main forms of brain ECM

The brain ECM, which surrounds all cells, occupies approximately 20% of the volume fraction in an adult brain (Sykova & Nicholson, 2008). There are several specialised forms of the ECM in the brain, which include but is not limited to the basement membrane, perineuronal nets (PNNs), and neural

interstitial matrix (Rauti et al., 2019). These specialised scaffolds contain a myriad of extracellular-resident macromolecules that serve vital functions in maintaining structural support and normal brain function (**Table 1.2**). The basement membrane refers to a collection of ECM protein layers that provides architectural support for epithelial and endothelial cells (Paulson, 1992). It surrounds the pial surface (boundary between gray matter and cerebrospinal fluid) of the CNS, essentially forming the blood-brain barrier (L. Xu et al., 2019). It is composed from a collection of protein complexes, namely collagen, fibronectin, laminin, and heparin sulfate proteoglycans (HSPGs) (Thomsen et al., 2017).

Category	Component	Function	Reference
Glycosaminoglycans (GAGS)	Hyaluronic Acid (HA)	Involved in PNNs formation, regulates neuronal migration and mediates axonal and dendritic growth	(Benarroch, 2015)
Proteoglycans	Aggrecan	Imperative for stabilisation of PNNs structure. Without aggrecans, the PNNs scaffold will not hold.	(Rowlands et al., 2018)
	Brevican	Contributes as one of the building blocks of PNNs, and contribute to the plasticity and tenacity in neural circuits	(Frischknecht & Seidenbecher, 2012)
	Versican	The role of versican is	(Novak &

		not established, however, it is suggested that it plays a role in neuronal cell adhesion and axonal growth	Kaye, 2000)
	Neurocan	Aids axonal and neurite growth during brain development	(Zhou et al., 2001)
	Phosphacan	Regulates neuronal and glial adhesion and neurite outgrowth	(Novak & Kaye, 2000)
	Syndecan	Suggested to be involved in growth factor signalling	(Beller & Snow, 2014)
	Glypican	Implicated in injury response of neurons	(Litwack et al., 1994)
	Agrin	Involves in the maintenance and formation of synapses, as well as supporting enhancing interneuronal synaptogenesis	(Daniels, 2012)
	Perlecan	Structure the basement membrane	(Benarroch, 2015)
Fibrous glycoproteins	Collagen	Although it is less abundant in the brain, collagen provides scaffold integrity,	(Frantz et al., 2010; Novak & Kaye, 2000)

	mediates cell adhesion, and involved in chemotaxis and cell migration	
Fibronectin	Although uncommon in the brain, fibronectin is involved in structural support and synaptogenesis	(Frantz et al., 2010; Novak & Kaye, 2000; Tonge et al., 2012)
Laminin	Mainly involved in the organisation of the interstitial ECM and mediates cell attachment	(Frantz et al., 2010)
Nidogen	Contributes to neuronal plasticity	(Köhling et al., 2006)
Tenascin	Supports cell adhesion and migration, growth, and differentiation due to their interaction with collagen and integrins	(Barbosa & Martins, 2017)

Table 1.2: Function of the ECM components in the brain. Table is adapted from (Rauti et al., 2019) with modifications.

PNNs are large meshworks of ECM molecules surrounding distinct neuronal cells, which after their first description in the 1890s by Golgi and Ramon Y Cajal were largely neglected due to an erroneous claim of being an artefact, only to be rediscovered in 1998 (Celio et al., 1998). These intricate structures mainly surround parvalbumin (PV)-expressing interneurons, which include chandelier and basket cells. PNNs are formed by several groups of ECM molecules including hyaluronan and its synthesizing enzymes hyaluronan synthases (HASs; HAS1 and HAS3), chondroitin sulfate proteoglycans (CSPGs), tenascins, and hyaluronan and proteoglycan link proteins (HAPLNs) (Sorg et al., 2016). PNNs functions have been associated with sleep regulation, maintenance of normal synaptic connectivity, learning and memory, and provides protection against amyloid beta neurotoxicity (Carulli & Verhaagen, 2021; Dankovich & Rizzoli, 2022; Gisabella et al., 2021; Miyata et al., 2007; Morawski et al., 2012).

Neural interstitial matrix, as the name suggests, are interconnected ECM constituents situated in the interstitial space between cells of the CNS parenchyma. Its main components are made of proteoglycans, hyaluronan, tenascins and link proteins (Rauch, 2007). Extracellular NG2, also known as CSPG4, can also be found in the interstitial matrix presumably shedded from NG2-expressing cells (Lau et al., 2013).

1.4.3 ECM remodelling

Degradation of the ECM is an important cellular mechanism involved in various functions such as cell migration (Leonard & Taneyhill, 2020), cell

differentiation (Streuli, 1999) and wound healing (Velnar et al., 2009). ECM remodelling is largely regulated by metalloproteinases, namely metzincins, a group of zinc-dependent proteases present in the extracellular matrix (ECM). The metzincin family of metalloproteinase includes matrix metalloproteainase (MMP), ADAM (a disintegrin and metalloproteinase), and ADAMTS (a disintegrin and metalloproteinase with thrombospondin motifs) (Bonnans et al., 2014).

In the brain, the ECM acts as a physical barrier to restrict neural plasticity, a process of reorganizing structural and functional capacity of neural networks in response to environmental stimuli and sensory input. However, this function can be restored through enzymatic degradation of the extracellular scaffold. Chondroitin sulfate proteoglycans (CSPG)-containing ECM is known to inhibit neurite outgrowth and regeneration (Fawcett, 2009). Intriguingly, removal of ECM increased neuronal network rearrangement upon stimuli input, as well as promoting cognitive flexibility in rodents (Happel et al., 2014). Indeed, enzymatic activity of MMP-9 is required for the formation of spinehead protrusions in mature neurons, which is implicated in long-term potentiation (Szepesi et al., 2013). Importantly, MMPs and ADAMTS4 have been shown to degrade CSPGs including brevican and aggrecan, suggesting further evidence for ECM remodelling in the mature brain (Nakamura et al., 2000; Tortorella et al., 1999). Proteolytically cleaved brevicans can be found widespread across different brain regions, however, a higher proportion of these fragments are present in paravalbumin-positive interneurons surrounded with PNNs (Valenzuela et al., 2014). In addition, the same study reported the presence of brevican fragments with varying

degrees in all cultured neurons, signifying ECM degradation in the mature brain as an active physiological phenomenon. Endopeptidases are also involved in restricting glial scarring. For instance, the proteolytic activity of MMP-2 aids immature astrocytes in reducing glial scars by removing excess CSPGs (Filous et al., 2010). Filous and colleagues also reported that the removal of CSPGs through exogenous proteolytic treatment showed an increase in axonal growth, suggesting the important role of ECM reconstitution in CNS axonal regeneration.

Although the removal of a physical barrier is a key event in ECM remodelling, it should not be regarded as its sole function. Biomaterials such as extracellular vesicles (EVs) and growth factors can be sequestered in the extracellular scaffold (Huleihel et al., 2016; Wilgus, 2012). Degradation of the ECM leads to the release of these bioactive components which interacts with nearby cells, triggering a myriad of cellular pathways. EVs entrapped in the ECM scaffolding are referred to as matrix-bound nanovesicles (MBVs). These vesicles contain microRNA (miRNA), cytokines, chemokines, and numeros proteins and lipids that can be endocytosed into recipient cells (Faust et al., 2017; Huleihel et al., 2016; Hussey et al., 2020; Quijano et al., 2020). Interestingly, exosomes extracted from prion-infected cultures are shown to harbour infectious abnormal PrP assemblies (Alais et al., 2008; Fevrier et al., 2004). Other than MBVs, infectious PrP conformers are also present in the extracellular mileu (Jeffrey et al., 2011; Marbiah et al., 2014). However, it is not known whether these sequestered aberrant biomaterials can promote infection upon its release via ECM remodelling.

1.4.4 Role of V-ATPase in ECM remodelling

The V-ATPase (Vacuolar-type H^+ ATPase) pump is highly conserved across eukaryotic organisms. It is comprised of two domains, namely the transmembrane V1 complex, and the membrane-embedded V0 complex (Wang et al., 2020)The V-ATPase pump can be effectively inhibited by bafilomycin A1. By using cryo-TEM, it was observed that six bafilomycin A1 molecules are bound to the c-ring. One bafilomycin A1 molecule engages with two c subunits and disrupts the interactions between the c-ring and subunit a, thereby preventing proton translocation (R. Wang et al., 2021). Mutations in the c-ring of the V-ATPase inhibits Bafilomycin A1 from binding to its target site (Bowman & Bowman, 2002). V-ATPase pumps are found within the membrane of various organelles, including endosomes, lysosomes, and secretory vesicles, and also present within the plasma membrane of a variety of cells (Beyenbach & Wieczorek, 2006; Forgac, 2007; Wagner et al., 2004). In lysosomes, a relatively low pH of approximately 4.5 must be maintained for optimal enzymatic proteolysis. This is achieved by V-ATPases actively pumping H+ ions from the cytosol and into the organelle.

The human lysosome houses a multitude of cysteine cathepsins (B, C, F, H, K, L, O, S, V, W and X) and aspartyl cathepsins (D and E) (Hsu et al., 2018; Rossi et al., 2004). Most cathepsins are known to degreade the extracellular resident proteins. ECM remodelling by cathepsins was demonstrated through shedding of extracellular receptors and cell adhesion molecules (Gocheva & Joyce, 2007; Mohamed & Sloane, 2006; Sobotič et al., 2015). For example, Cathepsin B degrades collagen type IV, laminin, fibronectin, and CSPG

(Buck et al., 1992), whereas Cathepsins K, L, S, F, and V digest elastin, collagen, and proteoglycans at varying degrees (V. Turk et al., 2012). Interestingly, cathepsin B degrades axon-inhibitory CSPGs, which led to axonal regeneration (Tran et al., 2018). On another note, Cathepsin L also exerts similar axonal remodelling properties, however, it is not known whether it targets CSPGs as well (Tohda & Tohda, 2017).

Other than maturing lysosomal enzymes, V-ATPases are also implicated in acidification of the extracellular environment, which can be observed in normal cell functions including bone resorption and renal acid-base regulation, as well as in pathological conditions such as tumor metastasis. Depletion of the Atp6ap1 (also known as Ac45), a component of V-ATPase pump, blocks physiological extracellular acidification in osteoclasts, a key event in bone resorption (Yang et al., 2012). Intriguingly, in the same study, removal of the Atp6ap1 did not affect V-ATPase assembly, however, it impaired the trafficking of proton pumps from reaching the plasma membrane. In pathological environments, particularly the tumor microenvironment, membrane-associated V-ATPases are upregulated and dysregulate the extracellular pH, leading to deleterious conditions including chemoresistance and tumor invansion (De Milito & Fais, 2005; Nishi & Forgac, 2002; Sennoune, Bakunts, et al., 2004; Sennoune, Luo, et al., 2004). In breast cancer cells, translocation of V-ATPase pump to the membrane is mediated by the a4 subunit, a component found within the A0 domain of the proton pump (Hinton et al., 2009).

Importantly, V-ATPases are also implicated in the trafficking and activating of MMPs, a group of proteases widely known for its ECM-degrading properties

(Bonnans et al., 2014). Although MMPs are not directly pH dependent, it can nevertheless be activated at low pH, particularly by cathepsin-dependent cleavage. For instance, cathepsins G and K are implicated in the cleavage and activation of pro-MMP9 (Christensen & Shastri, 2015). Cathepsin G is also involved in activating zymogens of MMP1 and MMP3 (Okada & Nakanishi, 1989; Son et al., 2009), which subsequently leads to ECM degradation (Bonnans et al., 2014). MMP14 is a metalloproteinase involved in activating collageneses leading to ECM degradation. Interestingly, perturbation of the Atp6ap1 (Ac45) gene, in which encodes for the accessory subunit of V-ATPases, impairs the translocation of membrane-associated MMP14, a known collagenase, from anchoring the plasma membrane. Hence, this diminishes the activation of ECM-digesting peptidases, which could lead to a decrease of scaffold remodelling (Smith et al., 2016). Currently, there are lack of studies linking V-ATPases in ECM remodelling with neurodegenerative disorders, however, in Parkinson's Disease, impaired V-ATPases regulation leads to the increased pH of lysosomes, followed by protein aggregation and neuronal cell death (Dubos et al., 2015; Hirose et al., 2019; Korvatska et al., 2013).

1.4.4 The role of V-ATPase in modulating prion infection

As cellular cargo journeys from the cell surface towards the depths of lysosomes, the luminal pH within endosomal organelles undergoes a progressive decline (Nishi & Forgac, 2002). This dynamic pH transition critically modulates integral cellular activities, including the release of

internalised ligands from their receptors and the activation of lysosomal enzymes. Central to the process of endosomal acidification is the vacuolar ATPase (V-ATPase), a multisubunit complex that actively transports protons from the cytoplasm into the organelle's lumen or outside the cell itself, depending on its localisation (Breton & Brown, 2013; M. P. Collins & Forgac, 2020).

Membrane bound PrP^{C} is internalised into endocytic compartments and are either recycled intact to the cell surface or degraded by lysosomes (Campana et al., 2005). The role of V-ATPases in TSEs is not well established. However, it is observed that PrP^{Sc} is partially accumulated in V-ATPase concentrated organelles such as endosomes and lysosomes in prion infected cells (Veith et al., 2009). Interestingly, extensive molecular-dynamics simulation studies have shown that the acidic environment plays a key role in misfolding PrP into its aberrant form (Lima et al., 2018; Van Der Kamp & Daggett, 2010). Indeed, human recombinant PrP requires a pH of 4 or lower to form a high proportion of β-sheet structures resembling that of PrP^{Sc} (Jackson et al., 1999). Moreover, the thermodynamic stability of PrP is markedly decreased when the pH is reduced from pH 7 to 4.8 (Apetri et al., 2006) or pH 4.5 (Calzolai & Zahn, 2003), setting the stage for prion pathology. Interestingly, raising the pH of intracellular vesicles using pharmacological inhibitors such as monensin and lysosomotropic amines does not increase the synthesis of PrP^{Sc} (Taraboulos et al., 1992). Although PrP^{Sc} can also be found in V-ATPase enriched autophagosomes, inhibition of proton pumps using bafilomycin A1 does not alter the concentration of PrP^{Sc} in these autophagic vesicles (Marzo et al., 2013), as well as not

altering the steady state levels of PrP^{Sc} in chronically infected N2a cells (Yamasaki et al., 2014).

Nevertheless, a notable gap exists in the body of research elucidating the role of V-ATPase in modulating infection within newly infected cells. Within the scope of this thesis, I have undertaken the task of unveiling this intricate interplay, however, under the context of degradation of prion-embedded ECM by V-ATPase dependent enzymes. In turn, the disassembly of prion-infected ECM will result in the release of infectious PrP conformers that leads to infection. We show that by blocking V-ATPases, which is involved in maturing matrix-degrading enzymes, infection was significantly attenuated, suggesting V-ATPases play an important role in prion diseases.

1.4.5 ECM in neurodegenerative disease

There is a considerable body of evidence suggesting that ECM protein regulation is severely altered in several neurodegenerative disorders such as Alzheimer's disease, Parkinson's disease (PD), amyotrophic lateral sclerosis (ALS), and prion diseases (Downs et al., 2022; Johnson et al., 2022; McBride et al., 1998; Phatnani et al., 2021; Snow et al., 1990). The main pathological hallmark of AD includes extracellular senile plaques (SPs) and intracellular neurofibrillary tangles (NFTs). SPs consist of amyloid-beta (Aβ) peptides and NFTs are formed by aggregated hyperphosphorylated tau protein (Masters et al., 2015; J. Wang et al., 2017). Interestingly, pathological studies have shown that SPs colocalise with collagen IV, laminin, and fibronectin in the ECM brains from AD patients (Howard & Pilkington, 1990;

Perlmutter et al., 1991). Proteoglycans, which are either found in secreted form or bound to the plasma membrane, are glycosylated proteins which are post-translationally modified by the addition of glycosaminoglycans. Studies have shown that glycosylated proteoglycans including heparan sulfate proteoglycans (HSPGs) and chondroitin sulfate proteoglycans (CSPGs), interact with abnormal protein aggregates such as tau and prion assemblies (Ben-Zaken et al., 2003; Holmes et al., 2013).

In human AD postmortem samples, it was observed that SP-positive basement membrane is thickened (Claudio, 1995; Lepelletier et al., 2017; Perlmutter & Helena Chang Chui, 1990; Serot et al., 1997; Zarow et al., 1997). Inspections on tissue samples affected by amyloid disorders in brain and in peripheral organs including AD, type II diabetes, light chain amyloidosis, and prion diseases have shown elevated HSPGs levels in the fibrillary amyloid aggregates (Hernández et al., 2002; Naiki & Nagai, 2009; Snow et al., 1990).

Intriguingly, heparan sulfate (HS), which is a type of glycosaminoglycan (GAG), has been shown to be involved in the formation and stabilisation of amyloidogenic deposits (Dulce et al., 2011; Snow et al., 2021). Studies have suggested that HS (1) promotes the misfolding of proteins or peptides into pre-amyloid structures (Elimova et al., 2009; Motamedi-Shad, Monsellier, Torrasa, et al., 2009; V. Schultz et al., 2017; D. Xu & Esko, 2014), (2) act as a platform for peptide-assembly, essentialy trigerring nucleation seeds (McLaurin et al., 1999; Motamedi-Shad, Monsellier, & Chiti, 2009; Rouvinski et al., 2014) and (3) stabilise oligomers assembly which forms amlyoid fibrils (Castillo et al., 1997; Rodriguez et al., 2017; Snow et al., 1994).

In prion diseases, numerous studies have demonstrated that aberrant PrP conformers bind to HS (Ben-Zaken et al., 2003; Horonchik et al., 2005; Snow et al., 1990). Treatment using HS mimetics is capable of abolishing cellular infectivity *in vitro* and significantly prolong the survival period of BSE-infected mice (Adjou et al., 2003). The success of this treatment could be due to HS mimetics acting as competitors to endogenous HS for sequestering infectious PrP assemblies. In 2014, Marbiah and colleagues demonstrated that the ECM played a crucial role in the deposition of extracellular PrP^{D}. Using immunostaining, it was observed that Fibronectin I is negatively correlated with extracellular prion deposition. Upon silencing ECM-associated genes such as Fn1 and Chga, prion-resistant cells were rendered susceptible to infection (Marbiah et al., 2014). The same researchers also concluded that inhibition of sulfation of HSPGs increases susceptibility of prion-resistant cells. On another note, disruption of perineuronal nets (PNNs) in prion-infected brain has been documented in both humans (Belichenko et al., 1999) and animals (Franklin et al., 2008; Guentchev et al., 1998). PNNs are extracellular matrix surrounding certain neurons, particularly inhibitory GABAergic parvalbumin-positive interneurons. PNNs play a pivotal role in memory and learning (Carulli & Verhaagen, 2021), thus, disruption of this functional scaffold might explain, in part, the cognitive deficits seen in prion diseases.

1.5 Cell-derived ECM scaffold

The ECM is composed of an internetwork of macromolecules that not only act as a physical barrier that provides cells with structural support and segregating tissues apart, it is also involved with important cellular functions including proliferation, differentiation, and wound healing. However, pathological conditions could alter the ECM composition and integrity, and subsequently, influence cell processes that would lead to deleterious effects such as chemoresistance and tumor invasion. To best study the cell-ECM interactions, scientists have developed a valuable tool called cell-derived ECM, or also known as decellularised ECM (dECM), a bioscaffold deposit devoid of cells. This acellular complex can be generated through decellularisation, a process that lyses adherent cells while retaining the structural and functional integrity of the ECM. The dECM is developed to mimic the native extracellular environment. It can be prepared either through the decellularisation of whole organs, tissue sections, organoids, or monolayer cultured cells. Production of ECM scaffolds are applied in numerous fields including regenerative medicine, drug discovery, food technology, and basic research.

1.5.1 Applications of cell-derived matrices

Cell-derived scaffolds are widely used in regenerative medicine. Articular cartilage damage can be treated with autologous chondrocyte implantation (ACI). It relies on autologous chondrocytes to produce the necessary extracellular resident proteins to stabilise the defected cartilage of the knee

joint. The first generation ACI involves extracting chondrocytes from patient, followed by *in vitro* expansion on culture dishes, and insertion into the patient's damaged cartilage under a grafted periosteum (Moradi et al., 2012). The second generation ACI works similarly to its predecessor, however, instead of grafting the patient's own periosteum as a cartilage patch, it utilises the porcine Type I/III collagen (Chondro-Gide®, Geistlich Pharma) to act as the cellular scaffold (Kon et al., 2011). However, problems arise as cells were disproportionally distributed throughout the native or synthetic periosteal patches in both of generations. Hence, the third generation ACI, or better known as matrix-induced ACI (MACI), was developed to address this concern. This involves growing patient-extracted chondrocytes directly on porcine-derived matrices on cell culture dishes. Following *in vitro* expansion, the cultured scaffold is trimmed according to the area of defect, and it is surgically inserted into the patient. The grafted tissue will subsequently fuse with its surrounding, producing the necessary ECM resident proteins to stabilise the damaged knee cartilage. Importantly, several independent studies showed significant positive clinical outcomes, with most patients reporting improved knee function with reduced pain and swelling (Bartlett et al., 2005; Basad et al., 2015; Gille et al., 2016). Upon 7 years follow up, the reported failure rate of MACI was only 10.7% (Filardo et al., 2014), a remarked enhancement compared to the first generation ACI, which has a failure rate of 33% (Ogura et al., 2017).

In 2010, Go and colleagues demonstrated that decellularised trachea seeded with autologous epithelial and mesenchymal stem cell-derived chondrocytes showed a functional restoration when transplanted into pigs (Go et al., 2010).

However, human surgical transplant of recellularised organs originating from either cardaver or synthetic materials remain controversial, as it was shown to be detrimental for patients (L. Schneider et al., 2022). Nevertheless, allogenic grafts using recellularised cell-derived ECM scaffold show some success in animal models such as rat esophagus (Eftekharzadeh et al., 2022), liver (Yaghoubi et al., 2022), testis (Kargar-Abarghouei et al., 2018), and mouse trachea (Tan et al., 2022).

In *in vitro* studies, acellular scaffolds are used to investigate native ECM structures, as well as understanding the cell-ECM interaction during physiological or pathological events. Hence, dECM characterisation can contribute to the mechanonistics understanding of the bioscaffold dynamics. Kaukonen and colleagues have shown that dECM generated from healthy fibroblasts, but not tumor-associated dECM, blocks cancer proliferation (Kaukonen et al., 2016). Following inspection using atomic force microscopy (AFM), the researchers discovered that acellular scaffold derived from cancerous fibrolasts are significantly stiffer than their healthy counterparts, which is a consistent feature in various cancer cells (Cavo et al., 2016; Reid et al., 2017; Rice et al., 2017). Interestingly, the tumor microenvironment is also implicated in invasiveness and drug resistance (Serebriiskii et al., 2008). The utilisation of dECM improves cancer models by recapitulating native tumor microenvironments using monolayer or complex 3D cultures, or organ-on-a-chip strategies (Gioiella et al., 2016; Hoshiba, 2018; Kargar-Abarghouei et al., 2018). Usage of dECM has also demonstrated that the ECM from highly malignant cultures facilitate epithelial-mesenchymal transition (EMT) and *ABCB1* upregulation, which further enhances chemoresistance

(Hoshiba, 2018), hence, demonstrating the impact of an aberrant ECM on cellular functions.

Thus, bioscaffolds denuded of cells could also be utilised in other field of studies, especially in prion diseases since aberrant PrP conformers are deposited and bind to ECM constituents (Horonchik et al., 2005). This could potentially allow researchers to understand how cells interact with extracellular PrP assemblies within the ECM, including in the context of ECM remodelling whereby cells degrade and release entrapped biocomponents within the extracellular scaffolding.

1.5.2 Decellularisation approaches

There are a multitude of ways to prepare decellularised scaffolds. Cells can either be removed through detergent treatment, enzymatic degradation, mechanical force, or lysis under hypotonic or hypertonic conditions. The objective of decellularisation, as the name implies, is to remove adherent cells from the extracellular scaffold. Decellularisation can be applied on numerous samples including whole organs, tissue sections, organoids, or monolayer cultures. In this section, I will focus on decellularisation techniques that are used on monolayer cells cultured on 2D surfaces, whenever applicable.

Cells can be stripped from the ECM by treating with detergents. There are several types of detergents that are commonly used for decellularisation, with each having its own strengths and weaknesses. For instance, Triton X-100, a non-ionic detergent, is suitable to remove cells from attaching on the

ECM by disrupting the protein-lipid and lipid-lipid interactions, but leaving protein-protein union unperturbed (Cartmell & Dunn, 2000; Woods & Gratzer, 2005). However, it is reported that triton X-100 disrupts GAGs bound within the ECM, hence rendering it less favourable for studies focusing on sulphated proteins (Ren et al., 2013). Ionic detergent such as sodium dodecyl sulphate (SDS) is also efficient in lysing adherent cells. It disrupts the cellular membranes and denature proteins by disrupting hydrophobic interactions in the tertiary structures (Bhuyan, 2010; R. N. Chen et al., 2004; Elder et al., 2010). This will affect studies that wish to use these cell-derived matrices by seeding reporter cells, as a denatured protein will lose its native functionality. On the other hand, zwitterionic detergents such as 3-[(3-cholamidopropyl) dimethylammonio]-1-propane sulfonate (CHAPS) and tri-n-butyl-phosphate (TNBP), are also used for decellularising the extracellular scaffolding. Although zwitterionic detergents do not alter the native state of proteins, it is less efficient in removing scaffold-adherent cells compared to SDS (Du et al., 2011).

Extracellular bioscaffolds can also be generated through enzymatic treatments. One of the most common proteinases used for releasing adherent cells is trypsin. Trypsin cleaves the C-side bonds found in arginine and lysine, and is commonly mixed with EDTA to facilitate breakdown of cell-ECM interactions. However, prolonged treatment using trypsin and EDTA causes a variety of problems including the alteration of the matrix scaffold, removal of laminin, and disruption of GAGs (Rieder et al., 2004). Pepsin is also an alternative enzyme used for generating acellular ECM. However, it was noted that although collagen fibers remained preserved following pepsin

digestion, only 12.9% of GAGs were left post-treatment (C. Schneider et al., 2016). Besides enzymatic approach, cells can be removed from extracellular scaffolds in a harsh tonicity environment. This creates a disruptive osmostic pressure that lyses cells, whilst leaving the ECM unperturbed. Unlike most of decellularisation techniques, hypertonic and hypotonic solution-based decellularisations have little to no effect on the ECM proteome along with effective nuclear waste removal (Bi, Karanth, et al., 2020; Bi, Ye, et al., 2020). In addition, these physical decellularisation technique also preserves the ultrastructure of the extracellular matrix as observed using scanning electron microscopy (Omid et al., 2023).

For whole organs, cells are treated with a solution containing relatively high amounts of NaCl (typically 10%) to induce lysis, followed by incubation and washes using hypotonic solution. Effective nuclear waste removal was also observed, with rates exceeding or comparable efficacies to common detergents used for decellularisation including SDS and Triton X-100 (Bi, Karanth, et al., 2020; Bi, Ye, et al., 2020; Hu et al., 2021). In 2022, Hoshiba and Yunoki conducted a study to compared decellularisation methods using 5 separate chemical treatments (Triton X-100, SDS, EDTA, Tween-20, NH_4OH) and 2 osmotic conditions (Hypotonic shock using water, hypertonic lysis using 1.5 M NaCl in aqueous solution). In monolayer murine NIH313 fibroblasts, all treatments showed efficient decellularisation outcomes, except for Triton X-100 and Tween 20. However, it is reported that hypotonic shock is not efficient in clearing cells from whole organs, hence, the application is limited to mostly monolayer cultures (Hoshiba & Yunoki, 2023). Nevertheless, hypoosmotic lysis is suitable in preparing cell-derived ECM as

it is efficient in removing adherent monolayer cells and does not alter the native state of the ECM (Hoshiba & Yunoki, 2023; Hu et al., 2021). Hence, this is favourable for studies that aim to elucidate the relationship between aberrant ECM with cells, such as prion diseases which contain prion-infected scaffolds (Ben-Zaken et al., 2003; Horonchik et al., 2005; Jeffrey & González, 2007; Marbiah et al., 2014).

1.6 Gene Candidates for ECM remodelling

In the process of selecting genes involved in ECM remodelling, we conducted an extensive literature review on proteins that either directly (ECM-degrading enzymes) or indirectly (proteins influencing ECM-degrading enzymes) contribute to the dismantling of the extracellular scaffold. The final list of genes was meticulously refined by considering their expression levels in our mouse neuroblastoma S7 cells. It is important to note that this particular gene expression data, which was assessed by Marbiah and colleagues (Marbiah et al., 2014), was not included in the published manuscript due to the comprehensive nature of the dataset, where only a subset of genes were highlighted in the study. Among these genes, we focused on those that exhibited relatively high expression levels in our cell model. The selected genes, namely *Adam10, Adam19, Adamts4, Htra2, Hpn, Mmp2, Mmp11, Mmp15, Mmp17,* and *Mmp24*, emerged as viable candidates for our study. We further studied the mRNA's brain regional distribution for each candidate gene, and found all, except for *MMP11*, to be detected in all regions. However, due to the intriguing role of MMP11 in

degrading fibronectin (Fernandez-Garcia et al., 2014), an essential component in prion-resistant cells (Marbiah et al., 2014), *Mmp11* was not omitted from the list.

Gene	mRNA regional distribution in brain	Brain expression clusters (mRNA)
ATP6AP1	Detected in all	Neurons – synaptic function
ADAM10	Detected in all	Oligodendrocytes – mixed function
ADAM19	Detected in all	Neurons – mixed function
ADAMTS4	Detected in all	White matter - myelination
HPN	Detected in all	White matter – signal transduction
HTRA2	Detected in all	Non-specific
MMP2	Detected in all	Macrophages & microglia – Immune response
MMP11	N/A	No clusters assigned
MMP15	Detected in all	Hindbrain – Mixed function
MMP17	Detected in all	Neurons – Mixed function
MMP24	Detected in all	Non-specific

Table 1.3: Human genes encoding for proteins involved in ECM degradation. All selected genes, with the exception of MMP11, are expressed in all brain regions, with mixed expression clusters (RNA). Information was retrieved from Protein Atlas (2023, https://www.proteinatlas.org/)

1.7 Rationale and aims

Albeit there are consistent findings that prions permeate the extracellular mileu, there is a lack of studies that aim to investigate the influence of prion-embedded ECM in infection. ECM remodelling, a process where cells degrade the surrounding extracellular scaffolding, causes the release of sequestered biomaterials such as growth factors and nanovesicles. It is not known whether ECM remodelling causes the release of aberrant PrP conformers that infect susceptible cells. Hence, our aim was to investigate the role of ECM remodelling in prion diseases and its impact on prion infection using a decellularised ECM (dECM) model. Our sub-aims include determining the localisation of prion subgroups (full length or truncated PrP^D) in our cell model, generating dECM that contains infectious extracellular prion aggregates, optimise a highly efficient gene silencing protocol to silence genes encoding for matrix-degrading enzymes, and determine the role of V-ATPases in mediating prion infection via ECM remodelling. We hypothesised that the degradation of the extracellular scaffolding will result in the release of infectious PrP isoforms that infect surrounding cells.

In this body of work, I have successfully generated a decellularised prion-embedded ECM that is highly infectious to S7 cells, a prion-susceptible neuroblastoma subclone. The generated dECM contains abundant full length PrP^D, a marker of extracellular prion aggregates, and ECM resident proteins such as Collagen IV and CSPG4. By silencing genes of reporter cells (cells seeded onto infectious dECM), we showed that the metalloproteases Adam19, Adamts4, and Mmp11 are involved in promoting infection via ECM remodelling. Gene perturbation of V-ATPase, a proton pump involved in

maturing ECM-degrading enzymes, also supports our hypothesis. The results of pharmacological inhibition of V-ATPases corroborated our finding that proton pumps play a role in facilitating infection through degradation of prion-embedded ECM. In the discussion, I have outlined the limitations of the decellularised model along with its results interpretations. Future experiments to further validate and extend the use of the dECM model is discussed in details as well.

Taken together, we have demonstrated the role of ECM remodelling in prion diseases *in vitro*. Our study highlights new therapeutic targets to treat prion infection, namely, the metalloproteases Adam19, Adamts4, and Mmp11, and the proton pump, V-ATPase.

2. Methodology

2.1 Cell culture

2.1.1 Nomenclature

This thesis employs various cell types for different purposes. The S7 cell line was derived from the parental cell line, N2a-PK1 cells (Klohn et al., 2003), which is a mouse neuroblastoma subclone that is susceptible to prion infection. S7 cells are highly susceptible to RML infection, a mouse prion strain. In contrast, iS7 cells were generated by chronically infecting S7 cells with RML brain homogenate using the Scrapie Cell Assay in End Point Format (SCEPA) (**Section 2.3.3**). Throughout this thesis, the word 'infected' is usually introduced prior to the term iS7 to remind the readers that this subclone is the infected counterpart of S7 cells. Additionally, N2a-*Prnp*$^{-/-}$ cells were derived from *Prnp* CRISPR knocked-out mouse neuroblastoma cells and validated by RT-qPCR, as conducted by Dr Juan Ribes from MRC Prion Unit.

2.1.2 Cell maintenance

S7, iS7, and N2a-*Prnp*$^{-/-}$ cells were maintained in Opti-MEM (Gibco™, Thermo Fisher Scientific, #31985-047) supplemented with 10% fetal bovine serum (FBS) (Gibco™, Thermo Fisher Scientific, #10270-106) and 1% penicillin/streptomycin (Merck, #P4333-100ML). Hereinafter, Opti-MEM with its supplementations is referred as 'cell culture medium'. Cells grown in 10-cm or 15 cm petri dishes in cell culture medium were incubated at 37°C with

5% CO_2 and split at 1:10 or 1:20 for 3 days or 4 days incubation, respectively. After 3 or 4 days, cell confluency was assessed using light microscopy. Cells that are 80 to 95% confluent (covering available space) were split for further usage. Cell culture beyond 5 passages were discarded in 10% (v/v) sodium hypochlorite for at least 1 hour at room temperature (RT).

2.1.3 Freezing

Cells in 10- or 15-cm dishes were resuspended in 10 or 20 ml of cell culture medium, respectively. Cell suspension concentration was determined using the Beckmann coulter counter. To achieve a 2x stock concentration of 12 million cells/ml, cells were centrifuged at 300 x g for 4 mins, followed by pellet resuspension with fresh cell culture medium at the appropriate volume. 250 µl of the resuspended cell pellet was added into a cryovial containing 250 µl of cell culture medium supplemented with 12% DMSO. The cryovials were stored in the Frosty™ Freezing (Thermo Fisher Scientific, #5100-0001) container filled with 100% isopropyl alcohol according to the manufacturer's guidelines. Cells were kept at -80°C overnight prior to long-term storage in liquid nitrogen.

2.1.4 Thawing

To thaw cells, frozen iS7, S7, or N2a-*Prnp*$^{-/-}$ cryovials were partially immersed in a clean 37°C water bath for about 2 minutes or until the cells

were visibly thawed. The following steps were done at room temperature unless otherwise indicated. Once cells were thawed, 500 µl of pre-warmed cell culture medium containing Opti-MEM (Gibco™, Thermo Fisher Scientific, #31985-047) supplemented with 10% fetal bovine serum (FBS) (Gibco™, Thermo Fisher Scientific, #10270-106) and 1% penicillin/streptomycin (Merck, #P4333-100ML) was added drop by drop followed by a gentle resuspension and left to stand for 4 mins. An additional 1000 µl of cell culture medium was added slowly and cells were carefully resuspended once. Cells were incubated for 4 minutes and were transferred to a 50 ml falcon tube containing 11 ml of cell culture medium. A 50 ml falcon tube is preferred since smaller falcon tubes (typically 15 ml) has a narrow lumen which increases cross contamination risks through accidental contact with the micropipette's shaft. Cells were then centrifuged for 4 minutes at 300 x g. The supernatant was discarded while leaving the cell pellet intact at the bottom. The cell pellet was then resuspended with 6 ml of cell culture medium. iS7, S7, or N2a-*Prnp*$^{-/-}$ cells were split 1:2 for 3 days or 1:3 for 4 days in a 10 cm dish containing 18 ml cell culture medium and incubated at 37°C with 5% CO_2. The cultured thawed cells were assigned as Passage 0 (P0).

2.1.5 Cell amplification

Cells were amplified whenever cell stocks are running low. To amplify cell culture stocks, a cryovial was thawed according to **Section 2.1.4**. After thawing, cells (P0) were grown to confluency (covering 80 to 95% of the

surface). Cells were split into appropriate amounts of 10 cm dishes (1:10 dilution) or 15 cm dishes (1:3 dilution). A confluent 10 cm dish contains approximately 10 million cells, which estimates a yield of 3x cryovials (3 million cells each), whereas a confluent 15 cm dish contains approximately 25 million cells (generating 7 or 8 cryovials). Cells were frozen as described in **Section 2.1.3**.

2.2 Cell imaging

2.2.1 Cell processing and immunostaining

All of the following steps were done in sterile condition at room temperature (25 ºC), unless otherwise stated. 500 µl of 5 x 10^4 cells/ml were added to each well of an 8-well chamber slides (Thermo Fisher Scientific, #155411PK) and grown for 4 days at 37°C with 5% CO_2 with a half medium change on day 3. Following supernatant removal, cells were fixed with 300 µl of 3.7% PFA in sterile Dulbecco's PBS (DPBS) (Thermo Fisher Scientific, #14190144) for 15 minutes followed by a single wash with DPBS. Cells were permeabilised using acetone (filled to the brim using a Pasteur pipette) for 1 minute in 8-well chamber slides. 'Wash' in this section refers to aspiration of treatment solution, followed by addition of DPBS prior to a secondary aspiration. Following permeabilisation, cells were washed once with DPBS, followed by treatment with or without 300 µl of 3.5 M guanidinium thiocyanate (GTC) in DPBS for 10 minutes. The treated cells were washed for 5x to remove residual GTC, and subsequently incubated with 300 µl/well primary antibody (**Table 2.1**) prepared in antibody diluent containing 25%

Superblock™ (Thermo Fisher Scientific, #37545) and 10% penicillin/streptomycin (Merck, #P4333-100ML) in DPBS with overnight incubation at 4°C. Cells were washed prior to addition of 300 µl/well of secondary antibody (**Table 2.2**) and 4′,6-diamidino-2-phenylindole (DAPI) (Invitrogen, #D1306) at a concentration of 0.5 µg/ml prepared in antibody diluent, and incubated for 2 hours at 37°C, followed by a single wash with DPBS. For storage, 10% penicillin/streptomycin in DPBS were added in copious amounts to prevent microbial growth.

Antibody	Host	Subtype	Company/ Catalogue	Stock conc. (mg/ml)	Application	Dilution
5B2	M	IgG1	Santa Cruz/ sc-47730	0.2	IF	1:500
6D11	M	IgG2a	BioLegend/ 808001	2	IF	1:10,000
AG4	M	IgG2b	TSE Resources Centre/ RC 059	1	WB	1:1000
Col-4	Rb	IgG (poly)	ABD Serotech/ 2150-1470	N/A	IF	1:500
ICSM35	M	IgG2b	MRC Prion Unit/ N/A	3	WB	1:12,000
NG2 (CSPG4)	Rb	IgG (poly)	Merck/ AB5320	0.1	IF	1:500

Table 2.1: Primary antibodies information. All antibodies are monoclonal unless stated as polyclonal (denoted as ‘poly’). Primary antibodies were incubated on cells following cell fixation, permeabilisation, and with or without denaturant treatment as specified in **Section 2.2.2.** Primary antibodies are diluted in antibody diluent containing 25% Superblock™, 10% Penicillin/Streptomycin in DPBS. M = Mouse, Rb = Rabbit, IF = Immunofluorescence, WB = Western blotting, N/A = Not available.

Antibody	Conjugate	Company	Catalogue	Stock conc. (mg/ml)	Application	Dilution
Goat anti-mouse IgG (H+L)	AF488	Jackson	115-545-003	1.25	IF	1:1000
	Rho	Jackson	115-295-003	1.25	IF	1:1000
Goat anti-mouse IgG1	AF488	Jackson	115-545-205	1.25	IF	1:1000
	Rho	Jackson	115-295-205	1.25	IF	1:1000
Goat anti-mouse IgG2a	AF488	Jackson	115-545-206	1.25	IF	1:1000
	Rho	Jackson	115-295-206	1.25	IF	1:1000
Goat anti-mouse IgG2b	AF488	Jackson	115-545-207	1.25	IF	1:1000
	Rho	Jackson	115-295-207	1.25	IF	1:1000
Goat Anti-Mouse	AP	Merck	A2179	1	WB	1:10,000
Goat anti-mouse IgG	AP	Southern Biotech	1030-04	N/A	SCA	1:4000
Horse anti-mouse IgG	AP	Vector Labs	MP-5402	N/A	SCA	1:25
Goat anti-rabbit IgG	AF488	Jackson	111-545-003	1.25	IF	

Table 2.2: Secondary antibodies information. Following primary antibody incubation, cells were washed with DPBS and incubated with secondary antibodies. Primary antibodies are diluted in antibody diluent containing 25% Superblock™, 10% Penicillin/Streptomycin in DPBS. AP = alkaline phosphatase, Rho = Rhodamine Red-X, IF = immunofluorescence, WB = western blotting, SCA = Scrapie Cell Assay.

2.2.2 Confocal imaging

Fluorescence images of processed cells in **Section 2.2.1** were acquired using Zeiss LSM 710 laser-scanning microscope, equipped with a 63x objective (1.4 oil, Plan-Aprochromat) using Immersol 518F Immersion Oil (Thermo Fisher Scientific, #Z4). Cells immunolabelled with Alexa Fluor 488

and Rhodamine Red-X fluorescence were measured using a 460-540 nm and 565-640 nm bandpass filters, respectively, following excitation with an argon laser at 488 nm and a diode-pumped solid state laser at 561 nm, respectively. To image cells at the extracellular matrix, in-focus detection was set to above substrate level, which coincides to basement of cell that is largely devoid of nuclei staining and positive with collagen IV immunolabelling. For z-stack imaging, the extracellular matrix level was arbitrarily denoted as ‘’zero µm’’ as a point of reference, and imaged at elevated z planes with an interval of 0.9 µm. All images were inspected and exported using the ZEN Black software.

2.2.3 Imaging via light microscopy

Image acquisition was performed using Olympus CKX411 equipped with QImaging Micropublisher 5.0 RTV. Confluent cells or decellularised extracellular matrix prepared in 8-well chamber slides (see **Section 2.4.1)** were placed on the stage, followed by in-focus adjustments using the focus knob. Cell images were taken at a 20x magnification, followed by processing using the QCapture-Pro software.

2.3 Quantifying PrP^{Sc} positive cell

2.3.1 Scrapie Cell Assay

The Scrapie Cell Assay is a highly sensitive and rapid technique in quantifying PrP^{Sc} propagation using prion-susceptible murine cells (Klohn et

al., 2003). We adapted and modified this procedure according to our purposes. All of the following steps were done at room temperature unless otherwise stated. S7 cells were seeded at 300 µl/well at the concentration of 5 x 10^4 cells/ml in a 96-well plate (Corning™ Costar™ 96-Well, Thermo Fisher Scientific, #10695951) containing dECM (**Section 2.4.1**) generated from infected iS7 or uninfected S7 cells, or challenged with varying concentrations of diluted 10% w/v brain homogenate from RML-infected or non-infected CD1 mice, followed by 3 to 4 days incubation at 37ºC with 5% CO_2. If reverse transfection (**Section 2.7.2**) is involved, 150 µl of 1.3 x 10^5 cells/ml are added to each well. Upon confluency, cells were split (1:6 for 3 days or 1:8 for 4 days) and collected on activated ELISPOT plates (clear 96-well filter plate, Merck, MAIPS4510). To activate ELISPOT plates, 50% ethanol in dH_20 was added to each well using a Vaccu-Pette (VWR, #612-6021) and incubated for 5 minutes, followed by two washes with PBS. Washing step was done using vacuum manifold aspiration from the base of the plate, followed by the addition of PBS using a Vaccu-Pette and a final aspiration. Following the two washes, approximately 150 µl of PBS were added to each well after the second wash. Cells from confluent 96-well cell culture plates were resuspended (20x clockwise, 20x anticlockwise) and diluted 1:10 using PBS in 0.5 ml 96-deep well plates (Merck, #BR701346-48EA).

For PrP^{Sc} spot revelation, 100 µl of diluted cells were transferred to activated ELISPOT plates, whereas 50 µl were added to a separate plate for hematoxylin staining (total cell quantification). The plates were aspirated, followed by overnight drying and fixation at 50°C. ELISPOT plates were

labelled according to the passage number of the transferred cells. For instance, ELISPOT plates containing cells on passage 3 are labelled as P3. For experiments involving transcriptional silencing (**Section 2.7.2**), P1 ELISPOT plates were collected. Alternatively, infected or mock-infected cells that were not implicated in gene silencing were transferred into ELISPOT plates at P2, P3, and P4. For PrP^{Sc} spot revelation, wells were treated with 60 µl of 1 µg/ml of PK or 10 ug/ml of pronase in lysis buffer (50 mM Tris HCl, pH 8 containing 150 mM NaCl, 0.5% (w/v) sodium deoxycholate and 0.5% (v/v) Triton-X 100) for 1 hour at 37°C, followed by 2 washes with PBS. 3 M of guanidinium thiocyanate (GTC) prepared in 10 mM Tris HCl pH 8.0 was added to each well and incubated for 20 minutes, followed by 8x washes with PBS. The wells were then blocked for 1 hour using Superblock™ solution (Thermo Fisher Scientific, #37545) filter sterilised in ddH_20. After blocking, wells were aspirated and the back-plastic cover of the plate was removed. The wells were incubated with 6D11 or 5B2 diluted in 1:10,000 or 1:500, respectively, in 2% (w/v) non-fat dry milk in TBS-Tween 20 (TBS-T) for 1 hour. TBS-T was acquired by diluting 20x TBS-T (Thermo Fisher Scientific, #28360) into a 1x working concentration in ddH_20.

All washing steps herewithin were done manually, where supernatant was removed by inverting and tapping the plates, followed by the addition of washing solution using a vacuupette, and discarded mechanically as stated earlier. Wells were washed 5x using TBS-T and further incubated with mouse alkaline phosphatase-conjugated anti-IgG (Southern Biotech, #1030-04) diluted 1:4000 in TBS-T containing 2% (w/v) non-fat dry milk for 6D11-labelled samples. For 5B2 immunostained wells, 1:20 of ImmPRESS-AP and

1:20 of 2.5% Normal Horse Serum (both acquired from antibody IgG-AP ImmPRESS kit (Vector Laboratories, #MP-5402)) diluted in TBS-T containing 2% (w/v) non-fat dry milk were added onto the treated samples and incubated for 1 hour. Wells were subjected to 5x washes using TBS-T, followed by incubation for 35 min with 60 µl AP dye/well (Bio-Rad, #1706432). The plates were then washed twice with dH20, dried and stored at 4°C or scanned immediately. Spot counts (reporting PK-resistant PrP-positive cells; see below) were determined with a Zeiss KS ELISPOT system (Stemi 2000-C stereo microscope equipped with a Hitachi HV-C20A color camera, a KL 1500 LCD scanner and Bioreader 5000-Eß system (BioSys, Karben, Germany).

2.3.2 Generation of chronically infected cell line

Chronically prion-infected iS7 cells used in this thesis was generated using the SCEPA (Scrapie Cell Assay in End Point Format) protocol, which was adapted and modified from Mahal and colleagues (Mahal et al., 2008). The infected cells were generated either through exposure of RML brain homogenate or infectious dECM. To produce chronically infected iS7 cells, 300 µl/well of 5 x 10^4 S7 cells/ml were seeded onto 12 wells of a 96-well plate (Corning™ Costar™ 96-Well, Thermo Fisher Scientific, #10695951) and incubated for 16 hours at 37°C with 5% CO_2. Cells were then infected with 3.3 x 10^{-4} dilution of RML brain homogenate or mock-infected with DPBS as control. To generate dECM-infected cells, reporter S7 cells with the

same volume and concentration were seeded onto infectious or non-infectious scaffolds (**Section 2.4.1**).

Cells that were either challenged with brain homogenate or dECM were grown to confluency, followed by a 1:3 split for every two days following a half medium change, for a total of 3 passages. In the 3 consecutive splits, wells were expanded into 24, 48, and finally 96 wells, covering the whole cell culture plate for each group. Next, cells were either passaged onto a 96 well plate with a 1:5 or 1:8 split for 3 or 4 days, or harvested into 10 cm dishes by transferring triturated 18 wells into a 10 cm dish containing 18 ml of cell culture medium. The cell culture dish was expanded into a 15 cm dish containing 40 ml of medium by splitting cells 1:3 for 3 days or 1:4 for 4 days incubation and used for inoculum preparation (**Section 2.5**), or expansion (**Section 2.1.5**) and subsequently freezing (**Section 2.1.3**). 96-well plates were serially passaged to obtain Passage 4, 5, and 6, followed by to spot revelation as described in **Section 2.3.1.**

2.4 Decellularised ECM

2.4.1 Decellularisation process

Decellularisation on a 2D plane is a process where cells grown on a surface are removed, leaving a layer of extracellular deposits. We employ a method which decellularise cells through hypoosmotic shock. All steps were done in sterile conditions. Briefly, 300 or 500 µl/well of infected iS7 or uninfected S7 cells were seeded down onto 96-well format plates including 96-well cell culture (Corning™ Costar™ 96-Well, Thermo Fisher Scientific, #10695951)

and ELISPOT plates (clear 96-well filter plate, Merck, MAIPS4510), or 8-well chamber slides (Thermo Fisher Scientific, #155411PK), respectively, at a concentration of 5 x 10^4 cells/ml in OPTI-MEM supplemented with 10% FBS (Gibco™, Thermo Fisher Scientific, #10270-106) and 1% Penicillin/streptomycin (Merck, #P4333-100ML) and incubated for 5 days. Cultured cells were subjected to a half fresh medium change on days 3 and 4 to avoid cell starvation.

On day 5, supernatant was aspirated and 300 or 500 µl/well of sterile distilled water (dH_2O) (Thermo Fisher Scientific, #15230204) was carefully added to 96-well format plates or 8-well chamber slides, followed by 15 minutes incubation at room temperature. Cells undergo three successive washes with copious amounts of sterile dH_2O, including a gentle resuspension in the third wash to remove remaining cell debri adhered to the surface. Following aspiration of supernatant, the generated dECM can be used immediately for downstream applications including immunocytochemistry (**Section 2.2.1** & **2.2.2**) or infection (**Section 2.4.2**), or stored at 4°C up to 1 week with 10% penicillin/streptomycin in DPBS.

2.4.2 Infection of cells on dECM

Since infectious extracellular scaffolding were generated *in situ*, reporter cells are to be seeded onto this layer for infection. Briefly, 300 µl/well of 5 x 10^4 uninfected S7 (reporter) cells prepared in cell culture medium comprising of OPTI-MEM supplemented with 10% FBS (Gibco™, Thermo Fisher Scientific, #10270-106) and 1% Penicillin/streptomycin (Merck, #P4333-

100ML) were seeded on 96-well culture plates (Corning™ Costar™ 96-Well, Thermo Fisher Scientific, #10695951) containing dECM generated from infected iS7 cells or uninfected cells (negative control) and incubated for 4 days at 37°C with 5% CO_2. Half fresh medium change was conducted on day 3. Cells were then subjected to serial passages and ELISPOT plate collections at Passage 2 (P2), P3, and P4 as explained **Section 2.3.1**. The collected ELISPOT plates were subjected to PrP^{Sc} spot count revelation using the Scrapie Cell Assay as specified in **Section 2.3.2.**

2.4.2.1 Cell viability assay

Cell viability was measured using the CellTiter-Glo® Luminescent Cell Viability Assay that detects metabolically active cells by quantitating the amount of ATP present. Briefly, 300 µl of 5 $x10^4$ cells/ml prepared in cell culture medium containing Opti-MEM (Gibco™, Thermo Fisher Scientific, #31985-047) supplemented with 10% fetal bovine serum (FBS) (Gibco™, Thermo Fisher Scientific, #10270-106) and 1% penicillin/streptomycin (Merck, #P4333-100ML), was added to wells containing infectious or non-infectious dECM prepared from infected iS7 or uninfected S7 cells (**Section 2.4.1**), respectively, or without dECM. In parallel, the same amount and concentration of cells were seeded down, with the addition of diluted 10% (w/v) RML or uninfected CD1 brain homogenate: 1 x 10^{-2}, 1 x 10^{-3}, 1 x 10^{-4}, 1 x 10^{-5}. Following 16h incubation at 37°C, cells were processed as per manufacturer's instructions (CellTiter-Glo® Luminescent Cell Viability Assay

manual) and luminescence signals were read using the Tecan Infinite Pro 200.

2.4.3 Probing for PrP^D internalisation

Decellularised infected iS7 or uninfected S7 cells were prepared in 8-well chamber slides (Thermo Fisher Scientific, #155411PK) according to **Section 2.9.1.** 500 µl/well of N2a-*Prnp*$^{-/-}$ cells were seeded at a concentration of 2, 1.5, or 1.25 x 10^5 cells/ml and incubated for 8, 16, or 24 h, respectively, at 37°C with 5% CO_2. Cells were processed according to **Section 2.2.1** with minor modifications. Briefly, reporter cells were fixed using 3.7% PFA in DPBS (Thermo Fisher Scientific, #14190144) and washed once with DPBS. Fixed cells were permeabilised using acetone for 1 minute, and washed with DPBS. Cells were treated with 3.5 M GTC for 10 mins, followed by 5x washes with DPBS.

To asses for PrP^D uptake, cells were incubated with CellMask™ Deep Red Plasma Membrane Stain (Thermo Fisher Scientific, #C10046) diluted 1:1000 for 10 mins, and consequently washed with DPBS. Cells were subsequently immunolabeled with anti-PrP antibody 6D11, washed with DPBS, and stained with Alexa Fluor 488 Goat anti-mouse igG2A and DAPI as described in **Section 2.2.1** and imaged according to **Section 2.2.2** with several amendments for scoring purposes.

Briefly, presence of 6D11-positive signals (signifying aggregated PrP uptake) was assessed through live scanning using Zeiss LSM 710. Scanning was performed above the extracellular matrix level (absence of dECM 6D11-

signals and presence of relatively weak DAPI positivity), denoted as 0 µm on the z-plane, and up until 30 µm (height of processed N2a-*Prnp*$^{-/-}$ cells is approximately 20 µm). Image acquisitions of 6D11, CellMask^{TM}, and DAPI fluorescence were taken (refer to **Section 2.2.2**) whenever a live scan displayed 6D11 positivity, which essentially means an imaging area may contain several images from different Z-planes. This was performed in such a way due to the presence of internalised PrP aggregates on different planes. A total of 10 areas were imaged with varying Z-plane image acquisitions, which represents a field of view. A total of 3 field of views were taken for scoring. Scoring was done by counting reporter cells that contain internalised PrP^{D} (6D11 positivity within cell boundary, depicted by CellMask^{TM} staining), membrane-bound PrP^{D} (6D11 signal within CellMask^{TM} staining or on the outer cell surface boundary), both internalised and membrane-bound PrP^{D}, or absence of PrP^{D} (negative of 6D11 immunofluorescence).

2.4.4 Assessing PrP^{D} truncation activity

To study the endogenous proteolytic cleavage of internalised aberrant PrP aggregates, the experimental setup was prepared as described in **Section 2.4.3** up until the step involving 5x washes with DPBS following GTC treatment. Following steps can be referred to **Section 2.2.1.** Briefly, processed reporter N2a-*Prnp*$^{-/-}$ cells were then incubated with anti-PrP antibodies 6D11 and 5B2 (**Table 2.1**) overnight at 4ºC, at 1:10,000 and 1:500 dilution, respectively. Samples were washed with DPBS and incubated

with goat anti-mouse AF488 IgG1 and Rhodamine IgG2a (**Table 2.2**) for 2 hours at 37 ºC, with a 1:1000 dilution each. Cells were washed with DPBS and added with 10% penicillin/streptomycin in DPBS. Immunocolocalisation of 6D11-positive PrP^D uptake was screened using the live scanning mode as mentioned in **Section 2.4.3.** Whenever 6D11-signals appeared on the live scan display, image acquisition of 4 channels involving 6D11, 5B2, and DAPI-staining, as well as bright-field imaging was performed. 5 random fields were screened, and representative images were taken as specified in **Section 2.2.2**.

2.4.5 Investigating the relationship of prion conformation and infectivity

The conformation-dependent immunoassay (CDI) was adapted and modified from Safar and colleagues (J. Safar et al., 1998). All steps were conducted at room temperature unless otherwise indicated. The dECM from infected iS7 or uninfected S7 cells were prepared according to **Section 2.4.1** in 8-well chamber slides (Thermo Fisher Scientific, #155411PK)**.** The acellular scaffolds were fixed using 300 µl/well of 3.7% PFA in DPBS for 15 mins, followed by washing with DPBS. Washing constitutes aspirating supernatant, followed by filling the well to the brim with DPBS, and lastly a final aspiration. After washing, 300 µl/well of 0, 0.5, 1, 1.5, 2, 2.5, 3, or 3.5 M of GTC prepared in DPBS was incubated in respective wells for 10 mins, and subsequently washed for 5x with DPBS. Processed dECM samples were subjected to immunostaining using 6D11 and 5B2 along with secondary antibodies IgG2a Rhodamine and IgG1 AF488 as specified in **Section 2.2.1.**

To test for infectivity of GTC-treated infectious or non-infectious control dECM, acellular scaffolds derived from iS7 or S7 cells were prepared on 96-well plates (Corning™ Costar™ 96-Well, Thermo Fisher Scientific, #10695951) according to **Section 2.4.1.** The prepared dECM was treated with differing concentrations of GTC as mentioned earlier in this section, followed by 5x washes with DPBS. Each dECM-containing well was seeded with 300 µl of 5 x 10^4 cells/ml of reporter S7 cells. Cells were subjected to the SCA as mentioned in **Section 2.3.1.**

2.5 Mouse inoculation using dECM-infected cells

All procedures involving live animals were performed under approval and licence granted by the UK Home Office Act 1986; Project Licence number: PP3260075, and in compliance to University College London institutional and Animal Research: Reporting of *In Vivo* Experiment (ARRIVE) guidelines. Wild type FVB mice, aged between 6 – 8 weeks, were housed individually in cages with ventilation and 12 h light/dark cycle. Food and water were provided *ad libitum*.

To prepare cell inoculum, reporter S7 cells were chronically infected or mock-infected on acellular scaffolds derived from iS7 or S7 cells (**Section 2.4.1**) using the SCEPA-end format (**Section 2.3.3**), respectively. The dECM-infected or mock infected reporter cells, as well as chronically infected iS7 cells (refer to **Section 2.1.1**) were subsequently expanded onto several 15-cm dishes and grown to confluency. The plates were placed on ice for 5 minutes, followed by supernatant removal and two gentle washes with 15 ml

of pre-cooled DPBS (4°C) twice. Following the second wash, the cells were resuspended with 25 ml of cold PBS and the 15 cm culture plates were pooled according to the infected or mock-infected cell group. Cells were counted with the Beckmann Coulter Counter and centrifuged at 300 x g for 5 mins at 4°C. The resulting pellet was diluted in cold PBS to obtain a concentration of 1.5 $x10^7$ of cells/ml. Benzonase (25-29 U/µl, Merck, #71205) was added to the cell suspension at a 1:250 dilution (4 µl/ml). Protease inhibitor (-EDTA) was added to the mixture at 1:100 dilution. The mixture was snap frozen with dry ice, prior to storing at -80°C. The cell lysates were then thawed on ice to achieve a complete freeze-thaw cycle. Samples were subjected to a total of 3 freeze-thaw cycles prior to inoculation. 30 µl of infected iS7, dECM-infected or mock-infected reporter cell lysates were inoculated intracerebrally into groups of wild type FVB mice (n=4). Humane endpoint culls were performed following two early indicators and one confirmatory sign, or two confirmatory signs based on the ‘’Scrapie Diagnostic Criteria’’ in protocol 9, PPL (PP3260075), as described in **Table 2.3**. All surviving animals were kept up until 300 days post-inoculation, which were then culled by competent staff at the BSF of MRC Prion Unit, University College London.

Scrapie diagnostic criteria	Observation
Early indicators	Piloerection
	Intermittent generalised tremor
	Penile erection
	Clasping hind legs when lifted by tail
	Rigid tail
	Unsustaine hunched posture
	Mild loss of coordination
Confirmatory signs	Ataxia
	Impairment of righting reflex
	Dragging of hind limbs
	Sustained hunched posture
	Significant abnormal breathing

Table 2.3: Determination of scrapie sick mice. Confirmation of prion disease in mice is based on the presence of two early indicators and one confirmatory sign, or two confirmatory signs observed by competent staff in the BSF. When these criterias are met, the programme leader will be contacted and the animal will be euthanised in allignment to the University College London institutional and ARRIVE guidelines. This stringent protocol underscores ethical compliance and the precise identification of prion-infected mice.

2.6 Pharmacological inhibitors treatment *in vitro*

S7 cells in cell culture medium containing Opti-MEM (Gibco™, Thermo Fisher Scientific, #31985-047) supplemented with 10% fetal bovine serum (FBS) (Gibco™, Thermo Fisher Scientific, #10270-106) and 1% penicillin/streptomycin (Merck, #P4333-100ML) were seeded 300 µl/well in a

96-well plate (Corning™ Costar™ 96-Well, Thermo Fisher Scientific, #10695951) at a density of 5 x 10^4 cells/ml. Cells were incubated for 3 days at 37°C with 5% CO_2. Bafilomycin A1 (Baf A1) stock at 1 mM was mixed with equal volumes with dimethyl sulfoxide (DMSO) to produce 500 µM Baf A1. The prepared solution was subjected to serial dilutions (1:2) in DMSO to obtain several concentrations: 250, 125, 62.5 and 31.3 uM. All prepared concentrations were further diluted 1:1000 in cell culture medium. The supernatant from 96-well plate containing confluent S7 cells prepared earlier was replaced by the newly prepared Baf A1 solutions (500, 250, 125, 62.5, 31.3, 15.1 nM) at 300 µl/well with each concentration covering a single row (12 wells) of the plate. The last two remaining rows were added with 300 µl/well of DMSO diluted 1:1000 in cell culture medium, which was denoted as 0 nM Baf A1. Cells were incubated for 2 hours at 37ºC following Baf A1 (500, 250, 125, 62.5, 31.3, 15.1 or 0 nM). The supernatant was removed and cells were washed once with 300 µl/well of cell culture medium, followed by the addition of fresh cell culture medium with the same volume.

The treated cells were split 1:3 into a 96-well cell culture plate containing infectious dECM (refer to **Section 2.4.1**), which was assigned as Passage 0. Following 1 day incubation at 37ºC with 5% CO_2, cells were inspected using an inverted light microscope to observe any morphological changes following Baf A1 treatment. Due to the physical changes observed such as lack of synapses and shape abnormality in cells treated with 500 nM Baf A1, analysis regarding treatment efficacy for this concentration was excluded. Cells undergo a half medium change, in which 150 µl of supernatant is replaced by 150 µl of fresh medium, followed by incubation at 37ºC with 5%

CO_2 for another 24h. Cells were serially passaged and ELISPOT plates were collected at P2, P3, and P4, as described in **Section 2.3.1**.

2.7 Screening for relevant genes in modulating ECM infectivity

2.7.1 Optimising gene silencing approach

To develop a gene silencing protocol for cells infected on decellularised ECM, several procedures were tested. Briefly, we tested 6 protocols: 3D-Std, 3D-Mod-1H, 3D-Mod-2H, 4D-Std, 4D-Mod-1H, and 4D-Mod-2H. 3D or 4D found in the beginning of the protocol's title indicate the total number of days of the entire transfection protocol prior to serial passages. The protocol code (Std = standard, Mod-1H = modified, single hit/transfection, Mod-2H = modified, double hit/transfection) comes after the prefix 3D or 4D. For Std, the 150 µl/well of 1.3 x 10^5 reporter uninfected S7 cells were seeded into 96-well plates containing infectious dECM (**Section 2.4.1**) and reverse transfected with 150 µl of cell culture medium containing *Prnp* siRNA-lipofactemine complex (**Section 2.7.2**). Cells were either incubated for 3 (3D-Std) or 4 (4D-Std) days at 37°C with 5% CO_2. In Mod=1H, 150 µl/well of 1.3 x 10^5 reporter uninfected S7 cells were seeded in wells containing 150 µl of *Prnp* siRNA-lipofectamine mixture. Following one day incubation at 37°C with 5% CO_2, cells were resuspended and transferred onto wells containing infectious dECM. Cells were incubated for another 2 or 3 days (3D-Mod-1H or 4D-Mod-2H, respectively) for 37°C with 5% CO_2. Mod-2H is similar to Mod-1H, with the exception of reverse transfected cells were transferred onto

infectious dECM containing pools of *Prnp* siRNA-lipofectamine complex, thus, administering a second gene silencing dose.

2.7.2 Gene silencing standard protocol

As the 4D-Std method was the gene silencing protocol of choice (refer to **Section 2.7.1** & **3.13**)**.** I have re-written it in this section to allow readers to understand the protocol on its own (without comparison to other tested protocols in **Section 2.7.1**) All steps were performed at room temperature unless otherwise indicated. Briefly, siRNA pools (siPOOL^{TM}, siTOOLs Biotech Gmbh) were reconstituted with nuclease-free water to a stock concentration of 10 µM. siPOOL^{TM} are highly complex and defined pools of 30 siRNAs which target different regions in the same gene. Each siRNA is present at picomolar working concentrations, which diminishes off-target signatures while elevating on-target specificity (Hannus et al., 2014). 4 µl of siRNA (siPOOL, siTOOLs Biotech GmbH) for each gene target shown in **Table 2.4** and an additional of 4 µl of siRNA if double-knockdown was administered, and 12 µl of RNAimax transfection reagent (Thermo Fisher Scientific, #13778150) were added to 34 µl (single knockdown) or 30 µl (double knockdown) of OPTIMEM without supplementations and incubated for 5 minutes following a 30 sec mixing on a vortex. After 5 mins, 1950 µl of cell culture medium containing Opti-MEM (Gibco^{TM}, Thermo Fisher Scientific, #31985-047) supplemented with 10% fetal bovine serum (FBS) (Gibco^{TM}, Thermo Fisher Scientific, #10270-106) and 1% penicillin/streptomycin (Merck, #P4333-100ML) was mixed with the 50 µl siRNA-lipofectamine

complex, and 150 µl of the mixture was added to each of 12 wells containing infectious dECM (**Section 2.4.1**). For non-silencing controls, 22 wells were used. Reporter uninfected S7 cells were seeded onto wells containing siRNA-lipofectamine complex and infectious dECM at a density of 1.3 $x10^5$ cells/ml with a volume of 150 µl/well. Cells were incubated for a total of 4 days at 37°C with 5% CO_2. Following incubation, cells were subjected to serial passages and ELISPOT plate collection and infectivity was determined by Scrapie Cell Assay (**Section 2.3.1**).

Target	Gene ID	Application
Atp6ap1	54411	Gene KD, RT-qPCR
Adam10	11487	Gene KD, RT-qPCR
Adam19	11492	Gene KD, RT-qPCR
Adamts4	240913	Gene KD, RT-qPCR
Hpn	15451	Gene KD, RT-qPCR
Htra2	67404	Gene KD, RT-qPCR
Mmp2	17390	Gene KD, RT-qPCR
Mmp11	17385	Gene KD, RT-qPCR
Mmp15	17388	Gene KD, RT-qPCR
Mmp17	23948	Gene KD, RT-qPCR
Mmp24	17391	Gene KD, RT-qPCR
Prnp	19122	Gene KD, RT-qPCR
Gapdh	14433	RT-qPCR
Actb	11461	RT-qPCR

Table 2.4: List of gene candidates involved in gene knockdown and/or RT-qPCR. The gene ID shown in the table were referenced to the suppliers for siRNA provided by SiTOOLS Biotech Gmbh and/or lyophilised primers acquired from Qiagen for gene expression analysis. Gene KD = Gene Knockdown, RT-qPCR = reverse transcription quantitative polymerase chain reaction.

2.7.3 Determine siRNA knockdown efficacies

To determine gene knockdown efficiencies, reverse transcription quantitative polymerase chain reaction (RT-qPCR) was employed. RT-qPCR was mostly performed by Mitali Patel based in the MRC Prion Unit. Following 72 hours of transfection of cells with siRNA-Lipofectamine complex (siPOOL, siTOOLs Biotech GmbH) (**Section 2.7.2**) and a non-targeting control, total RNA was isolated using Direct-zol RNA Mini-prep kit (Cambridge Bioscience, #R2050).

Briefly, the supernatant of siRNA-treated cells was aspirated, followed by a gentle rinse using DPBS. Cells lysates were prepared by resuspending cells using appropriate volume of TRI Reagent. To remove particulate debris from homogenised cells, samples were centrifuged briefly and the resulting supernatant was transferred into a new nuclease-free tube. Equal volumes of ethanol (95% - 100%) was added and mix thoroughly. The mixture was transferred into the Zymo-Spin Column and centrifuged. All centrifugation steps were performed at 16,000 x g for 1 minute, unless otherwise specified. Samples retained on the membrane were treated using DNase I for 15 minutes at room temperature, while the flowthrough was discarded. Washes were performed by adding 400 µl of Direct-zol™ RNA pre wash to the column, followed by centrifugation. The flow-through was discarded, and the washing step was repeated. The final wash was done by adding 700 µl of

RNA Wash Buffer to the column and centrifuged to ensure complete removal of wash buffer. The column was transferred into an RNase-free tube. To elute RNA, 50 µl of DNase/RNase-free water was added to the column matrix and centrifuged.

To assess purity and concentration of isolated RNA material, absorbance was read at 260 nm and 280 nm using the Nanodrop 2000 Spectrophotometer. A260/A280 ratio that was lower than 2.1 was omitted from further analysis. Total RNA (500 ng) was used to synthesise the first strand complementary DNA (cDNA) using QuantiTect Reverse Transcription kit (Qiagen, #205311). Briefly, gDNA elimination step was carried out on ice by mixing 2 µl of gDNA Wipeout Buffer, RNase-free water and up to 500 ng of RNA in a total volume of 14 µl for 2 mins at 42ºC. Reverse-transcription master mix was prepared on ice by adding 4 µl of Quantiscript RT Buffer, 1 µl of RT Primer Mix and 1 µl of Quantiscript Reverse Transcriptase. This was then added to the entire genomic DNA elimination reaction. Samples were incubated for 30 min at 42ºC and a further 3 min at 95ºC to inactivate the transcriptase. Control reactions were established with both no Reverse Transcriptase and no RNA template to monitor potential contaminations in RT-qPCR.

For the RT-qPCR assay, all reaction cycles were performed in triplicates along with ddH_2O control and the controls used during the transcriptase reaction. The assay was performed with QuantStudio 12K Flex (Applied Biosystems) with the following cycling parameters: 50°C, 2 mins; 94°C, 15 min; 40 cycles at 94°C, 15s; 60°C, 1 min. Samples were prepared in triplicates in 10 µl reactions containing QuantiTect SYBR Green (Qiagen), 1x

QuantiTect customised Primer Assay (lyophilized in TE buffer, pH 8.0) which was purchased according to the respective Gene IDs shown in **Table 2.4**, 25 ng of cDNA made to a final volume with ddH_20. To normalise target gene expression levels, housekeeping genes *Gapdh* and *Actb* were used as endogenous controls. At the end of the run, fluorescent signal was acquired to determine the expression of mRNA by evaluating threshold cycle (CT) values.

2.8 Assessment of cellular PrP^D truncation

2.8.1 Preparation of cell lysates

Uninfected S7 or infected iS7 cells were thawed (**Section 2.1.4**) and grown to confluence in 10 cm dishes. The dishes were placed on icy cold water to minimise endogenous proteolytic activities. Cell supernatant was aspirated, followed by two gentle washes with sterile DPBS (Thermo Fisher Scientific, #14190144). DPBS was aspirated and 1 ml of fresh cold RIPA buffer (50 mM Tris, 150 mM NaCl, 0.5% sodium deoxycholate, 1% Triton (v/v), benzonase (25-29 U/µl). Plates were tilted to allow the even spread of RIPA buffer on the surface, and tilted again every 5 minutes for a total of 4 times. Lysates of the same group from different plates were pooled together and mixed adequately. Lysates were subjected to BCA to determine total protein concentration prior to storage at -80°C.

2.8.2 Bicinchoninic acid assay (BCA)

Prior to loading cell lysates for electrophoresis, protein concentration was determined using BCA assay. Briefly, cell lysates prepared in (**Section 2.8.1**) was mixed with RIPA buffer in three dilutions; 1:25, 1:100, and 1:400. 25 µl of diluted samples were added into Nunc Maxisorp 96-well plates (Thermo Fisher Scientific, #44-2404-21) in triplicates. Bovine serum albumin (BSA) standards were prepared by diluting BSA in RIPA buffer at 1000, 800, 600, 400, 200, 100, 50, and 0 µg/ml and loaded at 25 µl/well in triplicates. RIPA buffer was used as blank. To quantify protein concentration of samples, the absorbance signal was read at 562 nm using the Tecan Infinite Pro 200 and compared to the known concentration of the BSA standards.

2.8.3 Western blot

Cell lysates were either treated with a final concentration of 10 µg/ml of proteinase-K (PK) (Roche, #3115887001) or pronase (Merck, # P5147), or mock-treated with DPBS (control) (Thermo Fisher Scientific, #14190144) for 30 minutes at 37°C. To stop proteolytic digestion, PK-treated or pronase-treated samples were treated with a final concentration of 1 mM of AEBSF (Thermo Fisher Scientific, #78431) or 10 mM of EDTA (Invitrogen, #15575-038), respectively. DPBS of the same volume as AEBSF or EDTA introduced in the experimental samples was added to the control group. Samples were further diluted in DPBS and mixed with equal volumes of 2x Sample Buffer (Thermo Fisher Scientific, #LC2676) containing 4% β-mercaptoethanol (BME) (Merck, #M6250) to achieve a concentration of 50 µg / 35 µL.

Samples were boiled at 100°C using a thermoblock for 10 mins. Samples were briefly centrifuged at 1000 x g for 30 sec to pool droplets formed on the inner lid after boiling. 35 µL of the prepared samples were loaded to the designated wells of a 12% bis/tris gel (Thermo Scientific, #NP0341BOX). Electrophoresis was done at 200 V for 80 mins, prior to transfer using a PVDF transfer membrane (Thermo Fisher Scientific, # 88518) at 15 V overnight. The blotted membranes were collected and blocked using 5% (w/v) non-fat milk in PBS-T (PBS containing 0.05% Tween-20) for 1 hour. Blots were incubated with 0.25 µg/ml of ICSM35 or 1 µg/ml of AG4 (**Table 2.1**) diluted in 5% (w/v) non-fat milk in PBS-T. After washing (3x consecutive washes followed by 3 washes with 15 mins interval), and incubated with a 1:10,000 dilution of alkaline-phosphatase-conjugated goat anti-mouse IgG secondary antibody (Merck, #A2179) (**Table 2.2.**) in PBST. The blots were washed with PBS-T as mentioned and further washed twice for 2 mins each with Activation Buffer (20 mM Tris (pH 9.8) + 1 mM $MgCl_2$) to achieve optimum pH for alkaline phosphatase activity. Blots were incubated for 5 mins in chemiluminescent substrate (CDP-Star; Tropix Inc) and visualized on Biomax MR film (Kodak).

2.9 Statistics

Data was analysed using Graphpad Instat 3.10 and Microsoft Excel. The Kolmogorov-Smirnov test was applied to test whether experimental data were normally distributed. Normally distributed data was analysed by parametric tests, including Student's t-test and Analysis of variance (ANOVA) followed by post-hoc Bonferroni test. In case of small sample sizes (<12) or data that did not fit the normal distribution, Kruskal Wallis and Mann Whitney U test were employed, followed by the Dunn's multiple range test. Unless otherwise stated, a p-value <0.01 was considered statistically significant.

3. Results

3.1 Rationale

There is an array of proteases involved in the degradation and remodelling of the extracellular matrix (ECM) under physiological and pathological conditions (Lu et al., 2011). To put matters into perspective, we are intrigued in understanding the implications of remodelling prion-infected ECM. ECM disintegration is a biological process that involves proteolytic degradation of ECM-resident proteins including collagen and fibronectin. Following degradation, the deconstructed scaffold releases sequestered growth factors and matrix-bound vesicles into the interstitial space, thus, interacting with nearby cells. Extracellular prion aggregates originating from the membrane, are embedded into the ECM. Hence, this study focuses on the role of proteases in controlling extracellular prion infection. We approached this matter by developing a protocol that generates infectious cell-free scaffolding, and utilised a highly efficient gene perturbation technique that removes selected endogenous proteases from reporter cells. The outcome of this study will give us a new perspective on the role of proteases in controlling prion infection, and potentially provide new therapeutic targets against prion diseases.

3.2 Protease resistance profile of full length PrP^D

In prion diseases, PrP^D can be found intra- and extracellularly (Rouvinski et al., 2014). Intracellular PrP^D is N-terminally truncated, however, the cleavage site is thought to be dependent on the prion strain (Bessen & Marsh, 1992;

Notari et al., 2008). On the other hand, non-intracellular PrP^D aggregates colocalise with cell membranes and the extracellular space (Jeffrey et al., 2011). In this study, we are interested in understanding the infectivity of extracellular PrP^D scaffolds. We aim to generate a decellularised extracellular matrix (dECM) model embedded with extracellular PrP^D amyloids and investigate the role of proteases in releasing infection from these cell-free matrices. We selected a set of genes that code for proteinases that are directly or indirectly involved in degrading ECM, potentially mobilising extracellular PrP^D.

As mentioned, full length PrP^D is exclusively formed extracellularly, making it a reliable marker to detect extracellular PrP^D in the ECM. Antibodies against the unstructured N-terminus of PrP^D could be used as a tool to further investigate the intricacies of extracellular prions. Presently, there is a lack of evidence that confirms N-terminal anti-PrP antibodies bind to full-length but not to N-terminally truncated PrP^D. The main reason is the commonality of using Proteinase K (PK) treatment to detect PrP^{Sc}. PK is an enzyme that digests the N-terminal region of PrP^{Sc} and completely digests PrP^C, hence, rendering detection of full length PrP^D futile. For our purposes, we use pronase, a multiproteolytic agent that destroys PrP^C but unlike PK, it does not digest the flexible tail as well as the resistance core, leaving the whole molecule intact (D'Castro et al., 2010). This enabled us to validate detection of exclusively full-length PrP^D using anti-PrP antibodies targeting the unstructured N-terminus.

The epitopes of the anti-PrP antibodies used for western blot, AG4 and ICSM35, are shown in **Figure 3.1 A**, along with 5B2 and 6D11 which were

used in immunocytochemistry. Since PrP^{Sc} is partially resistant to proteases, we first determined the appropriate concentration of PK or pronase treatment to avoid over digestion. We used ICSM35 as it detects both full length and truncated PrP^{Sc}. The working concentration for both PK (**Figure 3.1 B**) and pronase (**Figure 3.1 C**) was 10 µg/ml each, a concentration that digests PrP^{C} signal completely whilst retaining PrP^{Sc} signal.

We then treated uninfected S7 or infected iS7 lysates with either PBS (mock control), or pronase or PK at 10 µg/ml prior to electrophoresis. The outcome of treated samples immunolabelled with ICSM35 (**Figure 3.1 D**) were as expected; Pronase-treated infected sample retains high molecular weights of resistant material similar to that of PBS-treated infected lysate, however, no signal was seen in PBS-treated uninfected sample, suggesting complete digestion of PrP^{C}.

PK digestion cleaves the protease-sensitive N-terminus, leaving the resistant core fragments of un-, mono-, and diglycosylated PrP^{Sc} unperturbed. Interestingly, AG4, an anti-PrP antibody against the N-terminus, binds to only high molecular weight of PrP^{Sc} in pronase-treated infected lysate, but not in pronase-treated uninfected control (**Figure 3.1 D**). AG4 did not detect PK-treated infectious sample, which confirms the digestion of sensitive N-terminus in PrP^{Sc}. Taken together, we demonstrated that anti-PrP antibodies against the N-terminus are able to detect full-length PrP^{D} but not truncated PrP^{D}. A separate N-term anti-PrP antibody, 5B2, was used for further validation and experimentations to confirm the presence of extracellular PrP^{D} assemblies in our dECM model.

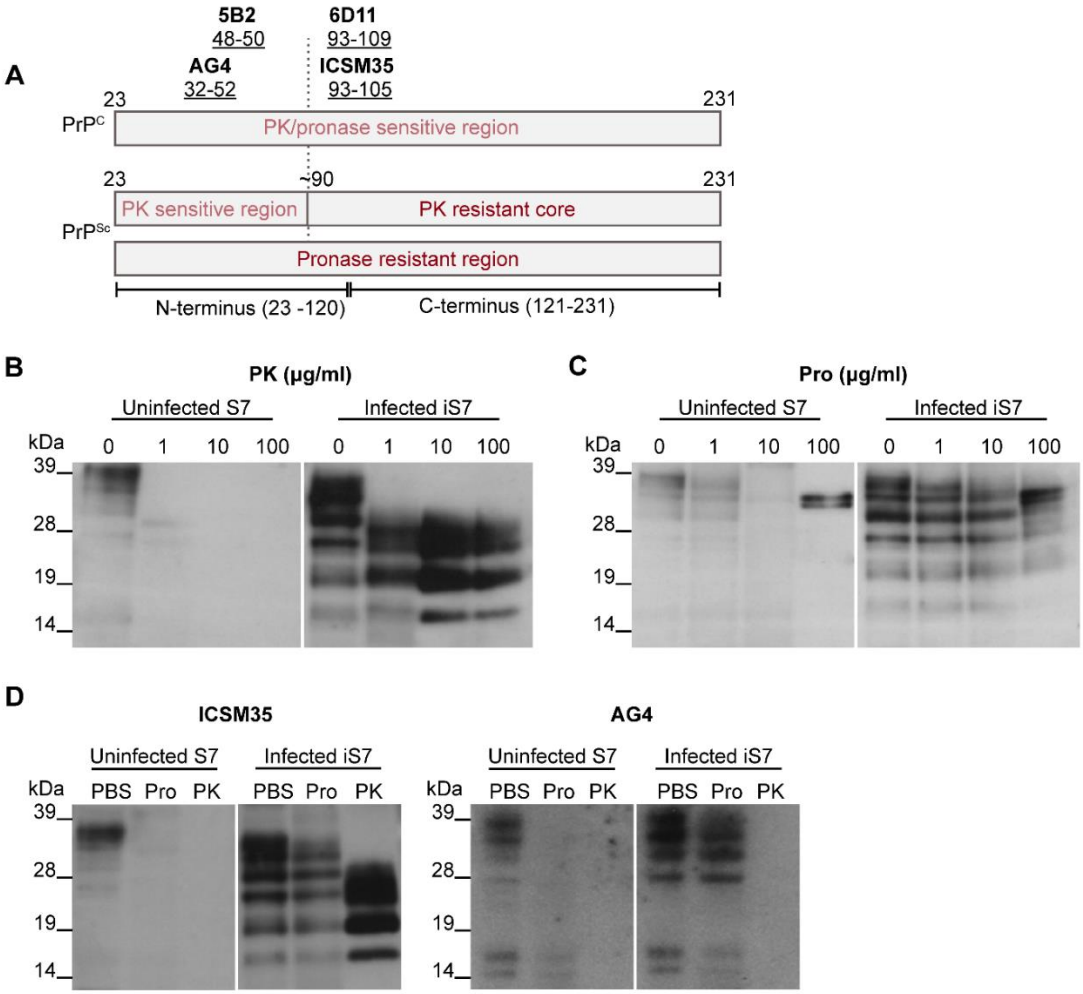

Figure 3.1: Anti-PrP antibodies against N-terminus detect full length pronase-resistant PrP from infected iS7 cell lysates. A) Schematic diagram of the epitopes of anti-PrP antibodies, along with the proteolytic sensitive or resistant regions that may affect the antibody binding site following protease treatment. **B** – **D)** Infected iS7 or uninfected S7 cells were lysed using RIPA buffer as described in Section 2.8.1. Following lysis, protein concentrations were determined using BCA. Samples were then treated with increasing concentration of **B)** Proteinase-K (PK) or **C)** pronase (Pro) for 30 mins at 37°C. Reactions were stopped using AEBSF or EDTA, respectively. 50 µg of samples were loaded onto a 12% Bis/Tris polyacrylamide gel and electrophoresis was conducted according to Section 2.8.3. Proteins were transferred onto PVDF membrane overnight and immunostained with ICSM35, an antibody against core PrP. In **D)**, ICSM35 (left panel) and AG4 (an antibody against the N-terminus of PrP) (right panel) were used on samples treated with 10 µg/ml of pronase or PK.

3.3 Localisation of full length PrP^D, an exclusive extracellular PrP^D marker

We next examined the localisation of full length PrP^D and truncated PrP^D in chronically infected iS7 cells. The rationale is to show that full length PrP^D is present extracellularly in our cell model, and further to demonstrate that extracellular PrP^D (using FL-PrP^D as the marker) is embedded in the dECM model. In **Figure 3.2,** we first fixed infected iS7 or uninfected S7 cells, followed by permeabilisation with acetone. Cells were then treated under denaturing conditions with GTC to allow the detection of steric hindered PrP^D core. A focal plane just above the substrate level is denoted as Z0 (z-plane 0), cells were then imaged at an interval of 0.8 μm 'upwards' to acquire several Z-stacks. In infected iS7 cells, Z0, which represents the extracellular matrix layer, showed 5B2 detection on surface. As cells were imaged at elevated Z-plane levels (Z1, Z2, and Z3), 5B2-positve PrP^D was only observed on the membrane, implying that full length PrP^D is intracellularly absent, but only exists extracellularly.

On the other hand, 6D11-positive PrP^D was detected both intra- and extracellularly, as this antibody binds to core PrP^D that includes both full length and truncated PrP^D isoforms. Uninfected controls did not show highly intense anti-PrP staining, suggesting no abnormal aggregated PrP^D was detected in the negative control. PrP^C signals were detected by both antibodies, predominantly on the membrane. Hence, this confirmed that full length PrP^D is present extracellularly in our system, which is an exclusive form of PrP^D found in the extracellular milieu. In turn, this will aid in the development and characterisation of infectious decellularised extracellular matrix.

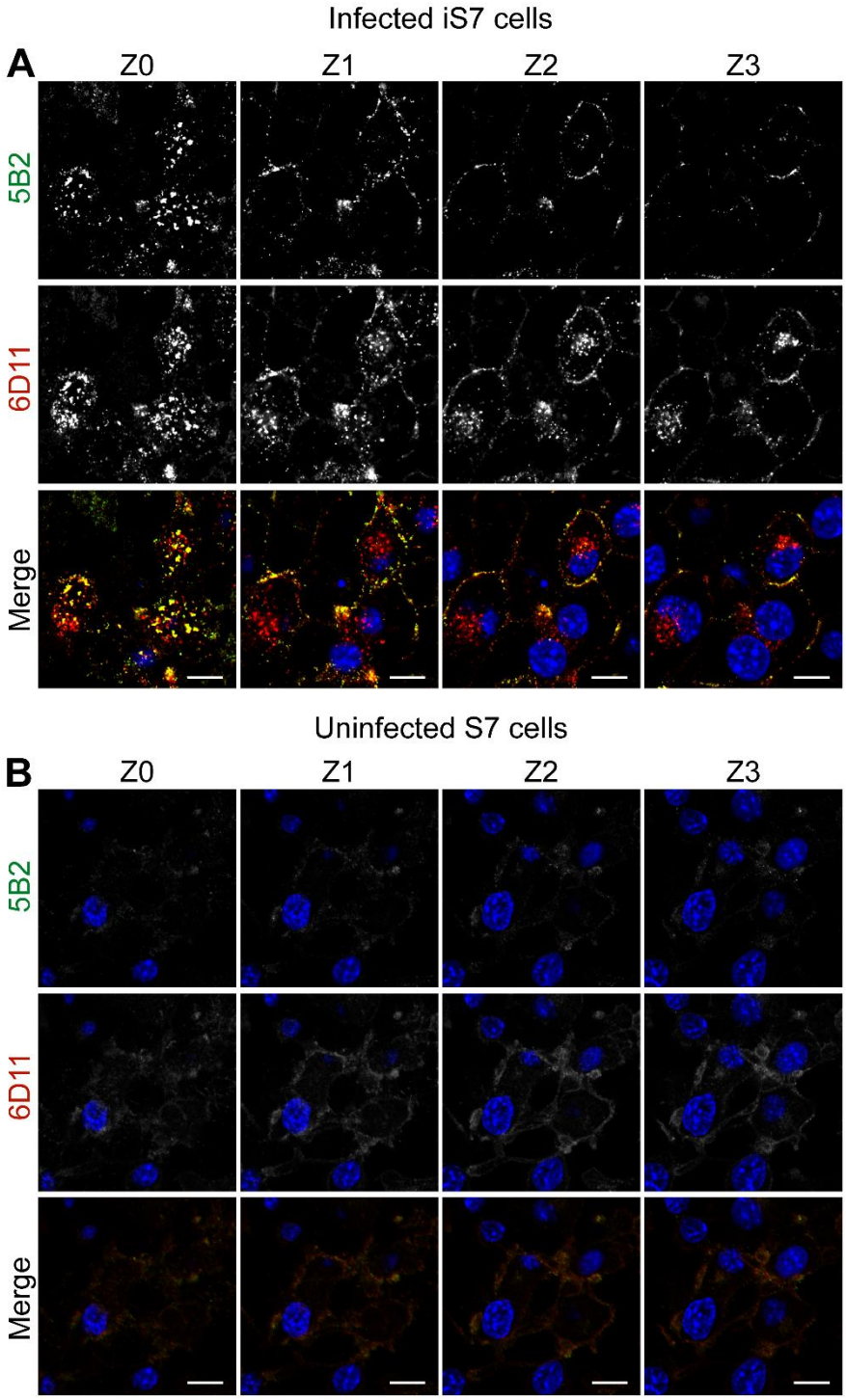

Figure 3.2: Subcellular localisation of full-length and truncated PrP^D. A) Infected iS7 or **B)** uninfected S7 cells were seeded on 8-well chamber slides and grown to confluency. Briefly, cells were fixed with 3.7% PFA, permeabilised with acetone, followed by treatment under denaturing conditions using 3.5 M GTC, as described in **Section 2.2.1**. Cells were double-labelled with primary antibodies 5B2 and 6D11, which targets the N-terminus and core PrP, respectively. Secondary antibodies conjugated to

AlexFluor 488 (against 5B2) and Red-Rhodamine X (against 6D11) were used for immunofluorescence. Z-stack acquisitions were acquired by first setting the extracellular matrix level as Z0 (details in **Section 2.2.2**), followed by imaging at elevated z-plane levels (Z1, Z2, Z3) with an interval of 0.9 µm between adjacent z-planes. 5B2 (anti-PrP against N-term) was used to label full length PrP^D whereas 6D11 decorated both full length and truncated aggregates. Scale bar = 5 µm.

3.4 Generating cell-free extracellular matrices using hypoosmotic buffer

After establishing that full length PrP^D is an extracellular prion marker, we developed our decellularised ECM using hypo-osmotic shock. As shown in **Figure 3.3 A**, infected iS7 or uninfected S7 cells were grown on 8-well chamber slides for 4 days with a half fresh medium change (250 µl/w of Opti-MEM + 10% FBS + 1% P/S) on day 3. Cells are typically 80 to 90% confluent on day 4. Cell supernatant was aspirated and replaced with sterile ddH20. Cells were incubated for 15 minutes at RT to allow gradual lysis. Wells were then subjected to 3 successive washes with sterile ddH20, and gentle resuspension (specified in **Section 2.4.1**). In **Figure 3.3 B**, infected iS7 (used as a representative image) were successfully lysed and removed from surface, based on light microscopy inspection. Gentle resuspension following washes is a necessary step to remove any remaining cells attached. Although no visible cells or cellular debri was seen upon examination, we would need to confirm the presence of PrP^D and the extracellular matrix on the decellularised surface.

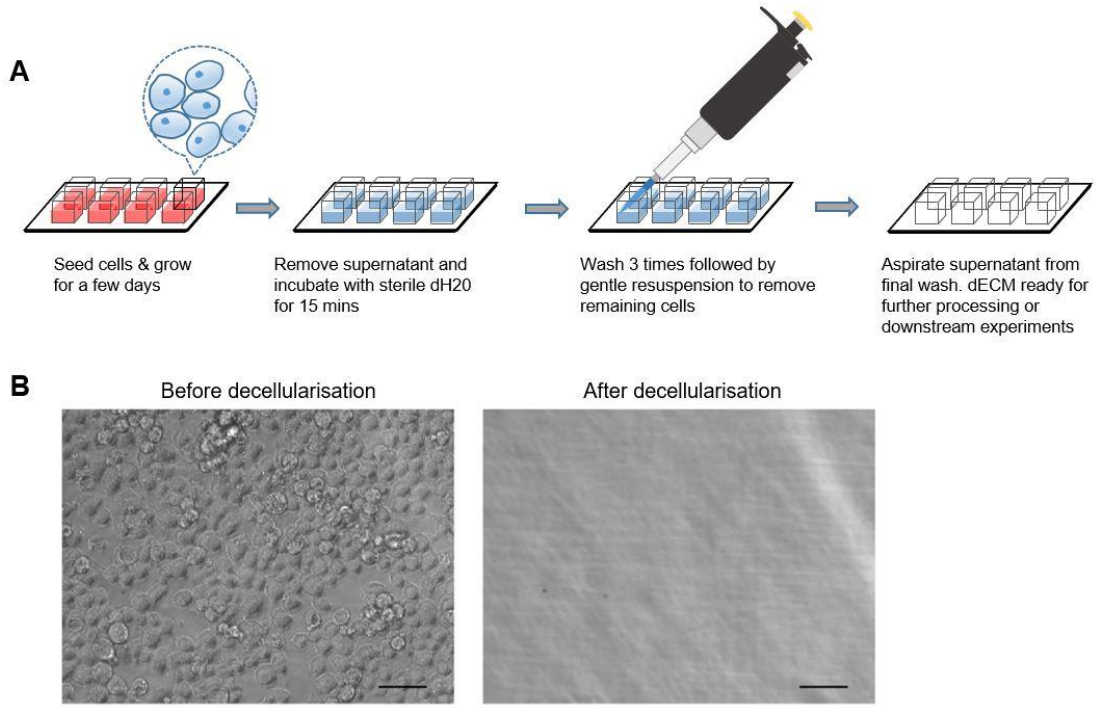

Figure 3.3: Decellularisation of cells to develop cell-free extracellular scaffolding on a 2D surface. A) Workflow to generate decellularised ECM under hypotonic condition. Briefly, infected iS7 or uninfected S7 cells were grown on 8-well chamber slides for 4 days, with a half medium change on day 3. Cell supernatant was removed, followed by the addition of sterile distilled water (dH20) and 15 mins incubation at room temperature. Cells were washed with sterile dH20 three times, while leaving the last wash on. The wells were carefully resuspended to remove residual cells adhered to the surface. Supernatant was aspirated, leaving a layer of decellularised material. **B)** Images acquired using an inverted light microscope that shows before and after decellularisation of infected iS7 cells. Scale bar is 50 µm.

3.5 Confirmation of deposited extracellular PrP^D following decellularisation

We next confirmed the presence of extracellular PrP^D on the surface of decellularised infected iS7 cells. Misfolded PrP conformers contain a sterically hindered core that blocks antibodies from binding (Rouvinski et al., 2014; Taraboulos et al., 1990). This epitope crypticity is one of its defining features, which allows the distinction between PrP^C and its aberrant conformers. Briefly, iS7 infected or uninfected S7 cells were decellularised or

left untouched prior to fixation. Samples were subsequently treated with or without GTC to induce denaturing or native conditions, respectively. For antibody labelling, 6D11 and 5B2 was added to each well and incubated overnight. Cells were then incubated with the respective secondary antibodies as described in **Section 2.2.2.** Intact cells (**Figure 3A, B**) or decellularised surface (**Figure 3C, D**) were imaged at the ECM level.

PrP^D was detected at the level of the ECM of intact cells (**Figure 3.4 A**). As mentioned, the core region of PrP^D is sterically hindered due to misfolding. This blocks 6D11, a core anti-PrP antibody, from binding to PrP^D. Immunodetection of PrP^D using 6D11 was only possible when the ECM of infected iS7 cells was treated under denaturing conditions (+GTC), which highlights epitope crypticity, a key feature of PrP^D. Following decellularisation of infected iS7 cells in **Figure 3.4 C**), we were still able to recover identical cryptic feature seen in intact infected cells (**Figure 3.4 A**), in which guanidinium treatment is still required to expose the core region of aberrant PrP conformers. This suggests that PrP^D was retained after removal of cells.

The main objective of this thesis is to investigate the modulation of extracellular prion infection by intervening with endogenous proteolytic activities. Hence, we would need an infectious model that contains extracellular prion assemblies. Full length PrP^D is found exclusively in the extracellular space, hence, a desirable marker to detect extracellular PrP^D assemblies. To detect full length PrP^D, we used 5B2, an antibody that binds to the N-term (sequence 48 – 50) of a PrP molecule. Highly intense 5B2 fluorescence observed in iS7 dECM in **Figure 3.4 C** suggests the presence of full length - extracellular PrP^D aggregates, which was also observed prior

to decellularisation (**Figure 3.4 A**). In our controls of intact (**Figure 3.4 B**) or decellularised (**Figure 3.4 D**) uninfected S7 cells, highly intense aggregates were not visible. Both antibodies (5B2 and 6D11) signals were positive, independent of denaturation. Overall, we can conclude that 5B2 is a suitable marker for extracellular PrP^D and can be used under native condition, making processing relatively quicker and feasible.

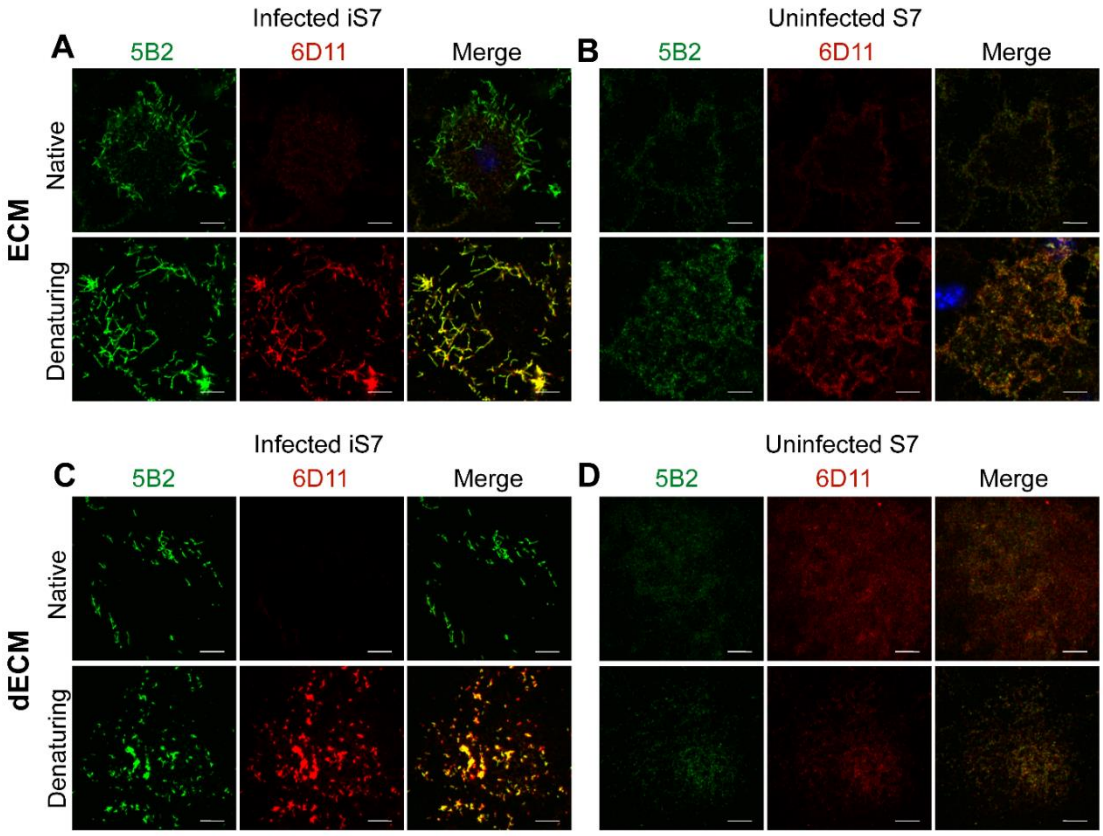

Figure 3.4: Extracellular PrP^D is retained following decellularisation. A) Infected iS7 or **B)** uninfected S7 cells were grown to confluency and fixed with PFA, pemeabilised with acetone and treated under denaturing (+GTC) or native (-GTC) conditions. Cells were immunostained using 5B2, an antibody against the N-terminus of PrP, and 6D11 that targets the PrP core. Primary antibodies were labelled with their respective fluorophore-tagged secondary antibodies (**Table 2.2**). C) Decellularised infected iS7 or decellularised uninfected D) were fixed and processed the same way. Immunofluorescence was assessed using confocal microscopy. Scale bar = 5 µm.

3.6 Optimal protocol for extracellular PrP^D deposition on substrate

Next, we sought to establish a protocol to obtain optimal extracellular PrP^D deposition on substrate. Hence, we deployed a number of cell growth protocols to optimise desirable 5B2 immunostaining in dECM. Here, we used two different 'medium change' procedures. In our lab group experience, FL-PrP^D is first detected using confocal microscopy after 3 days of cell growth, and subsequently increases on day 4. A half fresh medium change (250 µl of OptiMem + 10% FBS +1% P/S) on day 3 is required to replenish the necessary nutrients for cell survival. Hence, the first protocol is to grow cells for 4 to 7 days, with daily half medium change starting from day 3 post-seeding. On the other hand, we have also tested a separate protocol that involves full medium change (replacing cell supernatant with 500 µl/w of fresh cell culture medium). More details are found in **Table 3.1.**

20 images of 5B2-labelled decellularised surfaces were taken for each condition, followed by intensity analysis using ImageJ. In **Figure 3.5**, we showed that growing iS7 cells for 5 days with half medium changes on day 3 and 4 produced superior decellularised 5B2-positive fibrillary depositions ($p<0.0001$) when compared to the negative control (S7 dECM). From this point, we used the 5 days-half medium change procedure to grow infected iS7 or uninfected S7 cells prior to decellularisation, unless stated otherwise.

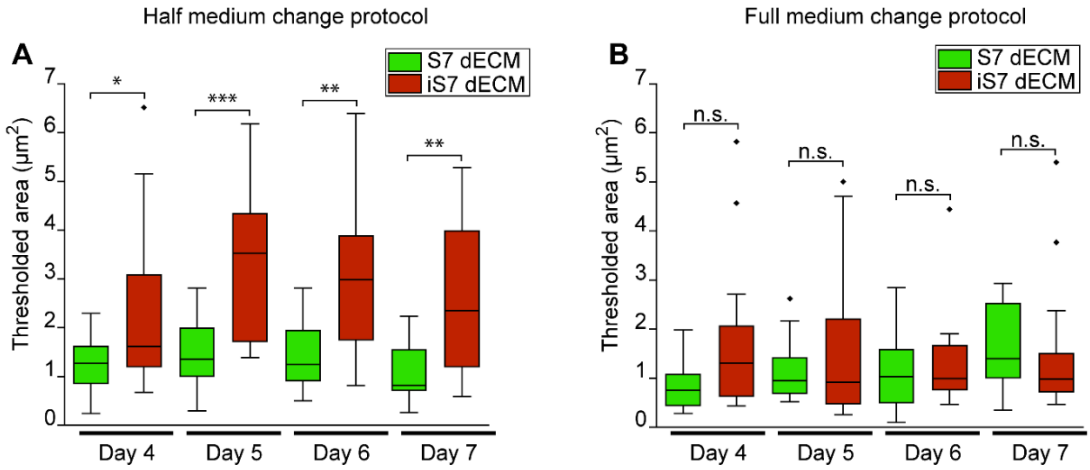

Figure 3.5: Comparison of cell culture protocols to obtain relatively high extracellular PrP^D deposition. Uninfected S7 or infected iS7 cells were seeded on 8-well chamber slides, and grown according to the **A)** half or **B)** full medium change protocol. After 4, 5, 6, or 7 days of growth, cells were decellularised through hypoosmolar conditions, followed by fixation using PFA. The decellularised layer was then immunolabelled with 5B2, an antibody recognising full length PrP, and subsequently labelled with a secondary antibody (AF488 IgG H+L, Jackson Affinipure). 20 images were taken per condition, followed by data analysis using ImageJ. Error bars represent standard deviation, whereas statistical analysis was assessed by Student's T-test, *p<0.01, **p<0.001, p***<0.0001.

Day(s) from cell seeding:	0	1	2	3	4	5	6	7
Half medium change (250 µL/w) of media with 10% FBS				✓	✓	✓	✓	
Full medium change (500 µL/w) of media with 5% FBS		✓			✓		✓	

Table 3.1: Tested cell growth protocols to obtain dECM with optimal extracellular PrPD deposition. Two types of protocols tested; half (written in blue) or full (written in green) medium change. Infected iS7 or uninfected S7 cells were grown for 4 to 7 days, with half or full medium changes according to the days specified in the table.

3.7 Extracellular matrix and fibrillar PrP^D assemblies remain intact post-decellularisation

Following establishment of a standard protocol for preparing decellularised material with high signals of extracellular PrP^D, we then investigated the presence of the ECM scaffold post decellularisation. We first grew cells according to the growth protocol, followed by decellularisation under hypo-osmolar conditions. Decellularised ECM was fixed using PFA, followed by double immunolabelling; 5B2 and either two of the ECM markers, collagen IV (Col4) (**Figure 3.6 B**) or chondroitin sulfate proteoglycan 4 (CSPG4) (**Figure 3.6 C**). The secondary antibody used is specified in **Table 2.2**. Here, we provided evidence that ECM-resident protein was retained, as determined by immunofluorescence, following cellular osmolysis. DAPI staining was negative in the dECM sample, indicating that cells were quantitatively removed from the surface. Hence, we have successfully developed a cell-free extracellular scaffold originating from either infected or uninfected cells.

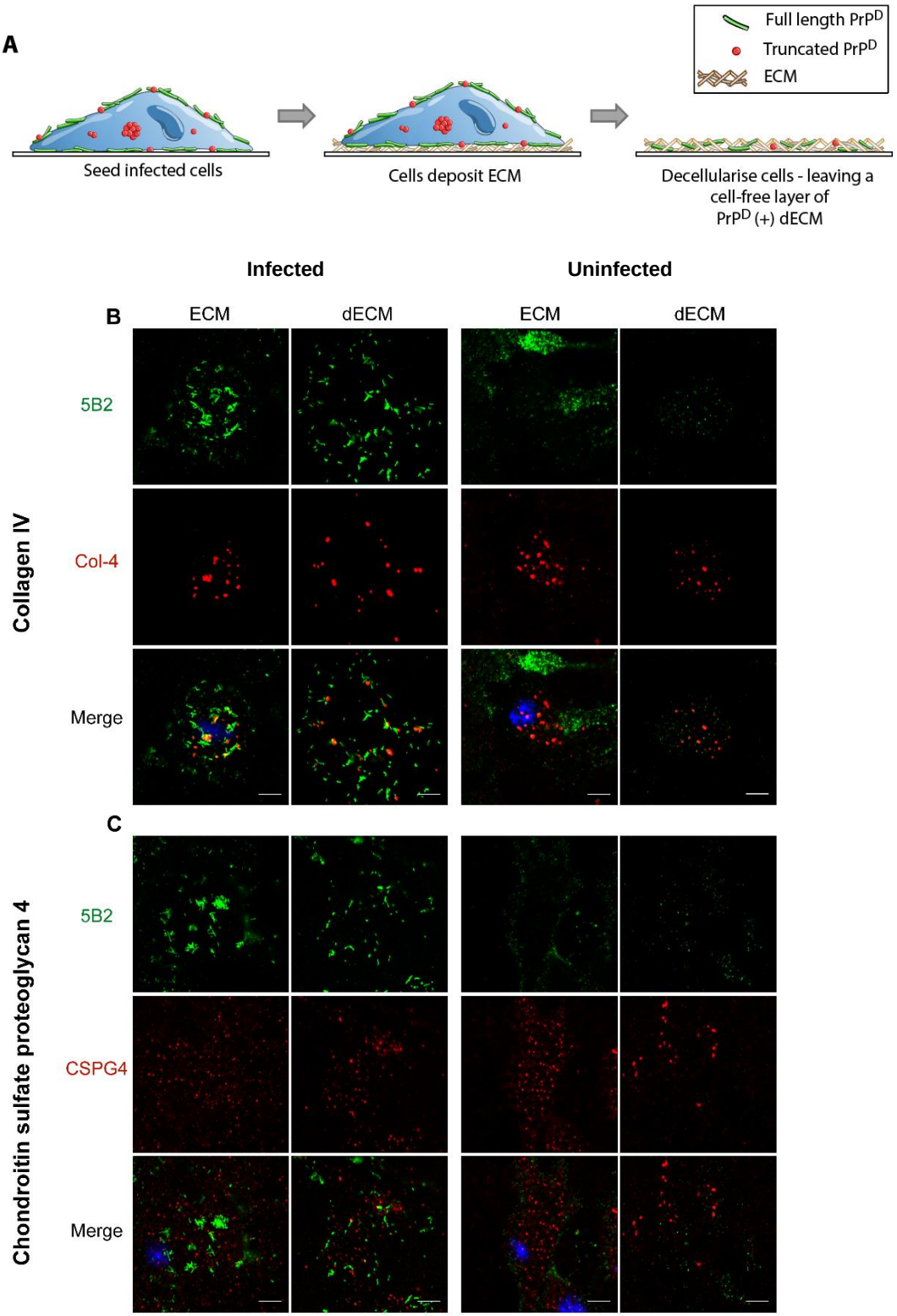

Figure 3.6: dECM model generated from chronically infected cells. A) Simplified workflow for generating PrP^D-positive dECM. **B**, **C)** Infected iS7 or uninfected S7 cells were seeded onto 8-well chamber slides and incubated for 5 days with a half medium change on days 3 and 4. Cells were treated with or without sterile distilled water (**Section 2.4.1**), leaving a decellularised surface or were left intact, respectively, prior to fixation using PFA. Intact

cells were permeabilised with acetone to permit antibody penetration. The decellularised (shown as dECM) and non-decellularised (shown as ECM) layer were immunolabelled with 5B2 to determine presence of extracellular PrP^D and B) collagen IV (Col IV) or C) chondroitin sulfate proteoglycan 4 (CSPG4) to detect presence of ECM-resident protein. Complementing secondary antibodies were used to fluorescently label their targets (**Table 2.2**). Immunofluorescence was assessed using the Zeiss LSM 710 confocal microscope, as described in **Section 2.2.2**. Scale bar = 5 µm.

3.8 Protease-resistant extracellular PrP aggregates present on decellularised surface

In **Figure 3.1,** we showed that full length PrP^D can be detected by treating infected samples with pronase, followed by immunolabelling using anti-PrP antibody against the N-terminus (AG4). As full length PrP^D serves as a marker for extracellular prions, I investigated whether decellularised ECM from infected iS7 cells contains full length pronase-resistant PrP. We selected a modified version of Scrapie Cell Assay (SCA) (Klohn et al., 2003). The SCA is a high throughput method that determines the number of cells (indicated as spots) positive with PrP-resistant material, which is present in infected cells. However, instead of using cell suspension, we generated decellularised scaffold from infected iS7 cells on 96-well ELISPOT plates (**Section 2.4.1**). Briefly, infected iS7 or uninfected S7 cells as a control were grown on a sterilised 96-well ELISPOT plate, which contains a layer of PVDF membrane on the surface of the well. The cells were then decellularised after 5 days and subjected to SCA (details in **Section 2.3.1**) using 10 µg/ml of pronase, 1 µg/ml of PK, or PBS as illustrated in **Figure 3.7 A**. In **Figure 3.7 B**, cell-free PrP^D scaffold (from infected iS7 cells) contains strong positivity (indicated by visible dark spots) of 5B2 and 6D11-protease resistant material.

This suggests that extracellular prions are adhered to the surface, whereas dECM generated from uninfected S7 cells were sensitive to pronase or PK treatment. In **Figure 3.7 C**, spot counts were saturated (spot count saturation is approximately 1500), whereas there were practically no spots (background of <25 spots) detected in uninfected dECM. Since limited light could pass through the membrane at the base of the well, we could not confirm the success of the decellularisation protocol via light microscopy. Therefore, we opted for hematoxylin staining, a cell nuclei marker to determine the presence of cells following decellularisation (**Figure 3.7 D**). No distinct spots or stain was observed following decellularisation, the background was comparable to the negative control (no seeded cells).

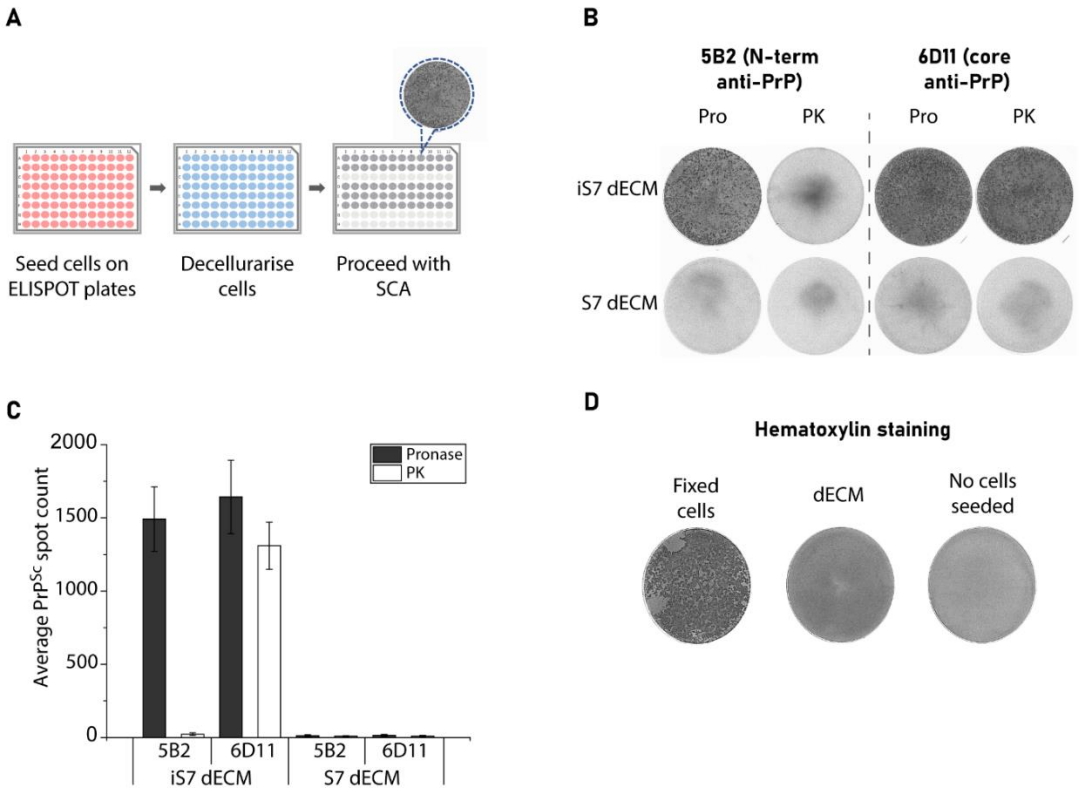

Figure 3.7: Presence of extracellular PrP^{Sc} on a decellularised surface. Infected iS7 or uninfected S7 cells were seeded onto ELISPOT plates. Cells were grown according to the standard protocol for decellularisation (**Section 2.4.1**). Cells were decellularised using copious amounts of sterile distilled water. Following decellularisation, the ELISPOT plate was subjected to the Scrapie Cell Assay (**Section 2.3.1**). Briefly, the wells were either treated with 10 ug/ml of pronase (Pro) or 1 ug/ml of proteinase-K (PK). After 1 hour at 37°C, proteases were removed by washing the plates sufficiently using PBS. The plates were treated with GTC to unfold PrP^{Sc} resistant core, followed by blocking, and anti-PrP antibodies incubation: 5B2 (against N-terminus) and 6D11 (targeting the core). The plates were labelled with a secondary anti-mouse IgG conjugated to HRP. The PrP^{Sc} spots were revealed upon treatment with the AP dye. **A)** Simplified workflow to prepare dECM and test for PrP-resistant material. **B)** Representative ELISPOT images of PrP^{Sc} spot count. **C)** Quantified average spot count of SCA data (technical repeats = 12), error bars represent SD. **D)** iS7 cells or S7 cells were grown on ELISPOT plates for 5 days with a half medium change on days 3 and 4. In parallel, cells that were grown under same conditions were decellularised according to **Section 2.4.1**. No seeded cells were used as a negative control. All of the wells were fixed, and incubated for 5 mins with hematoxylin diluted 1:20 in distilled water. Wells were washed with distilled water twice, followed by image acquisition.

3.9 Extracellular scaffolds are highly infectious *in vitro*

We thus far showed that dECM, generated from infected iS7 cells is devoid of adherent cells, consists of a layer of unperturbed ECM scaffold with extracellular PrP^D, and shows a proteinase resistance profile expected for PrP^D. We next tested whether dECM from infected iS7 cells is infectious and able to transmit disease to mice. To study the relative infectivity of extracellular prion assemblies, we seeded prion-susceptible reporter cells (uninfected S7 cells) on PrP^D-positive dECM or uninfected dECM as a control. In parallel, we infected reporter cells by adding varying concentrations of RML brain homogenate, or CD1 brain homogenate as a negative control. Following infection, cells were then split for 4 passages. **Figure 3.8 A** shows that extracellular PrP^D assemblies are highly infectious with infectious titres comparable to 3.3×10^{-5} of RML brain homogenate. This shows that dECM from persistently infected cells is highly infectious, and constitutes a novel route of infection.

To exclude that infectious dECM is cytotoxic, we challenged reporter cells either with dECM from uninfected or infected cells, brain homogenates from scrapie sick or healthy mice, or left untreated (**Figure 3.8 B**). Cytotoxicity was then measured by CellTiterGlo® Luminescent Cell Assay (**Section 2.4.2.1**), an assay that measures the cellular ATP concentration, an indicator of cell toxicity. The lower the amounts of ATP detected, the lower the luminescent unit depicted in **Figure 3.8 B**, only the highest concentration of RML brain homogenate (10^{-2}) dilution was toxic to the reporter cells ($p<0.05$, Kruskal Wallis with Dunn's Multiple Comparisons Test). This shows that

although the prion titer is relatively high, the infectious decellularised ECM is non-toxic for reporter cells.

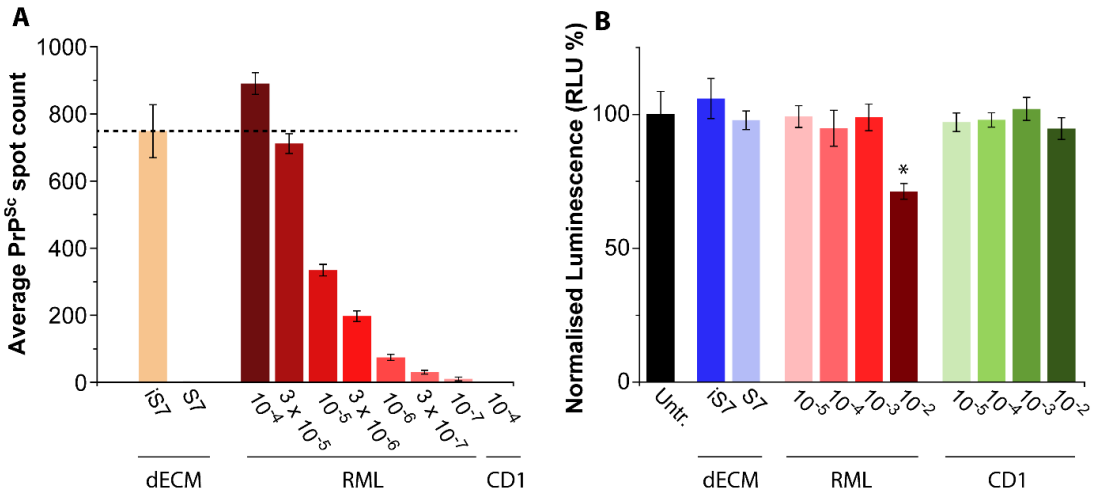

Figure 3.8: Infectivity of dECM and disease-transmissibility of infected reporter cells. A) Infected iS7 or uninfected S7 dECM was prepared as described in **Section 2.4.1**. Uninfected reporter S7 cells were seeded on top of the prepared bioscaffold, following serial passages to collect ELISPOT plates at passages 2, 3, and 4. In parallel, reporter S7 cells were infected with 10% RML brain homogenates prepared at varying concentrations and CD1 at the highest concentration (10^{-4}) as a negative control. Collected ELISPOT plates were subjected to Scrapie Cell Assay (**Section 2.3.1**) to asses average PrPSc positive cells seen as spots. Representative graph shown was obtained from passage 3. Each group has 12 technical repeats. Error bar represents Standard Error of the mean (SEM). **B)** Determination of cell viability after infection of dECM or brain homogenate using CellTiterGlo® Luminescent Cell Assay (**Section 2.4.2.1**). Error bars in the figure represent standard deviation. Significance level (* = $p < 0.05$) was determined using Kruskal Wallis with Tukey's Dunn's Multiple Comparisons Test. Bars represent average % of RLU from 6 wells, while error bars dictate its respective standard deviation.

3.10 Extracellular prion deposits transmit disease *in vivo*

To corroborate that extracellular prion assemblies are infectious (**Figure 3.8**), we set out to determine whether reporter cells that had been in contact with dECM transmit *bona fide* prion disease in mice. First, we prepared dECM from infected iS7 or uninfected S7 cells as shown in **Figure 3.9 A**. Susceptible S7 reporter cells were then seeded onto infectious or non-infectious dECM, followed by serial passages and SCA to determine infectivity. In addition to SCA, extracellular PrP^{D} was confirmed using immunofluorescence (**Figure 3.9 B**). We then prepared infected or mock-infected reporter cells (**Figure 3.9 A)** and inoculated them into wild-type FVB mice. In parallel, we inoculated mice with chronically infected iS7 as a positive control. In **Figure 3.9 C**, we demonstrated that dECM infected reporter cells transmit prion disease to wild-type FVB mice. Susceptible mice (n = 4 biological replicates) succumbed to prion disease at average incubation times of 171.6 ± 4.7 days post-inoculation (p.i.), whereas mice (n = 4 biological replicates) injected with persistently infectious cells succumbed to disease approximately at 158.4 ± 6.1 days p.i. This shows that dECM is infectious and thus represents bona fide prions. The infectious titre of chronically infected, dECM infected or mock-infected cells were measured as shown in **Figure 3.9 D.** dECM infected reporter cells PrP^{Sc} spot counts were significant when compared to mock-infected reporter cells ($p<0.001$), as determined by Student's T-test.

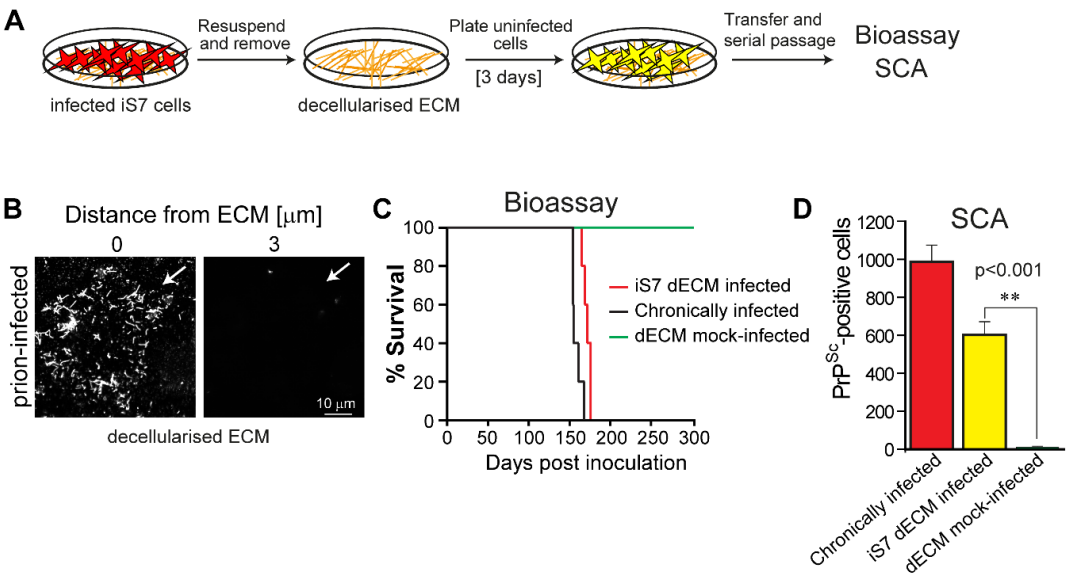

Figure 3.9: Extracellular PrP assemblies transmit prion disease *in vivo*. **A)** Schematic diagram for testing infectivity of decellularised ECM from chronically infected cells. Following trituration of cells under microscopic control, uninfected S7 reporter cells were seeded onto decellularised cell layers and cells were grown to confluency and serially passaged. **B)** Representative confocal image of a detached prion-infected cell with remaining 5B2-positive aggregates at the ECM. **C)** dECM-infected, uninfected, and chronically infected S7 cells were lysed and inoculated intracerebrally into FVB mice at a concentration of 3 x 10^7 cells/ml. Percent survival of inoculated mice is depicted in a Kaplan Meier survival plot. Disease incubation times of mice (n = 4 biological replicates), inoculated with dECM-infected S7 cells were 171.6 +/- 4.7 and 158 +/- 6.1, respectively. **D)** Infectivity of cells used for inoculation in C), as determined by SCA; significance determined by Student's t-test.

3.11 Conformation-dependent immunoassay of infectious dECM

While most anti-PrP antibodies readily recognise the cellular form of PrP (PrP^C) under native conditions in immunocytochemistry (ICC), the majority of antibodies fail to detect PrP^D aggregates in prion-infected cells. In contrast, PrP^D aggregates can be detected at perinuclear sites, at the plasma membrane and at the ECM under denaturing conditions in presence of high guanidinium salt conditions (Ribes et al., 2022 preprint; Taraboulos et al., 1990; Veith et al., 2009) at a concentration of 3.5M GTC, antibody binding sites are fully accessible, indicating that antibody epitopes are cryptic under native conditions. We here investigated how infectivity of PrP amyloids is affected by gradually increasing the denaturing strength following treatment of amyloids in a concentration range between 0 - 3.5M GTC. In **Figure 3.10 A**, infectious iS7 or uninfected S7 dECM were treated with varying concentrations of GTC. Wells were washed 5 times with DPBS, followed by seeding of uninfected S7 reporter cells. Cells were then split successively (P2, P3, and P4) and the number of infected cells determined by SCA. We show that 1.5 M of GTC is sufficient to completely abolish prion infectivity of extracellular prion assemblies.

Of interest, we also measured the colocalisation of 5B2/6D11. As mentioned before, anti-PrP antibodies against the unstructured N-terminus of PrP^D aggregates under native conditions, whilst antibodies against the PrP central region require denaturation due to the crypticity of epitopes. This corroborates data in **Figure 3.10 B**; increasing concentrations of GTC are associated with increasing levels of colocalisation between 5B2 and 6D11.

Colocalisation of 5B2/6D11 of iS7 dECM plateaued at 2.5 M of GTC treatment.

As for PrP^C, core epitopes are not hidden or buried, rendering its detection invariant to denaturants. This is in agreement with our control set (uninfected dECM) in **Figure 3.10 B** that shows a plateau polynomial curve. Representative images of the dataset in **Figure 3.10 B** are displayed in **Figure 3.10 C.** In **Figure 3.10 C**, images of the dECM generated from uninfected S7 cells were intentionally overexposed. This was done to clearly demonstrate that the immunostaining of PrP^C with 5B2 and 6D11 antibodies remains unaffected by GTC treatment, highlighting its independence from such treatment.

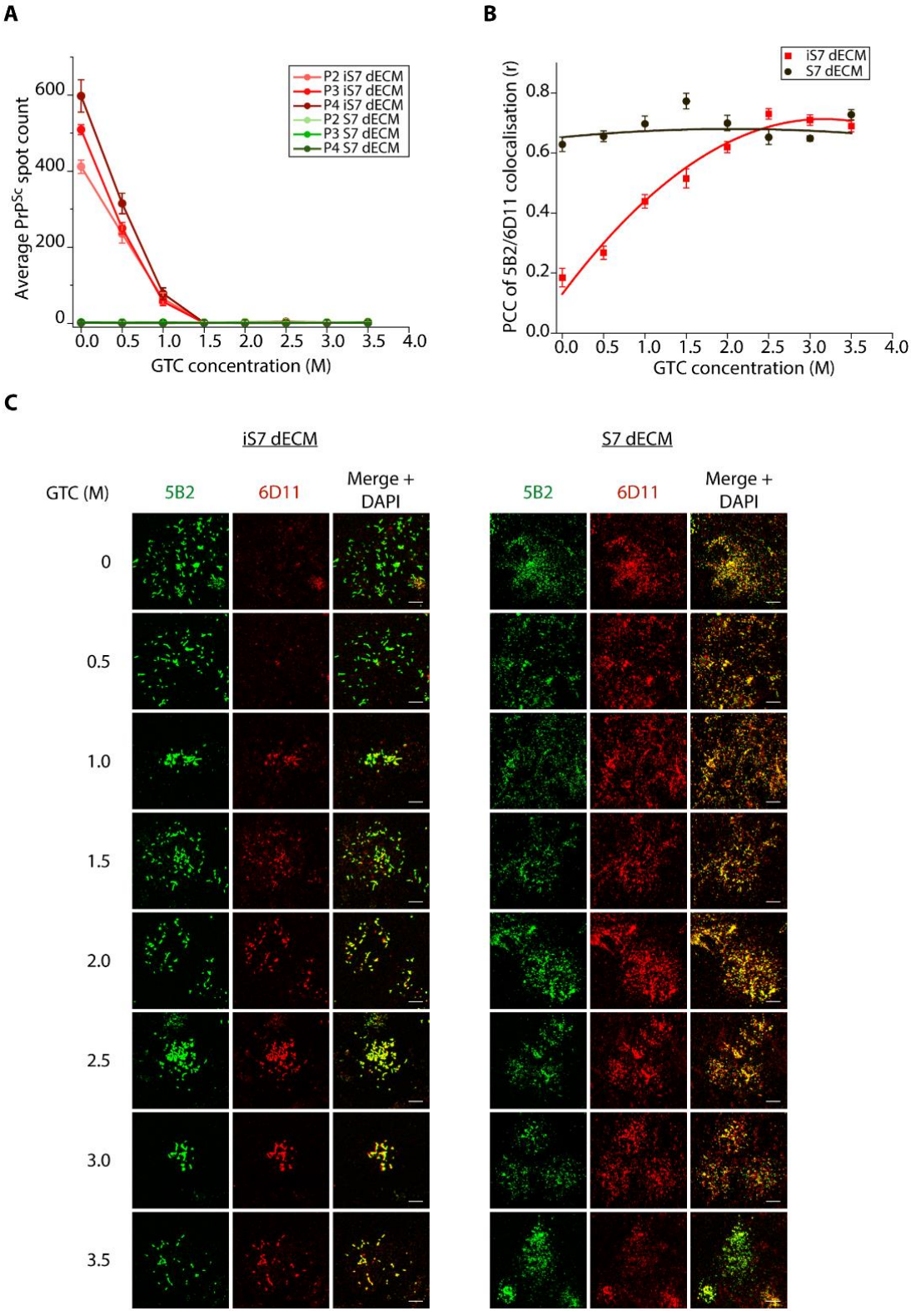

Figure 3.10: The relationship of denaturation state of extracellular PrP^D and infectivity: A) Decellularised ECM of infected iS7 or uninfected S7 cells prepared on 96-well cell culture plates (refer **Section 2.4.1**) were treated with varying concentrations of GTC. Following treatment, wells were sufficiently washed PBS. Uninfected S7 cells were seeded onto the treated wells and

serially passages to obtain ELISPOT plates at different stages (Passage 2 (P2), P3, and P4), refer to **Section 2.3.1**. **B**, **C)** Decellularised ECM generated on 8-well chamber slides was subjected to immunofluorescence (described in **Section 2.2.1** & **2.2.2**) using 5B2, an anti-PrP against the N-terminus and 6D11, targeting the PrP core. **B)** Analysis of Pearson's Correlation Coefficient (PCC) of 6D11 and 5B2 upon increasing concentration of GTC (increased core epitope exposure). **C)** Representative images of increasing GTC treatment of dECM from uninfected S7 or infected iS7 cells. 12 technical repeats for each sample in **A** and **B**. Error bars represent standard deviation.

3.12 Mobilisation of PrP^D-embedded in ECM scaffold through cell contact

Next, we asked whether immobilised PrP^D from ECM scaffolds can be mobilised and taken up by reporter cells. To answer this question, we used replication-refractory *Prnp* knockout cells (N2a-*Prnp*$^{-/-}$) to unambiguously identify exogenous PrP^D aggregates. N2a-*Prnp*$^{-/-}$ cells were seeded onto dECM scaffolds from infected iS7 and uninfected S7 cells, fixed after 8h, 16h, or 24h and processed as specified in the **Section 2.2.1**.

Representative images of the cell cultures are shown in **Figure 3.11 A**. At 8h post infection, 7.8% of N2a-*Prnp*$^{-/-}$ cells contained PrP^D at the vicinity of the plasma membrane, while detection of intracellular PrP^d was slightly lower (5.5%) (**Figure 3.11 B and Table 3.2**). Cells with both events had the lowest count, which accounts to 1.5%. Overall, a total of 14.8% of N2a-*Prnp*$^{-/-}$ cells were PrP^D-positive at 8 hours after seeding, whereas cells incubated for 24 hours were 40.8% PrP^D positive. This shows that *Prnp*$^{-/-}$ reporter cells are able to mobilise and internalise PrP^D embedded in the ECM. We repeated the same setup in **Figure 3.11 C**, but double-labelled cells with both 5B2 and 6D11. Fluorescence signals were acquired on the context of bright field

images to display cell membrane and surface boundaries due to a spectral overlap with the fluorescence dye CellMask. Of interest, we investigated whether ECM-bound PrP^D are endocytosed into reporter cells by virtue of contact, and if internalised prions are cleaved once internalisation occurs. Processed reporter cells were examined at 8h, 16h, or 24h following cell incubation. Images in **Figure 3.11 C** shown are representatives taken from the earliest fixation point (8h). Interestingly, all membrane bound PrP^D originating from ECM infection are full length PrP^D (5B2 and 6D11 positive), whereas internalised PrP^D aggregates were detected with 6D11 but not with 5B2, suggesting that the N-terminus is proteolytically processed upon internalisation of PrP^D.

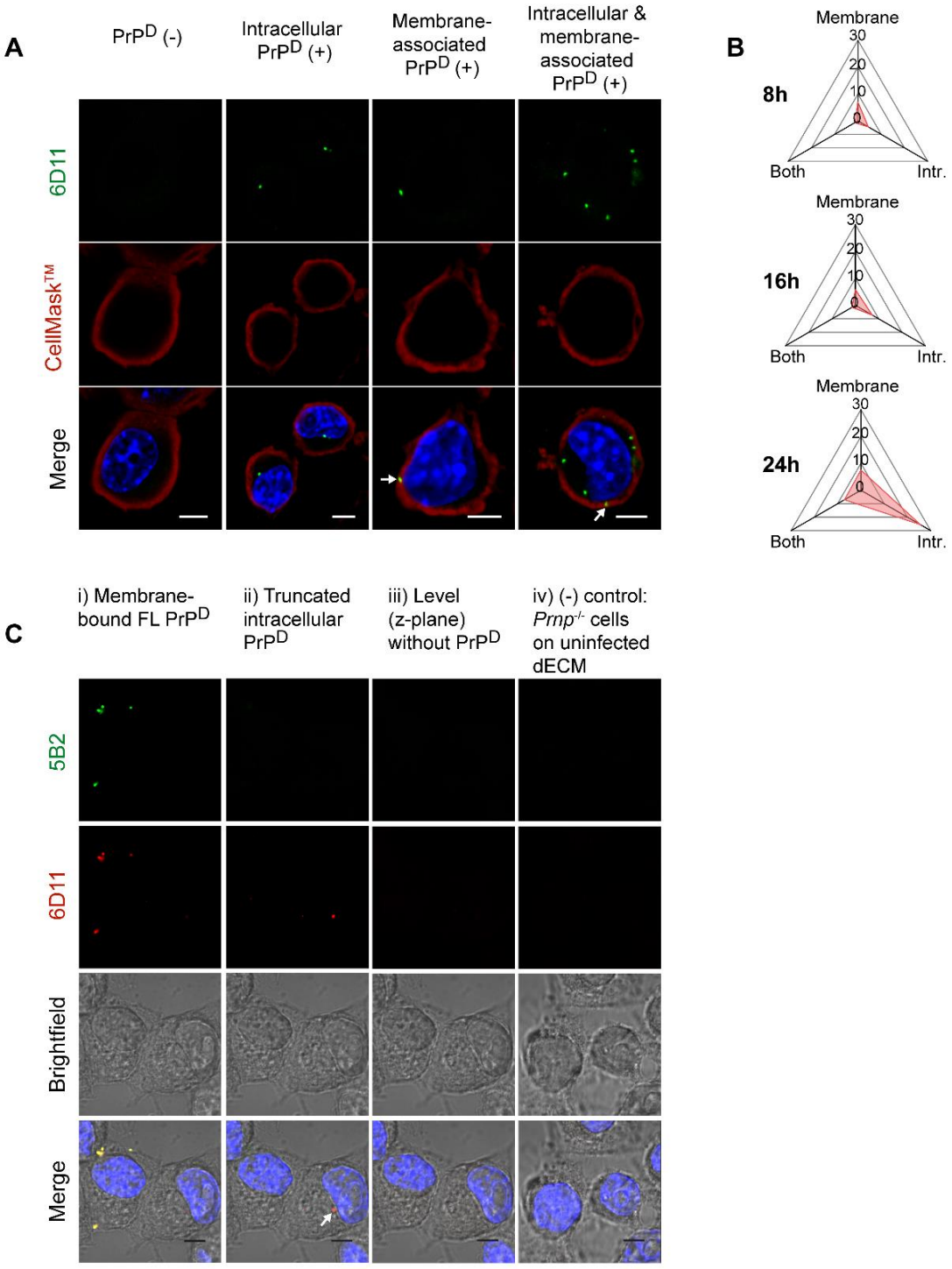

Figure 3.11: PrP^D uptake into N2a *Prnp*$^{-/-}$ cells from infected dECM scaffolds. A) Representative images of different PrP^D localisations following dECM contact. Arrow indicates PrP^D associated with the membrane. Briefly, N2a-*Prnp*$^{-/-}$ cells were seeded on dECM generated from S7 or iS7 cells and fixed after 8h, 16h, or 24h incubation. Cells were pemeabilised using acetone and treated with 3.5 M GTC to induce denaturing state. Samples were labelled with 6D11, followed by anti-mouse IgG (H+L) AF488 immunolabelling. Cells were also treated with CellMask™ Deep Red Plasma

Membrane Stain as a membrane marker. **B)** Percentage of PrP^D internalisation and localisation in **A)** at 8h, 16h, or 24h. 3 field of views (technical repeats) were scored per time point, each view contains 30 images taken at 63x magnification. Image was scored based on the PrP^D positivity associated with the membrane, intracellular (intr.) presence, or both. Full data set can be found in Table 3.2. **C)** Truncation phenomenon observed following PrP^D internalisation after 8h of incubation on dECM by using 5B2 (to detect full length PrP^D) and 6D11 to detect both truncated and full length PrP^D. The fixed, permeabilised, and denatured (see **Section 2.2.1**) N2a-*Prnp*$^{-/-}$ were double-labelled with 5B2 and 6D11. The boundary of cellular structure seen in brightfield imaging is considered as the membrane. Arrow indicates internalised PrP^D.

% of PrP^D-positive N2a-*Prnp*$^{-/-}$ after contact with infectious dECM						
Cellular site	8h		16h		24h	
	Avg	SD	Avg	SD	Avg	SD
Membrane-associated	7.0	1.5	5.8	2.0	7.5	1.3
Intracellular	4.5	2.0	7.2	2.6	25.5	4.9
Both	1.3	0.7	1.4	0.2	7.1	2.8

Table 3.2: Internalisation of PrP^D from ECM into cells. N2a-*Prnp*$^{-/-}$ cells were seeded on infectious dECM and fixed after 8, 16, or 24h. PrP^D-positive cells were quantified based on the criteria shown in Figure 3.11 A. Three field of views (Each field contains at least 30 images of 63x magnification, containing 15 to 40 cells per image).

3.13 Optimisation of gene silencing protocol

Gene perturbation remains an indispensable tool to identify cellular factors that block or facilitate prion infection. Based on evidence that mobilised prion seeds are taken up by cells (**Figure 3.12**), we next investigated whether proteases control the release of infectivity from extracellular PrP^D matrices. Hence, silencing protease-associated genes of cells infected on extracellular prion scaffolds is a favourable strategy. In standard experimental protocols, prion-susceptible cells are reverse transfected with siRNA and maximal

levels of gene silencing are obtained in the dish at day two or three after plating. Cells can then be infected at maximal levels of transcriptional silencing. However, our experimental approach of infecting reporter cells *in situ* by plating cells onto PrP^D scaffolds bears technical difficulties for obtaining maximal gene knockdown levels using transient gene silencing. Notably, replating of reverse transfected cells leads to rapid depletion of siRNA levels due to cell doubling. We therefore tested different protocols to obtain sufficient gene knockdown and infectivity of our reporter cells.

A schematic diagram, depicting six distinct protocols for transcriptional silencing of reporter cells, followed by infection with PrP^D scaffolds is shown in **Figure 3.12 A, B**. The prefix 3D and 4D refers to the number of days for each protocol, followed by the mode of transfection. For Std (standard transfection), uninfected S7 reporter cells were reverse transfected with pools of siRNA and subsequently seeded onto infectious dECM. In Mod-1H (modified, single hit), cells were reverse transfected with siPools and then grown on a plate without dECM, followed by resuspension and transfer onto a plate containing infectious dECM. For Mod-2H (modified, double hit), cells were reverse transfected, grown on a separate dish for one day, resuspended and reverse transfected with siPools for a second time before cells are seeded onto dECM. The rationale of Mod-1H or Mod-2H is to allow sufficient gene silencing to take place prior to infection.

Prnp was chosen as the target gene to optimise our gene perturbation protocol because the presence of *Prnp* is an absolute pre-requisite for prion propagation (Büeler et al., 1993). As a readout, effects on prion infection were measured and expressed as inhibition of infection (%).

Both, 3-day (**Figure 3.12 B**) or 4-day perturbation protocols (**Figure 3.12 C**), showed a ~70 to 85% reduction of prion infection after the first passage (P1) and gradually loses its inhibitory effect as cells are passaged, most likely due to the dilution of siRNA during cell doubling.

The 4D-Std protocol shows robust inhibition of cell infection (>80% effect during three serial passages) compared to other protocols in **Figure 3.12 B** and **C**. Henceforth, 4D-Std was selected as standard knockdown procedure to investigate the role of proteases during in situ infection of reporter cells with infectious dECM.

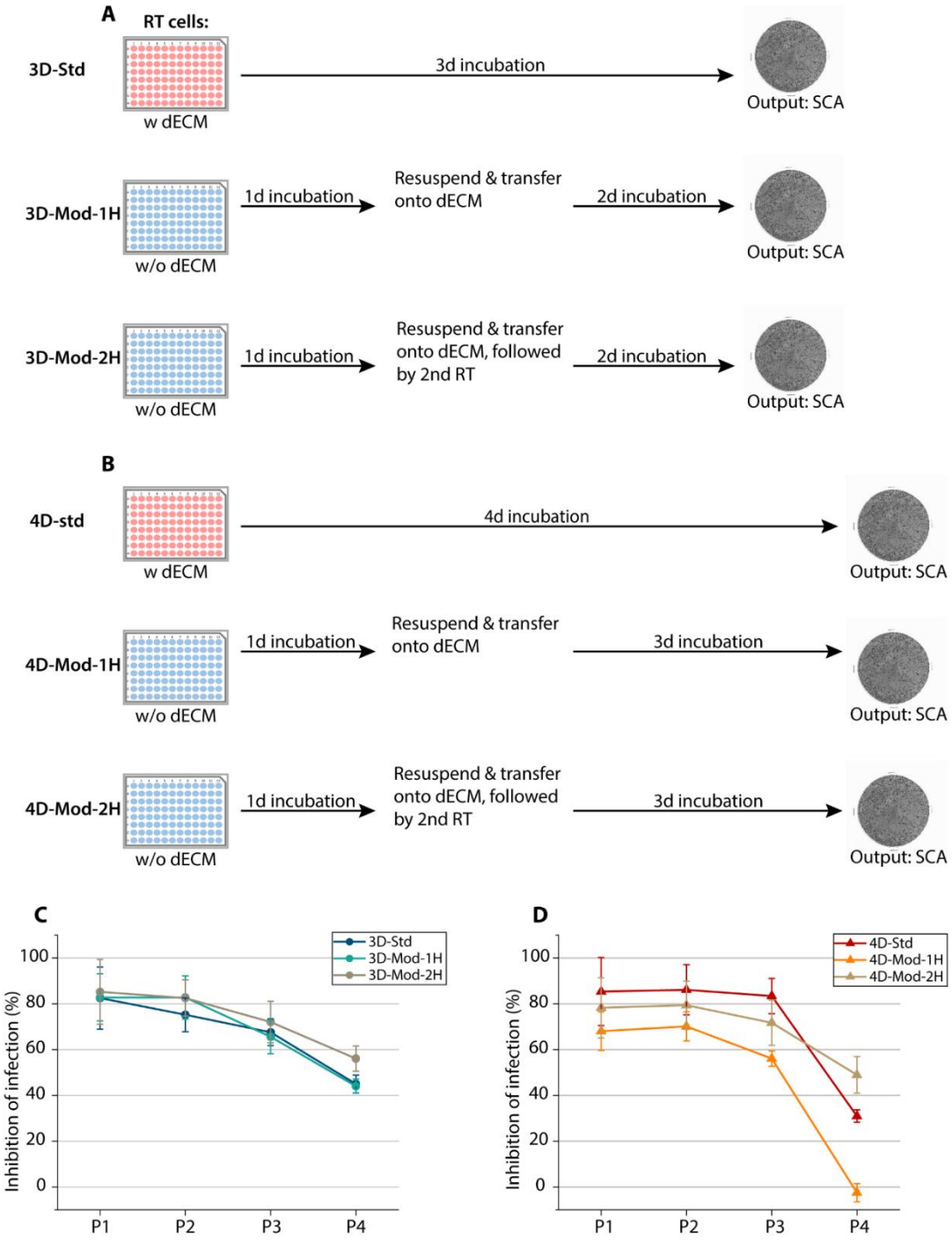

Figure 3.12: Optimising a gene silencing protocol on infectious dECM to obtain a highly efficient knockdown procedure. *Prnp* gene of uninfected S7 cells were silenced using pools of siRNA with or without the presence of infectious dECM, followed by an elaborate workflow explained in Section 2.7.1. Briefly, six silencing protocols were compared, which can be categorically divided into a **A)** 3-day or **B)** 4-day protocol. *Prnp* gene of uninfected S7 cells were silenced using pools of siRNAs with or without the presence of infectious dECM, followed by the respective steps shown in the elaborate workflow. Results for the **A)** 3-day and **D)** 4-day protocols are

shown in C and D, respectively. Error bars represent standard deviation. RT = reverse transfection, 3D = 3-day protocol, 4D = 4-day protocol, Mod = Modified protocol, Std = Standard protocol, 1H = Single transfection, 2H = Double transfection.

3.14 Identification of genes that affect infection of neuronal cells by ECM contact

Following optimisation of reverse transfection, I next investigated the role of proteases in the release of infection embedded in the extracellular scaffolds. Briefly, infectious dECM was prepared as described in the **Methods section 2.4.1**. Cells were seeded and reverse transfected using the 4D-Std protocol (**Figure 3.12 A**). Knockdown efficacies for gene candidates are reported in **Figure 3.13 C** (β-actin as housekeeping gene) and in **Figure 3.13 D**) (GAPDH as housekeeping gene) (see **Table 3.4** for summarised data set). In **Figure 3.13 A**, we observed a significant ($p<0.001$) reduction of PrP^{Sc} spot counts (more than 30%) following knockdown of either *Adam19*, *Adamts4*, or *Mmp11* when compared to non-silencing control (NSC). This suggests that proteases facilitate the release of infectious prions from the extracellular matrix. One could also speculate that these enzymes could directly be involved in altering the infectivity of PrP^{D} aggregates. For instance, it was hypothesised that peptidases including CTSB and CTSL is involved in disaggregating prion aggregates into smaller fragments which are more readily transmissible and infectious (Zhang et al., 2003). Although fragmentation of prion fibrils can be observed through mechanical force such as sonication (Saborio et al., 2001), there is a lack of experimental evidence that show endogenous enzymes are capable of replicating the same action.

We have also targeted *Atp6ap1*, a gene that encodes an accessory protein of the V-ATPase complex with a role in protease exocytosis (Yang et al., 2012). Notably, silencing of *Atp6ap1* resulted in a 44.5% ($p<0.001$) decrease in infectivity. Due to the favourable knockdown effect of *Atp6ap1*, we proceeded with double transcriptional silencing; *Atp6ap1* with either *Adam19*, *Adamts4*, or *Mmp11*. We found that silencing both *Atp6ap1* and *Mmp11* generated a synergistic effect, decreasing prion infection by more than 60% compared to NSC ($p<0.001$). Changes of PrP^{Sc} spot counts (%) are displayed in **Table 3.3**.

Notably, we observed a marked increase ($p<0.001$) of PrP^{Sc} spot counts by 60, 38, or 36% when *Mmp15, Mmp17,* or *Mmp24* was silenced, respectively (**Figure 3.13 A, Table 3.3**), which suggests a protective role of these genes during infection.

To investigate whether RNA expression levels of *Prnp* may change following silencing genes candidates, we conducted RT-qPCR on reverse transfected cells (**Figure 3.13 B**). Notably, *Prnp* expression levels of *Adam19*-silenced S7 cells were reduced by 75% (**Table 3.4**). Since *Prnp* expression is an indispensable determinant for prion infection, it is reasonable to speculate that a 75% decrease in *Prnp* expression may abrogate infection as shown in **Figure 3.13 A**.

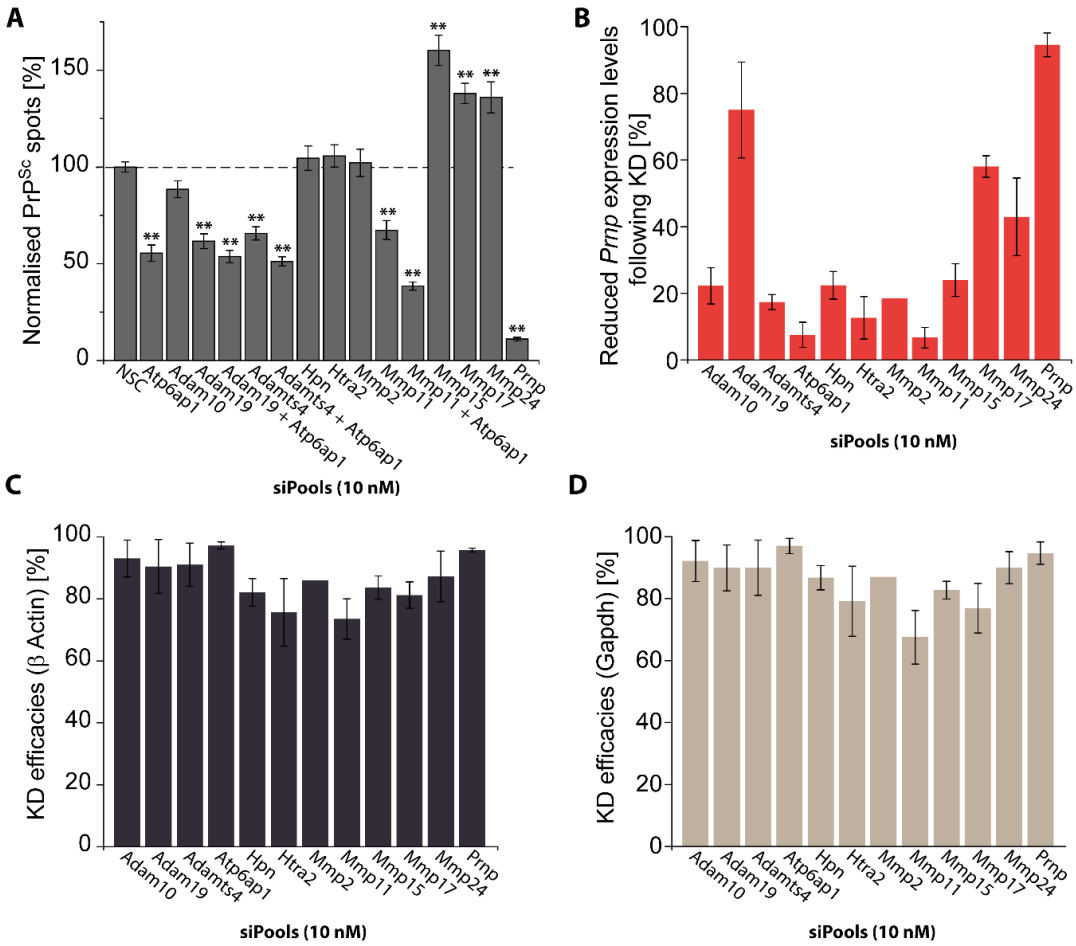

Figure 3.13: Proteases mediate infectivity of neuronal cells with extracellular PrP^D scaffolds. A) Uninfected S7 reporter cells, containing siRNA-lipofectamine complex against specific candidate genes were seeded onto infectious dECM (See **Section 2.11.2**). Cells were passaged twice, transferred onto ELISPOT plates and the number of PrP^{Sc}-infected cells were determined by Scrapie Cells Assay Section 2.3.2. Relative PrP^{Sc} spot counts, normalised to non-targeting controls, are shown. Data represent four independent repeats and standard error of the mean (SEM), ** = $p<0.0001$ (analysed using One Way Anova with Bonferonni corrections). **B)** Changes in *Prnp* gene expression levels of siRNA-treated cells in **A)**. Knockdown efficiencies of targeted genes were assessed using **C)** β-actin or **D)** GAPDH as the control genes. Three independent RT-qPCR experiments were performed for all gene targets in **B**, **C**, and **D**, except for *Mmp2* (single experiment), error bars represent standard deviation.

Silenced genes	Relative PrP^{Sc} spot count (%)	PrP^{Sc} spot count reduction (%)	PrP^{Sc} spot count increase (%)	p-value
NSC	100.0	n/a	n/a	n/a
Atp6ap1	55.5	44.5	-	p<0.001
Adam10	88.5	11.5	-	ns
Adam19	61.6	38.4	-	p<0.001
Adam19 + Atp6ap1	55.2	44.8	-	p<0.001
Adamts4	65.7	34.3	-	p<0.001
Adamts4 + Atp6ap1	51.2	48.8	-	p<0.001
Hpn	104.6	-	4.6	ns
Htra2	105.7	-	5.7	ns
Mmp2	102.1	-	2.1	ns
Mmp11	67.3	32.7	-	p<0.001
Mmp11 + Atp6ap1	38.5	61.5	-	p<0.001
Mmp15	160.2	-	60.2	p<0.001
Mmp17	138.0	-	38.0	p<0.001
Mmp24	136.0	-	36.0	p<0.001
Prnp	11.0	89.0	-	p<0.001

Table 3.3: Relative spot count changes when compared to non-silencing control (NSC) generated from Figure 3.13 A. Independent experiments were repeated four times. Analysis was done using One Way ANOVA with Bonferonni's correction. n/a = not available, ns = not signifcant.

Targeted genes	Decrease in *Prnp* expression levels		Decrease in expression levels of targeted genes with β-actin as control		Decrease in expression of targeted genes with GAPDH as control	
	Average	SD	Average	SD	Average	SD
Atp6ap1	7.5	3.8	97.2	1.2	97.0	2.5
Adam10	22.2	5.4	93.0	5.9	92.1	6.6
Adam19	75.0	14.4	90.4	8.7	89.9	7.4
Adamts4	17.3	2.3	91.0	7.0	89.9	8.9
Hpn	22.4	4.1	82.1	4.4	86.7	3.9
Htra2	12.6	6.4	75.6	10.9	79.1	11.3
Mmp2	#18.5	-	#86	-	#87	-
Mmp11	6.7	3.1	73.5	6.5	67.5	8.7
Mmp15	24.0	4.9	83.6	3.8	82.7	2.8
Mmp17	58.0	3.2	81.2	4.3	76.9	8.0
Mmp24	42.9	11.6	87.2	8.1	90.0	5.1
Prnp	94.6	3.6	95.7	0.6	94.7	3.6

Table 3.4: Gene expression levels of reverse transfected uninfected S7 reporter cells generated from Figure 3.13 B, C and D. % of changes in gene expression levels was conducted by RT-qPCR (3 independent experiment repeats). # refers to only 1 RT-qPCR dataset is available.

3.15 Bafilomycin treatment blocks infection of neuronal cells by extracellular prion scaffolds contact

We have provided evidence that proteases play a role in controlling infection of cells when in contact with extracellular PrP^D scaffolds (**Figure 3.13**). Notably, *Atp6ap1* play an important role in ECM-based prion infection. This gene encodes for the *Atp6ap1* protein, one of the components involved in the Vacuolar-ATPase (V-ATPase) pump. V-ATPases play a critical role in regulating lysosomal pH, ensuring a relatively low pH compared to the cytosol in order to activate ECM-degrading proteases. To test this, we treated unchallenged S7 reporter cells for 2 hours with increasing concentrations of bafilomycin A1, a potent V-ATPase pump inhibitor. The

concentrations tested were based upon a study that showed significant pH increase in Neuro2a cells using 100 nM bafilomycin A1 (Contu et al., 2023). We extended the range to see the limit where cells were able to tolerate the drug treatment by including 0 to 500 nM. Cells were then resuspended, transferred onto infectious dECM and grown to confluency. Cells were serially passaged three times to obtain P2, P3, and P4. Representative images (from P3) of S7 cells treated by bafilomycin A1 followed by dECM infection are shown in **Figure 3.14 A**, with noticeable drop in PrP^{Sc} spots as concentration of bafilomycin A1 is increased. This corroborates infectivity data of bafilomycin-treated S7 cells, shown in **Figure 3.14 B**. At 250 nM of bafilomycin A1 treatment, PrP^{Sc} spots were reduced approximately by 80%. However, a marked disparity in infection abrogation between Bafilomycin A1 and V-ATPase gene perturbation, to which resulted to a 45% decrease in infection, suggests the possibility of off-target effects pertaining to this pharmacological inhibitor. This is discussed further in **Section 4.3**. We excluded the data set of reporter S7 cells treated with 500 nM bafilomycin due to the toxic dosage that resulted in a decreased number of cells (**Figure 3.14 C**) as well as irregular morphological changes during routine cell check (done every 2 or 3 days) using light microscopy (results not shown).

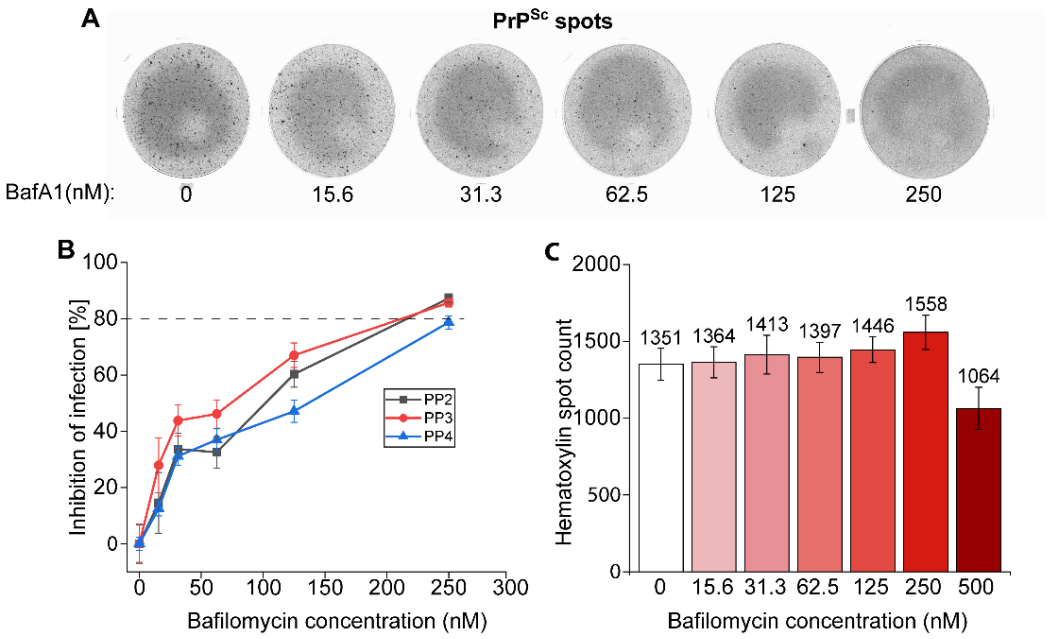

Figure 3.14: Blocking V-ATPase pump to perturb lysosomal enzyme maturation diminishes prion infectivity. Uninfected S7 cells were treated with increasing concentrations (0, 15.6, 31.3, 62.5, 125, or 250 nM) of bafilomycin A1 (Baf A1) for two hours, followed by resuspension and transfer onto infectious dECM wells (prepared according to **Section 2.4.1**). Cells were grown to confluency and serially passaged and subjected to SCA (see Section 2.3.1). **A)** Representative images of PrP^{Sc} spot counts taken at passage 3 (P3). **B)** % of PrP^{Sc} spots relative to mock-treated (DMSO vehicle), with 12 technical repeats for each group. **C)** Average number of cells treated with bafilomycin A1 at P2 (6 technical repeats per group). Error bars in **B)** and **C)** represent standard deviation.

4. Discussion

4.1 Project background

This project was set up to investigate the role of ECM remodelling in prion infection. To this end, we generated an infectious acellular bioscaffold that serves as a native microenvironment for susceptible cells. We further developed a highly efficient gene silencing protocol to perturb ECM-degrading peptidases. We show that Adam19, Adamts4, and Mmp11 are implicated in facilitating prion infection of reporter cells with infectious ECM scaffolds. This led us to target the V-ATPase complex, which is involved in the maturation of secreted proteases. We here show that proton pumps play a key role in mediating infection of reporter cells. Intriguingly, double-knockdown of genes pertaining to Mmp11 and Atp6ap1 led to a synergistic decrease in prion infection.

The context to this research enquiry stems from the presence of prion aggregates in the extracellular matrix (ECM). We recently found that aberrant PrP assemblies are tethered to the plasma membrane, and extend into the ECM (Ribes et al., 2022, preprint). These infectious conformers are sequestered in the biological scaffold, which is also the case for growth factors (G. S. Schultz & Wysocki, 2009; Wilgus, 2012) and extracellular vesicles, or otherwise known as matrix-bound vesicles (Huleihel et al., 2016). Biomaterials ‘entrapped’ in the extracellular meshwork are released into the interstitial space upon ECM degradation by endogenous proteases. Hence, since prions are embedded in the extracellular scaffold, would these infectious proteins be released upon matrix breakdown and infect cells? We

therefore presented evidence in this body of work to support our study model, visualised in **Figure 4.1.** Such mechanistic insight may inform therapeutic approaches, such as, targeting proteases that are implicated in promoting extracellular-oriented prion infection or generating ECM mimetics that can sequester and stabilise templating PrP aggregates. The implications of ECM remodelling in prion diseases have yet to be addressed. Part of the reason is due to the lack of a cell-free model of PrP amyloids. Decellularisation refers to the process of removing the cellular components of a scaffold while retaining the macrostructure and microstructure of the ECM (D. A. Taylor et al., 2020). Acellular matrices are typically used for tissue regeneration, although its applications have been extended to screen for drug treatments or identifying tumour-growth factors in cancer research (Dunne et al., 2014; Shologu et al., 2016; Wishart et al., 2020). Essentially, to investigate ECM-mediated prion infection, two critical setups were employed: A cell-free infectious ECM scaffold and candidate gene loss-of-function approach to target specific proteases. These core setups were accompanied with complementary experiments that further validate experimental outcomes.

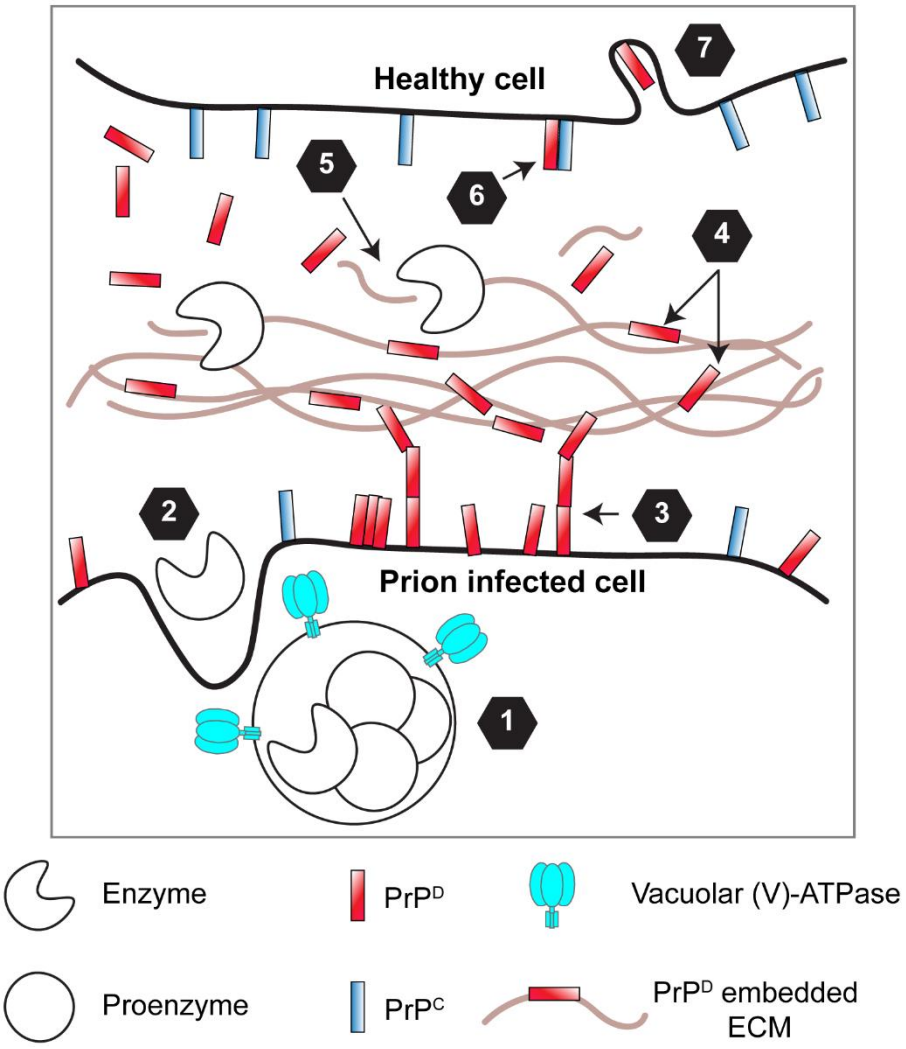

Figure 4.1: Proposed model for prion infection modulated by ECM remodelling. 1) V-ATPases acidifies lysosomes by translocating H^+ ions from the cytosol, facilitating enzyme maturation. **2)** Release of activated enzymes into the extracellular space. **3)** PrP^D extends from the cellular membrane into the extracellular mileu and **4)** binds to ECM components, forming PrP^D embedded ECM. **5)** Activated enzymes degrade prion infectious ECM, releasing PrP^D which infects healthy recipient cells by **6)** converting membrane-bound PrP^C into infectious PrP conformers and **7)** through internalisation via endocytic pathways.

4.2 Metalloproteases degrade prion-infected scaffolds, releasing infectious PrP assemblies

Through the perturbation of gene expression via transcriptional silencing, I have screened a panel of scaffold-altering proteases and discovered that Adam19, Adamts4, and Mmp11 were implicated in mediating infection stemming from prion-embedded ECM (**Figure 3.13 A**). The ECM-degrading peptidases were selected based on their relatively high expression levels in the S7 cells (more details in **Section 1.6**). Although most studies on prion-ECM interplay focuses on heparan sulfate (HS) as a ligand to abnormal PrP conformers (Adjou et al., 2003; Aguilar-Calvo et al., 2020; Ben-Zaken et al., 2003; Holmes et al., 2013; Horonchik et al., 2005; McBride et al., 1998; Motamedi-Shad, Monsellier, Torrasa, et al., 2009; Snow et al., 1990), none of the screened enzymes were capable of degrading this heavily sulfated glycosaminoglycan. However, this does not exclude that prions may interact with other ECM components as well.

As mentioned, transcriptional silencing of *Mmp11* resulted in significant reduction in infection through prion-positive ECM contact (**Figure 3.13 A**). The stromelysins (MMP3, MMP10, MMP11) are known to degrade fibronectin, laminin, and proteoglycans (Vincenti & Brinckerhoff, 2007). MMP11 plays a key role in remodelling fibronectin-based ECM. Breast cancer patients exhibiting fibronectin expression in breast cancer cells, in conjunction with MMP11 expression in mononuclear inflammatory cells (MICs), have a significantly higher likelihood of developing distant metastases. Conversely, patients who lack both fibronectin expression in tumour cells and MMP11 expression in MICs are less likely to develop

distant metastases (Fernandez-Garcia et al., 2014). Indeed, fibronectin 1 (FN1) expression levels are also elevated in prion-resistant cells, whereas susceptible cells express low amounts of FN1. Intriguingly, gene knockdown of *FN1* in prion-resistant cells resulted in a susceptible phenotype to scrapie infection (Marbiah et al., 2014). This corroborates our finding that *Mmp11* knockdown causes a significant decrease in extracellular scaffold-based infection.

We have also discovered that Adamts4 is involved in facilitating infection through prion-embedded scaffold contact (**Figure 3.13 A**). Although Adamts4 has been widely studied in the context of osteoarthritis (Glasson et al., 2004; Li et al., 2014; Majumdar et al., 2007; Verma & Dalal, 2011; Xue et al., 2013; Zhao et al., 2022) and spinal cord injury (Delarue et al., 2020; Demircan et al., 2014; Griffin et al., 2020; Lemarchant et al., 2014; Tauchi et al., 2012), literature on its direct or indirect interactions with prions is lacking. Adamts4 is known to degrade various CSPGs, including aggrecan, brevican, neurocan, and versican (Rose et al., 2021). Overexpression of *ADAMTS4* has been associated with ECM-altering conditions including lung microenvironment modification to promote immune cell migration (Boyd et al., 2020) and extracellular scaffold remodelling in cardiac fibrosis (Khanam et al., 2022). Currently, there is no evidence on Adamts4 capable of cleaving PrP^{C} or its rogue form, PrP^{D}. Therefore, considering the decellularised model used in this study, it is likely that Adamts4 is involved in mobilising prions that are bound to the ECM. It is worth noting that future studies should focus on the interaction between prions and substrates of Adamts4, namely, CSPGs.

As opposed to the secreted ADAMTS4 and MMP11, ADAM19 is a membrane-bound proteinase. ADAM19 is an endopeptidase that is involved in shedding growth factors and cytokines such as neuregulins, heparin-binding epidermal growth factor, and tumor necrosis factor (TNF)-α (Qi et al., 2009). It was also found to promote prion infection from dECM contact (**Figure 3.13 A**). In 2019, Peixoto and colleagues demonstrated that ADAM19 is upregulated in several distinct epithelial-mesenchymal transition (EMT) cell models, and the same outcome was observed *in vivo* (Peixoto et al., 2019). For context, EMT is a process involving ECM remodelling through regulation of ECM components and degradation of the core matriosome by upregulating enzyme-digesting bioscaffolds (Scott et al., 2019). It plays a crucial role in important biological processes including embryonic development, wound healing, and fibrosis (Boyer et al., 1999; Kalluri & Neilson, 2003; Marconi et al., 2021). Interestingly, inhibition of ADAM19 using miR-145 mimetic resulted in the repression of EMT in glioblastoma cells (X. Wang et al., 2017). This suggests that ADAM19 is involved in ECM remodelling, although it is not known whether ADAM19 cleaves stereotypic extracellular components such as collagen and proteoglycans. However, we discovered that silencing *Adam19* led to a 75% decrease in the *Prnp* gene expression of S7 cells. Currently, there is a lack of literature elucidating the gene regulatory mechanism between *Adam19* and *Prnp*. Regardless, such outcome may be the cause of significant drop in infectivity in *Adam19*-silenced S7 cells. More work needs to be done to further validate whether infection was reduced due to abrogated Adam19 activity on infectious dECM or simply because of a decreased in *Prnp* expression levels.

Interestingly, gene silencing of membrane-bound MMP15, 17, or 24 led to an increased in infection following contact with prion-infected scaffold. Due to the localisation of these membrane-bound enzymes, it can be speculated that these proteases shed surface PrP^{C}, which is the case for the membrane-anchored ADAM10. Indeed, mice devoid of ADAM10 in the forebrain, which is a known PrP sheddase (D. R. Taylor et al., 2009), significantly reduced the disease onset and increased PrP^{Sc} formation (Altmeppen et al., 2015), as its depletion may result to a posttranslational increase of PrP^{C} substrates. Hence, we speculated that membrane-bound MMP15, MMP17, and MMP24 are PrP sheddases. However, we observed no significant changes in infectivity following Adam10 loss-of-function in dECM-infected reporter cells, possibility due to the lack of a complex *in vivo* microenvironment in the generated cell-derived matrices. Unfortunately, I was not able to confirm whether these MMPs are indeed PrP sheddases due to time constraints. Future experiments such as confocal microscopy to confirm changes in membrane-bound PrP signal and quantitation of shed PrP in cell supernatant following gene perturbation could provide evidence on prospective PrP sheddases.

Intriguingly, although the gene knockdown of *Mmp17* resulted in a ~40% increase in infection (**Figure 3.13 A** & **Table 3.3**), it was also observed that the *Prnp* expression level was decreased by approximately 60% (**Figure 3.13 B** & **Table 3.4**). This is unexpected as a reduction in *Prnp* expression should abrogate infection rather than promote it. A limitation to interpret this discrepancy is the lack of a scrambled shRNA control, as such a control can ascertain whether the observed reduction in *Prnp* expression is specific to

Mmp17 knockdown or a general consequence of gene silencing. This control will establish a baseline for any potential variations in *Prnp* expression caused by experimental manipulations, thus enhancing the reliability and interpretation of our results.

4.3 V-ATPase promotes extracellular prion infection

In this thesis, I have demonstrated that the inhibition of functional V-ATPases led to the reduction of ECM-based prion infection, which suggests that V-ATPase activity exacerbates prion infection. Following gene perturbation of *Atp6ap1*, which encodes for a component involved in the assembly of proton pumps, almost half (45%) of PrP^{Sc} positive spot counts were reduced compared to non-silencing controls (**Figure 3.13 A**). To further confirm the functional role of V-ATPases in mediating extracellular prion infection, we treated uninfected S7 cells with bafilomycin A1, a potent inhibitor of V-ATPase pumps (R. Wang et al., 2021), followed by infection onto prion-containing scaffolds. As expected, inhibiting V-ATPases had a dose-dependent effect on prion infection, with the highest treatment efficacy being 80% reduction in infectivity at 250 nM concentration (**Figure 3.14 B**). This suggests a crucial role of V-ATPases in blocking prion infection.

V-ATPases are involved in maturing lysosomal enzymes that mobilise scaffold-entrapped biomaterials such as growth factors and nanovesicles (Huleihel et al., 2016; G. S. Schultz & Wysocki, 2009). By perturbing functional V-ATPases, we demonstrated that proton pumps are instrumental in mediating prion infection resulted from scrapie-infected ECM contact. This

suggests that V-ATPase-dependent peptidases are implicated in mobilising prions sequestered in the bioscaffold. These peptidases include secreted ECM-degrading cathepsins, such as cathepsin B (CTSB), -D (CTSD), and -L (CTSL), which are implicated in neurodegenerative proteopathies (Yadati et al., 2020). Indeed, the aforementioned 3 cathepsins are the most ubiquitously expressed among all lysosomal proteases (Vidoni et al., 2016; Yadati et al., 2020), and they are predominantly found in the CNS (Nakanishi, 2020; Repnik et al., 2012; Vidoni et al., 2016). CTSB and CTSL are upregulated in scrapie-infected mouse neuro2a cells (Zhang et al., 2003), and was shown to increase PrP^{Sc} levels when CTSB or CTSL is pharmacologically inhibited (Luhr et al., 2004). It is speculated that CTSB and CTSL are involved in the second autocatalytic loop of PrP^{Sc} formation, which involves breaking down large prion aggregates into smaller PrP assemblies that are more readily transmissible. In contradiction, the latter study also showed that silencing genes encoding for CTSB or CTSL led to a somewhat decrease levels of PrP^{Sc}, however this dataset was not quantified, only representative immunofluorescence and immunoblotting images were shown (Luhr et al., 2004). The *CTSD* gene is upregulated in scrapie sick mice, and genetic polymorphism of this gene is observed in sCJD patients (Bishop et al., 2008; Kovacs et al., 2010). CTSD is implicated in cleaving the GPI-anchor of PrP^{Sc}, but does not influence prion infectivity (P. A. Lewis et al., 2006). Overall, current evidence suggests that secreted V-ATPase-dependent lysosomal enzymes are implicated in prion diseases, however, the underpinning machinery is yet to be unravelled. However, although the results for silencing *Atp6ap1* (**Figure 3.13 A** & **Table 3.3**), a component of V-

ATPase, positively correlated with bafilomycin A1 treatment (**Figure 3.14 B**), a potent V-ATPase inhibitor, we observed a marked difference in blocking infection (45% vs 80%, respectively). Bafilomycin A1 is widely known for targeting V-ATPases (R. Wang et al., 2020, 2021; Yoshimori et al., 1991), affecting lysosomal acidification and consequently influencing the activation of matrix-degrading enzymes, however, it also blocks the formation of autophagosome-lysosome fusion (Yamamoto et al., 1998). This may aftect the rate of nascent PrP^{Sc} formation within newly infected cells, as infectious PrP seeds are also found in this vesicle (Marzo et al., 2013). However, no study in particular has focused on the off-target effects of Bafilomycin A1 in prion infection, suggesting a need for such research.

4.4 Infectious cell-derived matrices: A useful tool to investigate prion infection from bioscaffold contact

Presence of aberrant PrP conformers in the extracellular microenvironment have been reported in numerous studies (Jankovska et al., 2021; Jeffrey et al., 2011; Jeffrey & González, 2007; Marbiah et al., 2014; Van Everbroeck et al., 2004; D. Xu & Esko, 2014). Extracellular prions interact with ECM components such as heparan sulfates and laminin, thereby rendering the ECM as a buffer that sequesters abnormal PrP aggregates. Indeed, this has led to the use of polysulfated anions, including of heparan mimetics (HMs), to bind and abrogate prion propagation (Adjou et al., 2003; Hijazi et al., 2005; Schonberger et al., 2003). This piqued our interest as ECM remodelling releases entrapped bioactive substances, such as nanovesicles and growth factors, that influence cellular processes (Huleihel et al., 2016; Hussey et al.,

2020; G. S. Schultz & Wysocki, 2009). Hence, this led to the development of a decellularised model that enabled us to investigate prion infection originating from the ECM.

Infectious acellular scaffolds were prepared after flushing adherent prion-infected iS7 cells from the substrate by using sterile water. PrP^{D} aggregates were observed *in situ*, along with ECM components such as Collagen IV and CSPG4. However, due to restriction of time, I was not able to quantify the difference between pre- and postdecellularisation. This information will allow us to observe the efficiency of decellularisation whilst retaining PrP^{D} in the dECM. The decellularisation protocol did not produce retained membrane-bound PrP^{D} in the dECM, as integrin B1 (a membrane marker) immunostaining was negative during the pilot work (results not shown).

In **Figure 3.8 C**, we show that the average PrP^{Sc} spot count of dECM derived from infected iS7 cells reached saturation at approximately 1500 spot counts. In the standard SCA, each spot count represents a PrP^{Sc} positive cell. In our cell culture system, a confluent well could have more than ~70,000 cells or spots, as observed on processed ELISPOT plates. In this study, we grew the cells to confluency prior to decellularisation on ELISPOT plates. Consequently, the approximate average of 1500 PrP^{Sc} positive spot counts in **Figure 3.8 C** does not reflect the extent of infected dECM spots generated, but rather the upper limit of the system for defining a spot. As shown in **Figure 3.6 A**, infected cells need to grow for 5 days to allow deposition of ECM-bound prions. Following 5 days of growth, cells become confluent, rendering us unable to quantify spots between 20 (background) to

1200 (upper linear limit). This is not an issue for the standard SCA as resuspended cells are diluted prior to plating onto ELISPOT plates to avoid oversaturation. To circumvent this issue regarding oversaturated dECM PrP^{Sc} spots, a mixture of N2a-*Prnp*$^{-/-}$ cells and infected iS7 cells could attenuate oversaturation of PrP^{Sc} spots, although a mixed culture may contribute to confounding factors that could affect prion propagation and subsequently influencing prion-embedded ECM deposition.

Infectivity of the decellularised material was confirmed by seeding susceptible reporter cells onto iS7-dECM. Our SCA data demonstrates that the infectivity of the developed dECM was comparable to RML brain homogenate at the dilution of 3×10^{-5} (**Figure 3.8 A**). The presence of *bona fide* prions was verified following the death of scrapie sick mice when inoculated with S7 reporter cells infected using dECM (**Figure 3.9 C**). These findings highlight the significant role of the ECM in mediating extracellular infection in neuronal cells.

The development of an infectious non-cellular matrix allowed us to proceed with gene perturbation techniques to investigate the consequence of ECM remodelling in prion diseases. However, it is worth noting that in this study, reverse transfection was done in parallel with infection, as prion-embedded scaffold is readily attached on the surface. Hence, we should interpret the results with caution, as the gene silencing treatment may not be in ‘full swing’ to influence infectivity. To counteract this limitation, we tested several procedures to achieve optimal knockdown efficiencies. We compared against procedures that involves transcriptional silencing cells prior to transfer onto

infectious dECM. To our surprise, we found that the most effective approach involved treating cells concurrently with siRNAs (targeting the *Prnp* gene as a control) and infecting them on prion-embedded dECM. This resulted in the largest reduction in infection when compared to other tested procedures.

Nonetheless, the development of the acellular scaffold led to a series of experiments that allowed us to screen for prospective proteases involved in promoting ECM-based prion infection. This model is superior to synthetic matrices due to its deposition of a wide range of ECM proteins. The cell-derived matrices are easy to generate, labour-efficient, and cost-effective compared to decellularising whole organs for the same purpose, making them highly scalable and suitable for high throughput screening. However, this model has some limitations, such as limited physical contact between seeded reporter cells and substrate-bound dECM. Whole organ scaffolds, in contrast, allow seeded cells to interact with the core matrisome from various angles and offer a complex composition and structure that more closely resembles native tissue.

4.5 Internalisation of extracellular prion aggregates

The modification of the ECM requires proteolytic processing of ECM-resident proteins by peptidases. Our data indicates entrapped prions are mobilised and infect susceptible cells. To investigate this mechanism, we employed N2a-*Prnp*$^{-/-}$ cells to probe for abnormal PrP aggregate uptake from infectious dECM. Although it is more biologically relevant to use *Prnp*-expressing cells for this purpose, our attempts were unsuccessful as it is challenging to

distinguish *de novo* endogenous PrP signals from internalised extracellular PrP^D aggregates.

We have also opted for PrP-Myc tagged cells to allow the distinction between nascent PrP^D formation and inoculum, which refers to the prion aggregate originating from the infectious dECM. Essentially, immunofluorescent signals pertaining to newly formed PrP^D should be positive against anti-PrP and anti-Myc antibodies, whereas the inoculum should only be immunopositive against anti-PrP antibodies (Goold et al., 2011). However, the uninfected PrP-Myc tagged cells exerted a relatively strong immunofluorescence signal of PrP and Myc (results not shown), leading to false positive outcomes. This led to our decision to use *Prnp*-ablated reporter cells to study mobilisation and internalisation of prions bounded to the ECM, as the use of cells devoid of PrP eliminates the uncertainty of endogenous PrP signals. However, the main limitation of using *Prnp*-ablated reporter cells is the absence of infectious seed replication machinery that is observed in prion-susceptible cells. Although we were not successful in utilising PrP-Myc tagged cells in our experiment, it is possible to generate a subclone that does not exert highly intense Myc/PrP immunofluorescence. This is due to the difference in gene expression in different single colonies (Marbiah et al., 2014), which may affect the aggregation state and localisation of chimeric Myc-PrP. Since subcloning is a laborious and time-consuming method, I was not able to proceed with this experiment due to the restricted project timeframe.

Although a tagged PrP system is beneficial in tracking formation and localisation of aberrant *de novo* PrP aggregates, caution must be taken when

studying the endocytic route of seed uptake, as conformation of amyloids influences the internalisation pathways. For instance, (Barmada & Harris, 2005; Bian et al., 2006), different prion strains, such as RML and 22L, consists of distinctive conformational determinants (Hoyt et al., 2022), which ultimately affects the endocytic routes (Fehlinger et al., 2017).

Regardless, the use of cell-free scaffolding constitutes a new experimental approach to study internalisation of extracellular prion aggregates. This model is unique since most studies investigating abnormal PrP uptake utilises brain homogenates from terminally scrapie-sick animals (Borchelt et al., 1992; Veith et al., 2009; Yamasaki et al., 2014; Yim et al., 2015). These brain lysates contain a repertoire of prions associated with numerous cellular or acellular compartments, including extracellular vesicles, plasma membrane, intracellular organelles, and the matriosome, whereas this model is focused on ECM-associated prions only. Therefore, I argue that the development of cell-derived matrices to study prion diseases is an unmet need to understand the complex cell-ECM interplay during infection. In fact, this could also be used in other extracellular (or at least partly) proteinopathies with prion-like mechanisms including Alzheimer's disease (Sun et al., 2021) and Lewy Body diseases (Lee et al., 2014).

Considering the restricted project timeframe, I was only able to demonstrate the uptake of prions from the deposited infectious matrices. Experiments involving perturbation of endocytic pathways will be conducted in the future as it provides us valuable insights on extracellular prion uptake. Nonetheless, we observed that following 8 hours of incubating N2a-*Prnp*$^{-/-}$ cells onto

infectious dECM, 7% of cells contain PrP^D aggregates tethered to its membrane, whereas 4.5% of cells had intracellular PrP inclusions. Only a minute fraction, 1% of the entire culture population had both membrane-affiliated and intracellular PrP^D immunopositivity. However, following 24 hours of incubation, we observed a quarter of the cells contain intracellular PrP aggregates, while surface-bound PrP^D was only positive in 7.5% of cells, similar to the 8-hour incubation timepoint. Cells that contained both membrane-bound and intracellular PrP assemblies increased from 1% at 8 hours incubation, to 7% at 24 hours post-seeding (**Figure 3.11 A, B**). Overall, this suggests that cells were capable of degrading prion-embedded ECM and assimilate its dismantled constituents in a timely manner. However, future experiments should include treating the N2a-*Prnp*$^{-/-}$ cells with retinoic acid to inhibit proliferation (G. Wolf, 2008), as cell division may increase the amount of PrP^D-positive cells. Further validation such as the use of a live phase-contrast imaging is encouraged to confirm cell division is effectively halted.

Other than prion uptake, we also observed an interesting outcome where internalised PrP^D aggregates are always N-terminally cleaved. PrP^D are endogenously truncated at residue 89/90 to form the C2 fragment (Kovač & Šerbec, 2022). By using immunofluorescence, we were able to identify full length or truncated PrP^D through the use of two antibodies; 5B2 and 6D11, which targets the N-terminus and the core region of PrP, respectively. Merged signals of 5B2 and 6D11 indicates full length PrP^D, whereas sole 6D11 positivity labels a truncated determinant of PrP^D. Indeed, these antibodies label the physiological form of PrP as well, however, it can be

differentiated from PrP^D due to its relatively low signal intensity. Reporter cells seeded onto non-infectious dECM showed no visible internalised PrP signals. Nevertheless, we observed that the earliest incubation timepoint (8h) on infectious scaffolding, internalised extracellular aggregates are always 6D11-positive and 5B2-negative, indicating the presence of truncated PrP aggregates. Meanwhile, extracellular prion aggregates that colocalise at the cell periphery are full length in nature. Earlier timepoints were not possible due to the lack of proper cell adhesion on the substrate. Therefore, this suggests that internalised prions are cleaved, at most, a few hours following internalisation. This gives us a better understanding on the proteolytic processing of endocytosed aberrant PrP conformers. Future experiments targeting specific proteases may identify the peptidases involved in the truncation of internalised PrP^D. However, studies on proteolytic processing of prions suggest that truncation of full length PrP^D is strongly cell or tissue-dependent. For example, immunoblots of scrapie-infected Rov cells (epithelial cell lineage), MoVs cells (immortalized Schwann cells), and spleen tissue lysates contained predominantly truncated species of PrP^D, while primary neurons and astrocytes derived from scrapie-sick mice, along with prion-infected brain homogenates, displayed mostly full-length PrP^D bands on immunoblots (Dron et al., 2010). Therefore, future experiments aimed at delineating the endogenous cleavage of prions using infectious dECM should compare the results obtained from different types of reporter cells. To confirm the proteolytic actions of PrP^D truncation, complementary experiments such as Western blots or mass spectrometry should be

conducted. Taken together, the use of prion-infected acellular matrices is crucial in expanding our knowledge of extracellular prion spread.

4.6 Future studies

In this thesis, we show that ECM remodelling enzymes play a key role in modulating prion infection. In doing so, we have developed a novel infectious decellularised bioscaffold that serves as an investigative tool to identify peptidases involved in ECM-based prion infection. The use of this acellular model can enhance our understanding on cell-ECM interplay in prion diseases. In particular, infectious acellular matrices can be utilised to study the release of ECM-sequestered prions upon treatment with cell-derived or recombinant peptidases. This can be done by testing the presence of PrP^{Sc} in the supernatant of peptidase-treated decellularised ECM (dECM) through immunoblotting. Release of infectious particles can be determined by incubating susceptible cells with the supernatant sample, followed by infectivity titer determination using Scrapie Cell Assay (Klohn et al., 2003). Presence of *bona fide* prions can be confirmed by inoculating wild type mice, typically through intracerebral injection. The experimental group should succumb to scrapie sickness relatively earlier than mice injected with non-peptidase treated supernatant of infectious dECM. However, it is worth to note that these samples may contain low amounts of infectious prion seeds, leading to a significant delay in the disease onset. Hence, prior to inoculation, it is recommended to concentrate insoluble prion aggregates via centrifugation with phosphotungstic acid, a commonly used reagent to

precipitate abnormal PrP aggregates (D'Castro et al., 2010; Glatzel et al., 2003; Huang et al., 2005; Saá et al., 2006; Tennant et al., 2020; Wenborn et al., 2015; Wroe et al., 2006).

This thesis also provides valuable insights on the role of V-ATPases in mediating extracellular prion infection. Hence, the same experimental paradigm should also be applied on V-ATPase dependent lysosomal enzymes, or better known as acid hydrolases. For context, the V-ATPase pump is involved in maintaining the acidic environment in lysosomes, which in turn activates zymogens prior to its release to the interstitial space and consequently degrades the extracellular bioscaffold (Tancini et al., 2020). However, it should be noted that there are more than 60 lysosomal enzymes (Bouhamdani et al., 2021), which a great majority are dependent on functional V-ATPases. Interestingly, secreted V-ATPase dependent CTSB, CTSD, and CTSL are implicated in prion diseases (Bishop et al., 2008; Kovacs et al., 2010; Luhr et al., 2004; Zhang et al., 2003), which further supports that these peptidases are viable candidates in promoting extracellular-oriented prion infection.

The development of ECM-bound PrP^{D} also enables the investigation of extracellular prion endocytic routes. This is crucial in understanding how cells internalise prions from their surrounding matrices, leading to infection and pathological spread. The main question in hand is; to what extent does prion internalisation contribute to infection as opposed to mere physical contact against aberrant PrP assemblies? Answering this question helps us to further understand the pathological pathways of abnormal PrP conformers, possibly

offering us more prospective targets to block infection. To answer this query, endocytic pathways of cells infected onto prion-embedded ECM should be blocked by transcriptional silencing, or through the use of target-specific pharmacological inhibitors. These reporter cells are then subjected for immunocytochemistry and examined under a confocal microscope. Multiple image panels should be taken, with about 10 cells per image. Image analysis software such as ImageJ should be used to segregate and quantify PrP^{D}-positive cells. Cell groups that contain significantly lower rates of internalised PrP^{D} suggest that endocytic route X, for example, macropinocytosis, is critical in taking up extracellular prion aggregates. Once the internalisation route is determined, it would be interesting to include perturbation of protease-encoding genes that has been validated with the suggested experiments. Taken together, this creates a comprehensive view on prion release from the ECM, followed by its uptake into reporter cells. This will offer researchers prospective therapeutic targets against prion diseases.

In terms of the decellularised model itself, it can be improved by using a more biologically relevant scaffold; decellularised brain matrices (DBM). However, it is worth to mention that DBM is not feasible to generate relative to dECM, as it involves animal life stock maintenance and a lengthy decellularisation protocol (~24 hours) (Granato et al., 2020), as compared to *in vitro* cell-derived dECM which takes about 20 to 30 minutes (**Section 2.4.1**). Putting the disadvantages aside, this model will offer a more complex and realistic interaction between cells and ECM, compared to acellular matrices derived from immortalised cell lines. The decellularised brain scaffolds generated by Granato and colleagues were also successfully

repopulated with seeded neuro2a cells, suggesting essential ECM components were retained to support cell attachment and cell growth (Granato et al., 2020). Consequently, we aim to apply this procedure to scrapie-sick mice and load the generated DBMs with S7 cells, either with a gene knockout or overexpression of the gene of interest. This enables us to investigate ECM-based prion infection using a biologically relevant acellular scaffold.

4.7 Concluding remarks

Based on the data presented, I have demonstrated that ECM-degrading proteases play a crucial role in facilitating extracellular prion infection. By silencing genes encoding for ECM-degrading enzymes, I have identified Adam19, Adamts4, and Mmp11 as specific proteases involved in exacerbating extracellular prion infection. Additionally, I found that V-ATPases, crucial components for intracellular and extracellular peptidase maturation, also played a critical role in facilitating ECM-based prion infection. Targeting of both, V-ATPase and Mmp11, reduced prion infection synergistically. Further, I showed that ECM-sequestered prions can be taken up by cells in a time-dependent manner. Notably, these experiments were only possible because of the development of the infectious dECM, which contained *bona fide* prions that caused scrapie sickness in mice. Importantly, our focus on prion infection stemming from prion-embedded ECM has unveiled new insights on the duration of disease onset and its progression. The revelation of proteases as key players in prion diseases opens up

avenues for potential therapeutic interventions aimed at blocking infection, potentially delaying disease onset and slowing disease progression. This study model may also be applied in other research areas where extracellular prion-like aggregates are relevant, such as senile plaques in Alzheimer's disease, underscoring its importance in future research endeavours.

References

Abounit, S., Bousset, L., Loria, F., Zhu, S., Chaumont, F., Pieri, L., Olivo-Marin, J., Melki, R., & Zurzolo, C. (2016). Tunneling nanotubes spread fibrillar α-synuclein by intercellular trafficking of lysosomes. *The EMBO Journal*, *35*(19). https://doi.org/10.15252/embj.201593411

Abounit, S., Wu, J. W., Duff, K., Victoria, G. S., & Zurzolo, C. (2016). Tunneling nanotubes: A possible highway in the spreading of tau and other prion-like proteins in neurodegenerative diseases. *Prion*, *10*(5). https://doi.org/10.1080/19336896.2016.1223003

Adjou, K. T., Simoneau, S., Salès, N., Lamoury, F., Dormont, D., Papy-Garcia, D., Barritault, D., Deslys, J. P., & Lasmézas, C. I. (2003). A novel generation of heparan sulfate mimetics for the treatment of prion diseases. *Journal of General Virology, 84*(9). https://doi.org/10.1099/vir.0.19073-0

Admyre, C., Johansson, S. M., Qazi, K. R., Filén, J.-J., Lahesmaa, R., Norman, M., Neve, E. P. A., Scheynius, A., & Gabrielsson, S. (2007). Exosomes with Immune Modulatory Features Are Present in Human Breast Milk. *The Journal of Immunology*, *179*(3). https://doi.org/10.4049/jimmunol.179.3.1969

Aguilar-Calvo, P., Sevillano, A. M., Bapat, J., Soldau, K., Sandoval, D. R., Altmeppen, H. C., Linsenmeier, L., Pizzo, D. P., Geschwind, M. D., Sanchez, H., Appleby, B. S., Cohen, M. L., Safar, J. G., Edland, S. D., Glatzel, M., Nilsson, K. P. R., Esko, J. D., & Sigurdson, C. J. (2020). Shortening heparan sulfate chains prolongs survival and reduces parenchymal plaques in prion disease caused by mobile, ADAM10-cleaved prions. *Acta Neuropathologica*, *139*(3). https://doi.org/10.1007/s00401-019-02085-x

Alais, S., Simoes, S., Baas, D., Lehmann, S., Raposo, G., Darlix, J. L., & Leblanc, P. (2008). Mouse neuroblastoma cells release prion infectivity associated with exosomal vesicles. *Biology of the Cell*, *100*(10). https://doi.org/10.1042/bc20080025

Alonso-Nocelo, M., Raimondo, T. M., Vining, K. H., López-López, R., De La Fuente, M., & Mooney, D. J. (2018). Matrix stiffness and tumor-Associated macrophages modulate epithelial to mesenchymal transition of human adenocarcinoma cells. *Biofabrication*, *10*(3). https://doi.org/10.1088/1758-5090/aaafbc

Alpers, M. P. (2008). Review. The epidemiology of kuru: Monitoring the epidemic from its peak to its end. *Philosophical Transactions of the Royal Society B: Biological Sciences*, *363*(1510). https://doi.org/10.1098/rstb.2008.0071

Altmeppen, H. C., Prox, J., Krasemann, S., Puig, B., Kruszewski, K., Dohler, F., Bernreuther, C., Hoxha, A., Linsenmeier, L., Sikorska, B., Liberski, P. P., Bartsch, U., Saftig, P., & Glatze, M. (2015). The sheddase ADAM10 is a potent modulator of prion disease. *ELife*, *2015*(4). https://doi.org/10.7554/eLife.04260

Altmeppen, H. C., Prox, J., Puig, B., Kluth, M. A., Bernreuther, C., Thurm, D., Jorissen, E., Petrowitz, B., Bartsch, U., De Strooper, B., Saftig, P., & Glatzel, M. (2011). Lack of a-disintegrin-and-metalloproteinase ADAM10 leads to intracellular accumulation and loss of shedding of the cellular prion protein in vivo. *Molecular Neurodegeneration*, *6*(1). https://doi.org/10.1186/1750-1326-6-36

Altmeppen, H. C., Puig, B., Dohler, F., Thurm, D. K., Falker, C., Krasemann, S., & Glatzel, M. (2012). Proteolytic processing of the prion protein in health and disease. In *American Journal of Neurodegenerative Diseases, 1*(1). https://doi.org/10.1080/19336896.2016.1223003

Apetri, A. C., Maki, K., Roder, H., & Surewicz, W. K. (2006). Early intermediate in human prion protein folding as evidenced by ultrarapid mixing experiments. *Journal of the American Chemical Society*, *128*(35). https://doi.org/10.1021/ja063880b

Asante, E. A., Linehan, J. M., Desbruslais, M., Joiner, S., Gowland, I., Wood, A. L., Welch, J., Hill, A. F., Lloyd, S. E., Wadsworth, J. D. F., & Collinge, J. (2002). BSE prions propagate as either variant CJD-like or sporadic CJD-like prion strains in transgenic mice expressing human prion protein. *EMBO Journal*, *21*(23). https://doi.org/10.1093/emboj/cdf653

Barbosa, M. A., & Martins, M. C. L. (2017). Chapter 2: Extracellular matrix constitution and function for tissue regeneration and repair, Peptides and Proteins as Biomaterials for Tissue Regeneration and Repair. In *Peptides and Proteins as Biomaterials for Tissue Regeneration and Repair*. https://doi.org/10.1016/C2015-0-01811-1

Barmada, S. J., & Harris, D. A. (2005). Visualization of prion infection in transgenic mice expressing green fluorescent protein-tagged prion protein. *Journal of Neuroscience*, *25*(24). https://doi.org/10.1523/JNEUROSCI.1192-05.2005

Bartlett, W., Gooding, C. R., J Carrington, R. W., Skinner, J. A., R Briggs, T. W., & Bentley, G. (2005). Autologous chondrocyte implantation at the knee using a bilayer collagen membrane with bone graft A PRELIMINARY REPORT. *THE JOURNAL OF BONE AND JOINT SURGERY*, *87*(3). https://doi.org/10.1302/0301-620x.87b3.15552

Basad, E., Wissing, F. R., Fehrenbach, P., Rickert, M., Steinmeyer, J., & Ishaque, B. (2015). Matrix-induced autologous chondrocyte implantation (MACI) in the knee: clinical outcomes and challenges. *Knee Surgery,*

Sports Traumatology, Arthroscopy, *23*(12), 3729–3735. https://doi.org/10.1007/s00167-014-3295-8

Basler, K., Oesch, B., Scott, M., Westaway, D., Wälchli, M., Groth, D. F., McKinley, M. P., Prusiner, S. B., & Weissmann, C. (1986). Scrapie and cellular PrP isoforms are encoded by the same chromosomal gene. *Cell*, *46*(3). https://doi.org/10.1016/0092-8674(86)90662-8

Baumann, F., Tolnay, M., Brabeck, C., Pahnke, J., Kloz, U., Niemann, H. H., Heikenwalder, M., Rülicke, T., Bürkle, A., & Aguzzi, A. (2007). Lethal recessive myelin toxicity of prion protein lacking its central domain. *EMBO Journal*, *26*(2). https://doi.org/10.1038/sj.emboj.7601510

Beck, E., Daniel, P. M., Alpers, M., Gajdusek, D. C., & Gibbs, C. J. (1966). Experimental “kuru” in chimpanzees. A pathological report. *Lancet*, *2*(7472). https://doi.org/10.1016/s0140-6736(66)92031-9

Begué, C., Martinetto, H., Schultz, M., Rojas, E., Romero, C., D’Giano, C., Sevlever, G., Somoza, M., & Taratuto, A. L. (2011). Creutzfeldt-Jakob disease surveillance in Argentina, 1997-2008. *Neuroepidemiology*, *37*(3–4). https://doi.org/10.1159/000331907

Beller, J. A., & Snow, D. M. (2014). Proteoglycans: Road signs for neurite outgrowth. *Neural Regeneration Research*, *9*(4). https://doi.org/10.4103/1673-5374.128235

Bellingham, S. A., Coleman, B. M., & Hill, A. F. (2012). Small RNA deep sequencing reveals a distinct miRNA signature released in exosomes from prion-infected neuronal cells. *Nucleic Acids Research*, *40*(21). https://doi.org/10.1093/nar/gks832

Benarroch, E. E. (2015). Extracellular matrix in the CNS. Dynamic structure and clinical correlations. *Neurology*, *85*(16). https://doi.org/10.1212/WNL.0000000000002044

Ben-Zaken, O., Tzaban, S., Tal, Y., Horonchik, L., Esko, J. D., Vlodavsky, I., & Taraboulos, A. (2003). Cellular heparan sulfate participates in the metabolism of prions. *Journal of Biological Chemistry*, *278*(41). https://doi.org/10.1074/jbc.M301152200

Bessen, R. A., & Marsh, R. F. (1992). Biochemical and physical properties of the prion protein from two strains of the transmissible mink encephalopathy agent. *Journal of Virology*, *66*(4). https://doi.org/10.1128/jvi.66.4.2096-2101.1992

Beyenbach, K. W., & Wieczorek, H. (2006). The V-type H+ ATPase: Molecular structure and function, physiological roles and regulation. *Journal of Experimental Biology,* *209*(4). https://doi.org/10.1242/jeb.02014

Bhuyan, A. K. (2010). On the mechanism of SDS-induced protein denaturation. *Biopolymers*, *93*(2). https://doi.org/10.1002/bip.21318

Bi, H., Karanth, S. S., Ye, K., Stein, R., & Jin, S. (2020). Decellularized Tissue Matrix Enhances Self-Assembly of Islet Organoids from Pluripotent Stem Cell Differentiation. *ACS Biomaterials Science and Engineering*, *6*(7). https://doi.org/10.1021/acsbiomaterials.0c00088

Bi, H., Ye, K., & Jin, S. (2020). Proteomic analysis of decellularized pancreatic matrix identifies collagen V as a critical regulator for islet organogenesis from human pluripotent stem cells. *Biomaterials*, *233*, 119673. https://doi.org/10.1016/j.biomaterials.2019.119673

Bian, J., Nazor, K. E., Angers, R., Jernigan, M., Seward, T., Centers, A., Green, M., & Telling, G. C. (2006). GFP-tagged PrP supports compromised prion replication in transgenic mice. *Biochemical and Biophysical Research Communications*, *340*(3). https://doi.org/10.1016/j.bbrc.2005.12.085

Bishop, M. T., Kovacs, G. G., Sanchez-Juan, P., & Knight, R. S. G. (2008). Cathepsin D SNP associated with increased risk of variant Creutzfeldt-Jakob disease. *BMC Medical Genetics*, *9*. https://doi.org/10.1186/1471-2350-9-31

Bolton, D. C., Mckinley, M. P., & Prusiner, S. B. (1982). Identification of a protein that purifies with the scrapie prion. *Science*, *218*(4579). https://doi.org/10.1126/science.6815801

Bolton, D. C., Meyer, R. K., & Prusiner, S. B. (1985). Scrapie PrP 27-30 is a sialoglycoprotein. *Journal of Virology*, *53*(2). https://doi.org/10.1128/jvi.53.2.596-606.1985

Bonnans, C., Chou, J., & Werb, Z. (2014). Remodelling the extracellular matrix in development and disease. In *Nature Reviews Molecular Cell Biology, 15*(12). https://doi.org/10.1038/nrm3904

Borchelt, D. R., Koliatsos, V. E., Guarnieri, M., Pardo, C. A., Sisodia, S. S., & Price, D. L. (1994). Rapid anterograde axonal transport of the cellular prion glycoprotein in the peripheral and central nervous systems. *Journal of Biological Chemistry*, *269*(20). https://doi.org/10.1016/s0021-9258(17)36683-8

Borchelt, D. R., Taraboulos, A., & Prusiner, S. B. (1992). Evidence for synthesis of scrapie prion proteins in the endocytic pathway. *Journal of Biological Chemistry*, *267*(23). https://doi.org/10.1016/s0021-9258(18)41985-0

Bouhamdani, N., Comeau, D., & Turcotte, S. (2021). A Compendium of Information on the Lysosome. *Frontiers in Cell and Developmental Biology*, *9,* 798262. https://doi.org/10.3389/fcell.2021.798262

Bowman, B. J., & Bowman, E. J. (2002). Mutations in subunit c of the vacuolar ATPase confer resistance to bafilomycin and identify a

conserved antibiotic binding site. *Journal of Biological Chemistry*, *277*(6). https://doi.org/10.1074/jbc.M109756200

Boyd, D. F., Allen, E. K., Randolph, A. G., Guo, X. zhi J., Weng, Y., Sanders, C. J., Bajracharya, R., Lee, N. K., Guy, C. S., Vogel, P., Guan, W., Li, Y., Liu, X., Novak, T., Newhams, M. M., Fabrizio, T. P., Wohlgemuth, N., Mourani, P. M., Kong, M., … Thomas, P. G. (2020). Exuberant fibroblast activity compromises lung function via ADAMTS4. *Nature*, *587*(7834). https://doi.org/10.1038/s41586-020-2877-5

Boyer, A. S., Ayerinskas, I. I., Vincent, E. B., McKinney, L. A., Weeks, D. L., & Runyan, R. B. (1999). TGFβ2 and TGFβ3 have separate and sequential activities during epithelial-mesenchymal cell transformation in the embryonic heart. *Developmental Biology*, *208*(2). https://doi.org/10.1006/dbio.1999.9211

Bremer, J., Baumann, F., Tiberi, C., Wessig, C., Fischer, H., Schwarz, P., Steele, A. D., Toyka, K. V., Nave, K. A., Weis, J., & Aguzzi, A. (2010). Axonal prion protein is required for peripheral myelin maintenance. *Nature Neuroscience*, *13*(3). https://doi.org/10.1038/nn.2483

Breton, S., & Brown, D. (2013). Regulation of luminal acidification by the V-ATPase. *Physiology, 28*(5). https://doi.org/10.1152/physiol.00007.2013

Brown, P., Brandel, J. P., Sato, T., Nakamura, Y., MacKenzie, J., Will, R. G., Ladogana, A., Pocchiari, M., Leschek, E. W., & Schonberger, L. B. (2012). Iatrogenic creutzfeldt-Jakob disease, final assessment. *Emerging Infectious Diseases*, *18*(6), 901–907. https://doi.org/10.3201/eid1806.120116

Brown, P., Cathala, F., Castaigne, P., & Gajdusek, D. C. (1986). Creutzfeldt-Jakob disease: Clinical analysis of a consecutive series of 230 neuropathologically verified cases. *Annals of Neurology*, *20*(5). https://doi.org/10.1002/ana.410200507

Bruce, M. E., Will, R. G., Ironside, J. W., McConnell, I., Drummond, D., Suttie, A., McCardle, L., Chree, A., Hope, J., Birkett, C., Cousens, S., Fraser, H., & Bostock, C. J. (1997). Transmissions to mice indicate that “new variant” CJD is caused by the BSE agent. *Nature*, *389*(6650). https://doi.org/10.1038/39057

Buck, M. R., Karustis, D. G., Day, N. A., Honn, K. V., & Sloane, B. F. (1992). Degradation of extracellular-matrix proteins by human cathepsin B from normal and tumour tissues. *Biochemical Journal*, *282*(1). https://doi.org/10.1042/bj2820273

Büeler, H., Aguzzi, A., Sailer, A., Greiner, R. A., Autenried, P., Aguet, M., & Weissmann, C. (1993). Mice devoid of PrP are resistant to scrapie. *Cell*, *73*(7). https://doi.org/10.1016/0092-8674(93)90360-3

Caby, M. P., Lankar, D., Vincendeau-Scherrer, C., Raposo, G., & Bonnerot, C. (2005). Exosomal-like vesicles are present in human blood plasma. *International Immunology*, *17*(7). https://doi.org/10.1093/intimm/dxh267

Calzolai, L., & Zahn, R. (2003). Influence of pH on NMR structure and stability of the human prion protein globular domain. *Journal of Biological Chemistry*, *278*(37). https://doi.org/10.1074/jbc.M303005200

Campana, V., Sarnataro, D., & Zurzolo, C. (2005). The highways and byways of prion protein trafficking. *Trends in Cell Biology, 15*(2). https://doi.org/10.1016/j.tcb.2004.12.002

Cartmell, J. S., & Dunn, M. G. (2000). Effect of chemical treatments on tendon cellularity and mechanical properties. *Journal of Biomedical Materials Research*, *49*(1). https://doi.org/10.1002/(SICI)1097-4636(200001)49:1<134::AID-JBM17>3.0.CO;2-D

Carulli, D., & Verhaagen, J. (2021). An extracellular perspective on cns maturation: Perineuronal nets and the control of plasticity. *International Journal of Molecular Sciences, 22*(5). https://doi.org/10.3390/ijms22052434

Castillo, G. M., Ngo, C., Cummings, J., Wight, T. N., & Snow, A. D. (1997). Perlecan binds to the β-amyloid proteins (aβ) of Alzheimer's disease, accelerates aβ fibril formation, and maintains aβ fibril stability. *Journal of Neurochemistry*, *69*(6). https://doi.org/10.1046/j.1471-4159.1997.69062452.x

Caughey, B., Race, R. E., Ernst, D., Buchmeier, M. J., & Chesebro, B. (1989). Prion protein biosynthesis in scrapie-infected and uninfected neuroblastoma cells. *Journal of Virology*, *63*(1). https://doi.org/10.1128/jvi.63.1.175-181.1989

Cavo, M., Fato, M., Peñuela, L., Beltrame, F., Raiteri, R., & Scaglione, S. (2016). Microenvironment complexity and matrix stiffness regulate breast cancer cell activity in a 3D in vitro model. *Scientific Reports*, *6*, 353567. https://doi.org/10.1038/srep35367

Celio, M. R., Spreafico, R., De Biasi, S., & Vitellaro-Zuccarello, L. (1998). Perineuronal nets: Past and present. *Trends in Neurosciences*, *21*(12). https://doi.org/10.1016/S0166-2236(98)01298-3

Chen, R. N., Ho, H. O., Tsai, Y. T., & Sheu, M. T. (2004). Process development of an acellular dermal matrix (ADM) for biomedical applications. *Biomaterials*, *25*(13). https://doi.org/10.1016/j.biomaterials.2003.09.070

Chen, S. G., Teplow, D. B., Parchi, P., Teller, J. K., Gambetti, P., & Autilio-Gambetti, L. (1995). Truncated forms of the human prion protein in normal brain and in prion diseases. *Journal of Biological Chemistry*, *270*(32). https://doi.org/10.1074/jbc.270.32.19173

Christensen, J., & Shastri, V. P. (2015). Matrix-metalloproteinase-9 is cleaved and activated by Cathepsin K. *BMC Research Notes*, *8*(1). https://doi.org/10.1186/s13104-015-1284-8

Claudio, L. (1995). Ultrastructural features of the blood-brain barrier in biopsy tissue from Alzheimer's disease patients. *Acta Neuropathologica*, *91*(1). https://doi.org/10.1007/s004010050386

Coleman, B. M., Hanssen, E., Lawson, V. A., & Hill, A. F. (2012). Prion-infected cells regulate the release of exosomes with distinct ultrastructural features. *FASEB Journal*, *26*(10). https://doi.org/10.1096/fj.11-202077

Collins, M. P., & Forgac, M. (2020). Regulation and function of V-ATPases in physiology and disease. *Biochimica et Biophysica Acta – Biomembranes, 1862*(12). https://doi.org/10.1016/j.bbamem.2020.183341

Collins, S. J., Sanchez-Juan, P., Masters, C. L., Klug, G. M., Van Duijn, C., Poleggi, A., Pocchiari, M., Almonti, S., Cuadrado-Corrales, N., De Pedro-Cuesta, J., Budka, H., Gelpi, E., Glatzel, M., Tolnay, M., Hewer, E., Zerr, I., Heinemann, U., Kretszchmar, H. A., Jansen, G. H., … Will, R. G. (2006). Determinants of diagnostic investigation sensitivities across the clinical spectrum of sporadic Creutzfeldt-Jakob disease. *Brain*, *129*(9). https://doi.org/10.1093/brain/awl159

Colucci, M., Moleres, F. J., Xie, Z. L., Ray-Chaudhury, A., Gutti, S., Butefisch, C. M., Cervenakova, L., Wang, W., Goldfarb, L. G., Kong, Q., Ghetti, B., Chen, S. G., & Gambetti, P. (2006). Gerstmann-Sträussler-Scheinker: A new phenotype with "curly" PrP deposits. *Journal of Neuropathology and Experimental Neurology*, *65*(7). https://doi.org/10.1097/01.jnen.0000228198.81797.4d

Contu, V. R., Sakai, R., Fujiwara, Y., Kabuta, C., Wada, K., & Kabuta, T. (2023). Nucleic acid uptake occurs independent of lysosomal acidification but dependent on ATP consumption during RNautophagy/DNautophagy. *Biochemical and Biophysical Research Communications*, *644,* 105-111. https://doi.org/10.1016/j.bbrc.2022.12.090

Costanzo, M., Abounit, S., Marzo, L., Danckaert, A., Chamoun, Z., Roux, P., & Zurzolo, C. (2013). Transfer of polyglutamine aggregates in neuronal cells occurs in tunneling nanotubes. *Journal of Cell Science*, *126*(16). https://doi.org/10.1242/jcs.126086

Daley, W. P., Peters, S. B., & Larsen, M. (2008). Extracellular matrix dynamics in development and regenerative medicine. In *Journal of Cell Science, 121*(3). https://doi.org/10.1242/jcs.006064

Daniels, M. P. (2012). The role of agrin in synaptic development, plasticity and signaling in the central nervous system. *Neurochemistry International*, *61*(6). https://doi.org/10.1016/j.neuint.2012.02.028

Dankovich, T. M., & Rizzoli, S. O. (2022). The Synaptic Extracellular Matrix: Long-Lived, Stable, and Still Remarkably Dynamic. *Frontiers in Synaptic Neuroscience, 14,* 854956. https://doi.org/10.3389/fnsyn.2022.854956

D'Castro, L., Wenborn, A., Gros, N., Joiner, S., Cronier, S., Collinge, J., & Wadsworth, J. D. F. (2010). Isolation of proteinase K-sensitive prions using pronase E and phosphotungstic acid. *PLoS ONE*, *5*(12). https://doi.org/10.1371/journal.pone.0015679

De Milito, A., & Fais, S. (2005). Tumor acidity, chemoresistance and proton pump inhibitors. *Future Oncology*, *1*(6). https://doi.org/10.2217/14796694.1.6.779

Delarue, Q., Mayeur, A., Chalfouh, C., Honoré, A., Duclos, C., Di Giovanni, M., Li, X., Salaun, M., Dampierre, J., Vaudry, D., Marie, J. P., & Guérout, N. (2020). Inhibition of ADAMTS-4 Expression in Olfactory Ensheathing Cells Enhances Recovery after Transplantation within Spinal Cord Injury. *Journal of Neurotrauma*, *37*(3). https://doi.org/10.1089/neu.2019.6481

Demircan, K., Topcu, V., Takigawa, T., Akyol, S., Yonezawa, T., Ozturk, G., Ugurcu, V., Hasgul, R., Yigitoglu, M. R., Akyol, O., McCulloch, D. R., & Hirohata, S. (2014). ADAMTS4 and ADAMTS5 knockout mice are protected from versican but not aggrecan or brevican proteolysis during spinal cord injury. *BioMed Research International*, *2014*, 693746. https://doi.org/10.1155/2014/693746

Downs, M., Sethi, M. K., Raghunathan, R., Layne, M. D., & Zaia, J. (2022). Matrisome changes in Parkinson's disease. *Analytical and Bioanalytical Chemistry*, *414*(9). https://doi.org/10.1007/s00216-022-03929-4

Dron, M., Moudjou, M., Chapuis, J., Farooq Salamat, M. K., Bernard, J., Cronier, S., Langevin, C., & Laude, H. (2010). Endogenous proteolytic cleavage of disease-associated prion protein to produce C2 fragments is strongly cell- and tissue-dependent. *Journal of Biological Chemistry*, *285*(14). https://doi.org/10.1074/jbc.M109.083857

Du, L., Wu, X., Pang, K., & Yang, Y. (2011). Histological evaluation and biomechanical characterisation of an acellular porcine cornea scaffold. *British Journal of Ophthalmology*, *95*(3). https://doi.org/10.1136/bjo.2008.142539

Dubey, G. P., & Ben-Yehuda, S. (2011). Intercellular nanotubes mediate bacterial communication. *Cell*, *144*(4). https://doi.org/10.1016/j.cell.2011.01.015

Dubos, A., Castells-Nobau, A., Meziane, H., Oortveld, M. A. W., Houbaert, X., Iacono, G., Martin, C., Mittelhaeuser, C., Lalanne, V., Kramer, J. M., Bhukel, A., Quentin, C., Slabbert, J., Verstreken, P., Sigrist, S. J., Messaddeq, N., Birling, M. C., Selloum, M., Stunnenberg, H. G., … Herault, Y. (2015). Conditional depletion of intellectual disability and Parkinsonism candidate gene ATP6AP2 in fly and mouse induces cognitive impairment and neurodegeneration. *Human Molecular Genetics*, *24*(23). https://doi.org/10.1093/hmg/ddv380

Duffy, P., Wolf, J., Collins, G., DeVoe, A., Streeten, B., & Cowen, D. (1974). Possible Person-to-Person Transmission of Creutzfeldt-Jakob Disease. *New England Journal of Medicine*, *290*(12). https://doi.org/10.1056/nejm197403212901220

Dulce, P.-G., Christophe, M., Minh Bao, H., Fernando, S., Ludmilla, S., Diaz Julia Elisa, S., & Rita, R.-V. (2011). Glycosaminoglycans, Protein Aggregation and Neurodegeneration. *Current Protein & Peptide Science*, *12*(3). https://doi.org/10.2174/138920311795860188

Dunne, L. W., Huang, Z., Meng, W., Fan, X., Zhang, N., Zhang, Q., & An, Z. (2014). Human decellularized adipose tissue scaffold as a model for breast cancer cell growth and drug treatments. *Biomaterials*, *35*(18). https://doi.org/10.1016/j.biomaterials.2014.03.003

Eftekharzadeh, S., Akbarzadeh, A., Sabetkish, N., Rostami, M., Zabolian, A. H., Hashemi, J., Tavangar, S. M., & Kajbafzadeh, A. M. (2022). Esophagus tissue engineering: from decellularization to in vivo recellularization in two sites. *Cell and Tissue Banking*, *23*(2). https://doi.org/10.1007/s10561-021-09944-6

Elder, B. D., Kim, D. H., & Athanasiou, K. A. (2010). Developing an articular cartilage decellularization process toward facet joint cartilage replacement. *Neurosurgery*, *66*(4). https://doi.org/10.1227/01.NEU.0000367616.49291.9F

Elimova, E., Kisilevsky, R., & Ancsin, J. B. (2009). Heparan sulfate promotes the aggregation of HDL-associated serum amyloid A: evidence for a proamyloidogenic histidine molecular switch. *The FASEB Journal*, *23*(10). https://doi.org/10.1096/fj.09-134981

Faust, A., Kandakatla, A., Van Der Merwe, Y., Ren, T., Huleihel, L., Hussey, G., Naranjo, J. D., Johnson, S., Badylak, S., & Steketee, M. (2017). Urinary bladder extracellular matrix hydrogels and matrix-bound vesicles differentially regulate central nervous system neuron viability and axon growth and branching. *Journal of Biomaterials Applications*, *31*(9). https://doi.org/10.1177/0885328217698062

Fawcett, J. W. (2009). Recovery from spinal cord injury: Regeneration, plasticity and rehabilitation. *Brain, 132*(6). https://doi.org/10.1093/brain/awp121

Fehlinger, A., Wolf, H., Hossinger, A., Duernberger, Y., Pleschka, C., Riemschoss, K., Liu, S., Bester, R., Paulsen, L., Priola, S. A., Groschup, M. H., Schätzl, H. M., & Vorberg, I. M. (2017). Prion strains depend on different endocytic routes for productive infection. *Scientific Reports*, *7*(1). https://doi.org/10.1038/s41598-017-07260-2

Fernandez-Garcia, B., Eiró, N., Marín, L., González-Reyes, S., González, L. O., Lamelas, M. L., & Vizoso, F. J. (2014). Expression and prognostic significance of fibronectin and matrix metalloproteases in breast cancer metastasis. *Histopathology*, *64*(4). https://doi.org/10.1111/his.12300

Fevrier, B., Vilette, D., Archer, F., Loew, D., Faigle, W., Vidal, M., Laude, H., & Raposo, G. (2004). Cells release prions in association with exosomes. *Proceedings of the National Academy of Sciences of the United States of America*, *101*(26). https://doi.org/10.1073/pnas.0308413101

Filardo, G., Kon, E., Andriolo, L., Matteo, B. Di, Balboni, F., & Marcacci, M. (2014). Clinical Profiling in Cartilage Regeneration: Prognostic Factors for Midterm Results of Matrix-Assisted Autologous Chondrocyte Transplantation. *The American Journal of Sports Medicine*, *42*(4), 898–905. https://doi.org/10.1177/0363546513518552

Filous, A. R., Miller, J. H., Coulson-Thomas, Y. M., Horn, K. P., Alilain, W. J., & Silver, J. (2010). Immature astrocytes promote CNS axonal regeneration when combined with chondroitinase ABC. *Developmental Neurobiology*, *70*(12). https://doi.org/10.1002/dneu.20820

Forgac, M. (2007). Vacuolar ATPases: Rotary proton pumps in physiology and pathophysiology. *Nature Reviews Molecular Cell Biology, 8*(11). https://doi.org/10.1038/nrm2272

Franklin, S. L., Love, S., Greene, J. R. T., & Betmouni, S. (2008). Loss of perineuronal net in ME7 prion disease. *Journal of Neuropathology and Experimental Neurology*, *67*(3). https://doi.org/10.1097/NEN.0b013e3181654386

Frantz, C., Stewart, K. M., & Weaver, V. M. (2010). The extracellular matrix at a glance. *Journal of Cell Science, 123*(24). https://doi.org/10.1242/jcs.023820

Frischknecht, R., & Seidenbecher, C. I. (2012). Brevican: A key proteoglycan in the perisynaptic extracellular matrix of the brain. *International Journal of Biochemistry and Cell Biology, 44*(7). https://doi.org/10.1016/j.biocel.2012.03.022

Gambetti, P., Dong, Z., Yuan, J., Xiao, X., Zheng, M., Alshekhlee, A., Castellani, R., Cohen, M., Barria, M. A., Gonzalez-Romero, D., Belay, E. D., Schonberger, L. B., Marder, K., Harris, C., Burke, J. R., Montine, T., Wisniewski, T., Dickson, D. W., Soto, C., … Zou, W. Q. (2008). A novel human disease with abnormal prion protein sensitive to protease. *Annals of Neurology, 63*(6). https://doi.org/10.1002/ana.21420

Gambetti, P., Parchi, P., Petersen, R. B., Chen, S. G., & Lugaresi, E. (1995). Fatal Familial Insomnia and Familial Creutzfeldt-Jakob Disease: Clinical, Pathological and Molecular Features. *Brain Pathology*, *5*(1). https://doi.org/10.1111/j.1750-3639.1995.tb00576.x

Gibbs, C. J., Gajdusek, D. C., Asher, D. M., Alpers, M. P., Beck, E., Daniel, P. M., & Matthews, W. B. (1968). Creutzfeldt-Jakob disease (spongiform encephalopathy): Transmission to the chimpanzee. *Science*, *161*(3839). https://doi.org/10.1126/science.161.3839.388

Gille, J., Behrens, P., Schulz, A. P., Oheim, R., & Kienast, B. (2016). Matrix-Associated Autologous Chondrocyte Implantation: A Clinical Follow-Up at 15 Years. *Cartilage*, *7*(4), 309–315. https://doi.org/10.1177/1947603516638901

Gioiella, F., Urciuolo, F., Imparato, G., Brancato, V., & Netti, P. A. (2016). An Engineered Breast Cancer Model on a Chip to Replicate ECM-Activation In Vitro during Tumor Progression. *Advanced Healthcare Materials*, *5*(23). https://doi.org/10.1002/adhm.201600772

Gisabella, B., Babu, J., Valeri, J., Rexrode, L., & Pantazopoulos, H. (2021). Sleep and Memory Consolidation Dysfunction in Psychiatric Disorders: Evidence for the Involvement of Extracellular Matrix Molecules. In *Frontiers in Neuroscience, 15*, 646678. https://doi.org/10.3389/fnins.2021.646678

Glasson, S. S., Askew, R., Sheppard, B., Carito, B. A., Blanchet, T., Ma, H. L., Flannery, C. R., Kanki, K., Wang, E., Peluso, D., Yang, Z., Majumdar, M. K., & Morris, E. A. (2004). Characterization of and osteoarthritis susceptibility in ADAMTS-4-knockout mice. *Arthritis and Rheumatism*, *50*(8). https://doi.org/10.1002/art.20558

Glatzel, M., Abela, E., Maissen, M., & Aguzzi, A. (2003). Extraneural Pathologic Prion Protein in Sporadic Creutzfeldt–Jakob Disease. *New England Journal of Medicine*, *349*(19). https://doi.org/10.1056/nejmoa030351

Go, T., Jungebluth, P., Baiguero, S., Asnaghi, A., Martorell, J., Ostertag, H., Mantero, S., Birchall, M., Bader, A., & Macchiarini, P. (2010). Both epithelial cells and mesenchymal stem cell-derived chondrocytes contribute to the survival of tissue-engineered airway transplants in pigs. *Journal of Thoracic and Cardiovascular Surgery*, *139*(2). https://doi.org/10.1016/j.jtcvs.2009.10.002

Gocheva, V., & Joyce, J. A. (2007). Cysteine cathepsins and the cutting edge of cancer invasion. In *Cell Cycle, 6*(1). https://doi.org/10.4161/cc.6.1.3669

Godsave, S. F., Wille, H., Pierson, J., Prusiner, S. B., & Peters, P. J. (2013). Plasma membrane invaginations containing clusters of full-length PrPSc are an early form of prion-associated neuropathology in vivo.

Neurobiology of Aging, *34*(6). https://doi.org/10.1016/j.neurobiolaging.2012.12.015

Goold, R., Rabbanian, S., Sutton, L., Andre, R., Arora, P., Moonga, J., Clarke, A. R., Schiavo, G., Jat, P., Collinge, J., & Tabrizi, S. J. (2011). Rapid cell-surface prion protein conversion revealed using a novel cell system. *Nature Communications*, *2*(1). https://doi.org/10.1038/ncomms1282

Gousset, K., Schiff, E., Langevin, C., Marijanovic, Z., Caputo, A., Browman, D. T., Chenouard, N., de Chaumont, F., Martino, A., Enninga, J., Olivo-Marin, J. C., Männel, D., & Zurzolo, C. (2009). Prions hijack tunnelling nanotubes for intercellular spread. *Nature Cell Biology*, *11*(3). https://doi.org/10.1038/ncb1841

Granato, A. E. C., da Cruz, E. F., Rodrigues-Junior, D. M., Mosini, A. C., Ulrich, H., Rodrigues, B. V. M., Cheffer, A., & Porcionatto, M. (2020). A novel decellularization method to produce brain scaffolds. *Tissue and Cell*, *67,* 101412. https://doi.org/10.1016/j.tice.2020.101412

Griffin, J. M., Fackelmeier, B., Clemett, C. A., Fong, D. M., Mouravlev, A., Young, D., & O'Carroll, S. J. (2020). Astrocyte-selective AAV-ADAMTS4 gene therapy combined with hindlimb rehabilitation promotes functional recovery after spinal cord injury. *Experimental Neurology*, *327,* 113232. https://doi.org/10.1016/j.expneurol.2020.113232

Griffith, J. S. (1967). Nature of the scrapie agent: Self-replication and scrapie. *Nature*, *215*(5105). https://doi.org/10.1038/2151043a0

Guentchev, M., Groschup, M. H., Kordek, R., Liberski, P. P., & Budka, H. (1998). Severe, early and selective loss of a subpopulation of GABAergic inhibitory neurons in experimental transmissible spongiform encephalopathies. *Brain Pathology*, *8*(4). https://doi.org/10.1111/j.1750-3639.1998.tb00188.x

Gurke, S., Barroso, J. F. V., Hodneland, E., Bukoreshtliev, N. V., Schlicker, O., & Gerdes, H. H. (2008). Tunneling nanotube (TNT)-like structures facilitate a constitutive, actomyosin-dependent exchange of endocytic organelles between normal rat kidney cells. *Experimental Cell Research*, *314*(20). https://doi.org/10.1016/j.yexcr.2008.08.022

Hadlow, W. J. (1959). SCRAPIE AND KURU. *The Lancet, 274*, 7097. https://doi.org/10.1016/S0140-6736(59)92081-1

Haigh, C. L., & Collins, S. J. (2016). Endoproteolytic cleavage as a molecular switch regulating and diversifying prion protein function. *Neural Regeneration Research, 11*(2). https://doi.org/10.4103/1673-5374.177726

Hannus, M., Beitzinger, M., Engelmann, J. C., Weickert, M. T., Spang, R., Hannus, S., & Meister, G. (2014). SiPools: Highly complex but

accurately defined siRNA pools eliminate off-target effects. *Nucleic Acids Research*, *42*(12). https://doi.org/10.1093/nar/gku480

Happel, M. F. K., Niekisch, H., Castiblanco Rivera, L. L., Ohl, F. W., Deliano, M., & Frischknecht, R. (2014). Enhanced cognitive flexibility in reversal learning induced by removal of the extracellular matrix in auditory cortex. *Proceedings of the National Academy of Sciences of the United States of America*, *111*(7). https://doi.org/10.1073/pnas.1310272111

Harding, C., Heuser, J., & Stahl, P. (1984). Endocytosis and intracellular processing of transferrin and colloidal gold-transferrin in rat reticulocytes: Demonstration of a pathway for receptor shedding. *European Journal of Cell Biology*, *35*(2). PMID: 6151502

Harris, D. A. (2003). Trafficking, turnover and membrane topology of PrP. In *British Medical Bulletin, 66*. 72-85. https://doi.org/10.1093/bmb/66.1.71

Herms, J., Tings, T., Gall, S., Madlung, A., Giese, A., Siebert, H., Peter Schürmann, O., Windl, T., Brose, N., & Kretzschmar, H. (1999). Evidence of presynaptic location and function of the prion protein. *Journal of Neuroscience*, *19*(20). https://doi.org/10.1523/jneurosci.19-20-08866.1999

Hernández, F., Pérez, M., Lucas, J. J., & Avila, J. (2002). Sulfo-glycosaminoglycan content affects PHF-tau solubility and allows the identification of different types of PHFs. *Brain Research*, *935*(1–2). https://doi.org/10.1016/S0006-8993(02)02455-1

Hijazi, N., Kariv-Inbal, Z., Gasset, M., & Gabizon, R. (2005). PrPSc incorporation to cells requires endogenous glycosaminoglycan expression. *Journal of Biological Chemistry*, *280*(17). https://doi.org/10.1074/jbc.M411314200

Hill, A. F., Desbruslais, M., Joiner, S., Sidle, K. C. L., Gowland, I., Collinge, J., Doey, L. J., & Lantos, P. (1997). The same prion strain causes vCJD and BSE. *Nature, 389*(6650). https://doi.org/10.1038/38925

Hinton, A., Sennoune, S. R., Bond, S., Fang, M., Reuveni, M., Sahagian, G. G., Jay, D., Martinez-Zaguilan, R., & Forgac, M. (2009). Function of a subunit isoforms of the V-ATPase in pH homeostasis and in vitro invasion of MDA-MB231 human breast cancer cells. *Journal of Biological Chemistry*, *284*(24). https://doi.org/10.1074/jbc.M901201200

Hirose, T., Cabrera-Socorro, A., Chitayat, D., Lemonnier, T., Féraud, O., Cifuentes-Diaz, C., Gervasi, N., Mombereau, C., Ghosh, T., Stoica, L., d'Arc Al Bacha, J., Yamada, H., Lauterbach, M. A., Guillon, M., Kaneko, K., Norris, J. W., Siriwardena, K., Blasér, S., Teillon, J., … Groszer, M. (2019). ATP6AP2 variant impairs CNS development and neuronal survival to cause fulminant neurodegeneration. *Journal of Clinical Investigation*, *129*(5). https://doi.org/10.1172/JCI79990

Holmes, B. B., DeVos, S. L., Kfoury, N., Li, M., Jacks, R., Yanamandra, K., Ouidja, M. O., Brodsky, F. M., Marasa, J., Bagchi, D. P., Kotzbauer, P. T., Miller, T. M., Papy-Garcia, D., & Diamond, M. I. (2013). Heparan sulfate proteoglycans mediate internalization and propagation of specific proteopathic seeds. *Proceedings of the National Academy of Sciences of the United States of America*, *110*(33). https://doi.org/10.1073/pnas.1301440110

Horonchik, L., Tzaban, S., Ben-Zaken, O., Yedidia, Y., Rouvinski, A., Papy-Garcia, D., Barritault, D., Vlodavsky, I., & Taraboulos, A. (2005). Heparan sulfate is a cellular receptor for purified infectious prions. *Journal of Biological Chemistry*, *280*(17). https://doi.org/10.1074/jbc.M500122200

Hoshiba, T. (2018). An extracellular matrix (ECM) model at high malignant colorectal tumor increases chondroitin sulfate chains to promote epithelial-mesenchymal transition and chemoresistance acquisition. *Experimental Cell Research*, *370*(2), 571–578. https://doi.org/10.1016/j.yexcr.2018.07.022

Hoshiba, T., & Yunoki, S. (2023). Comparison of decellularization protocols for cultured cell-derived extracellular matrix—Effects on decellularization efficacy, extracellular matrix retention, and cell functions. *Journal of Biomedical Materials Research - Part B Applied Biomaterials*, *111*(1), 85–94. https://doi.org/10.1002/jbm.b.35135

Howard, J., & Pilkington, G. J. (1990). Antibodies to fibronectin bind to plaques and other structures in Alzheimer's disease and control brain. *Neuroscience Letters*, *118*(1). https://doi.org/10.1016/0304-3940(90)90251-4

Hoyt, F., Alam, P., Artikis, E., Schwartz, C. L., Hughson, A. G., Race, B., Baune, C., Raymond, G. J., Baron, G. S., Kraus, A., & Caughey, B. (2022). Cryo-EM of prion strains from the same genotype of host identifies conformational determinants. *PLoS Pathogens*, *18*(11). https://doi.org/10.1371/journal.ppat.1010947

Hsu, A., Podvin, S., & Hook, V. (2018). Lysosomal Cathepsin Protease Gene Expression Profiles in the Human Brain During Normal Development. *Journal of Molecular Neuroscience*, *65*(4). https://doi.org/10.1007/s12031-018-1110-6

Hu, M., Bi, H., Moffat, D., Blystone, M., Decostanza, P., Alayi, T., Ye, K., Hathout, Y., & Jin, S. (2021). Proteomic and bioinformatic analysis of decellularized pancreatic extracellular matrices. *Molecules*, *26*(21). https://doi.org/10.3390/molecules26216740

Huang, H., Rendulich, J., Stevenson, D., O'Rourke, K., & Balachandran, A. (2005). Evaluation of Western blotting methods using samples with or without sodium phosphotungstic acid precipitation for diagnosis of

scrapie and chronic wasting disease. *Canadian Journal of Veterinary Research*, *69*(3).

Huleihel, L., Hussey, G. S., Naranjo, J. D., Zhang, L., Dziki, J. L., Turner, N. J., Stolz, D. B., & Badylak, S. F. (2016). Matrix-bound nanovesicles within ECM bioscaffolds. *Science Advances*, *2*(6). https://doi.org/10.1126/sciadv.1600502

Hussey, G. S., Molina, C. P., Cramer, M. C., Tyurina, Y. Y., Tyurin, V. A., Lee, Y. C., El-Mossier, S. O., Murdock, M. H., Timashev, P. S., Kagan, V. E., & Badylak, S. F. (2020). Lipidomics and RNA sequencing reveal a novel subpopulation of nanovesicle within extracellular matrix biomaterials. *Science Advances*, *6*(12). https://doi.org/10.1126/sciadv.aay4361

Jackson, G. S., Hill, A. F., Joseph, C., Hosszu, L., Power, A., Waltho, J. P., Clarke, A. R., & Collinge, J. (1999). Multiple folding pathways for heterologously expressed human prion protein. *Biochimica et Biophysica Acta - Protein Structure and Molecular Enzymology*, *1431*(1). https://doi.org/10.1016/S0167-4838(99)00038-2

Jankovska, N., Matej, R., & Olejar, T. (2021). Extracellular prion protein aggregates in nine gerstmann–sträussler–scheinker syndrome subjects with mutation p102l: A micromorphological study and comparison with literature data. *International Journal of Molecular Sciences*, *22*(24). https://doi.org/10.3390/ijms222413303

Jeffrey, M., & González, L. (2007). Classical sheep transmissible spongiform encephalopathies: Pathogenesis, pathological phenotypes and clinical disease. *Neuropathology and Applied Neurobiology*, *33*(4). https://doi.org/10.1111/j.1365-2990.2007.00868.x

Jeffrey, M., McGovern, G., Sisó, S., & González, L. (2011). Cellular and sub-cellular pathology of animal prion diseases: Relationship between morphological changes, accumulation of abnormal prion protein and clinical disease. *Acta Neuropathologica, 121*(1). https://doi.org/10.1007/s00401-010-0700-3

Jiménez-Huete, A., Lievens, P. M. J., Vidal, R., Piccardo, P., Ghetti, B., Tagliavini, F., Frangione, B., & Prelli, F. (1998). Endogenous proteolytic cleavage of normal and disease-associated isoforms of the human prion protein in neural and non-neural tissues. *American Journal of Pathology*, *153*(5). https://doi.org/10.1016/S0002-9440(10)65744-6

Johnson, E. C. B., Carter, E. K., Dammer, E. B., Duong, D. M., Gerasimov, E. S., Liu, Y., Liu, J., Betarbet, R., Ping, L., Yin, L., Serrano, G. E., Beach, T. G., Peng, J., De Jager, P. L., Haroutunian, V., Zhang, B., Gaiteri, C., Bennett, D. A., Gearing, M., … Seyfried, N. T. (2022). Large-scale deep multi-layer analysis of Alzheimer's disease brain reveals strong proteomic disease-related changes not observed at the RNA

level. *Nature Neuroscience*, *25*(2). https://doi.org/10.1038/s41593-021-00999-y

Kalluri, R., & Neilson, E. G. (2003). Epithelial-mesenchymal transition and its implications for fibrosis. *Journal of Clinical Investigation 112*(12). https://doi.org/10.1172/JCI200320530

Kanaani, J., Prusiner, S. B., Diacovo, J., Baekkeskov, S., & Legname, G. (2005). Recombinant prion protein induces rapid polarization and development of synapses in embryonic rat hippocampal neurons in vitro. *Journal of Neurochemistry*, *95*(5). https://doi.org/10.1111/j.1471-4159.2005.03469.x

Kanchanawong, P., & Calderwood, D. A. (2022). Organization, dynamics and mechanoregulation of integrin-mediated cell–ECM adhesions. *Nature Reviews Molecular Cell Biology*, *24*(2). https://doi.org/10.1038/s41580-022-00531-5

Kanu, N., Imokawa, Y., Drechsel, D. N., Williamson, R. A., Birkett, C. R., Bostock, C. J., & Brockes, J. P. (2002). Transfer of scrapie prion infectivity by cell contact in culture. *Current Biology*, *12*(7). https://doi.org/10.1016/S0960-9822(02)00722-4

Kargar-Abarghouei, E., Vojdani, Z., Hassanpour, A., Alaee, S., & Talaei-Khozani, T. (2018). Characterization, recellularization, and transplantation of rat decellularized testis scaffold with bone marrow-derived mesenchymal stem cells. *Stem Cell Research and Therapy*, *9*(1). https://doi.org/10.1186/s13287-018-1062-3

Kaukonen, R., Mai, A., Georgiadou, M., Saari, M., De Franceschi, N., Betz, T., Sihto, H., Ventelä, S., Elo, L., Jokitalo, E., Westermarck, J., Kellokumpu-Lehtinen, P. L., Joensuu, H., Grenman, R., & Ivaska, J. (2016). Normal stroma suppresses cancer cell proliferation via mechanosensitive regulation of JMJD1a-mediated transcription. *Nature Communications*, *7*, 12237. https://doi.org/10.1038/ncomms12237

Khanam, R., Sengupta, A., Mukhopadhyay, D., & Chakraborty, S. (2022). Identification of Adamts4 as a novel adult cardiac injury biomarker with therapeutic implications in patients with cardiac injuries. *Scientific Reports*, *12*(1). https://doi.org/10.1038/s41598-022-13918-3

Klohn, P.-C., Stoltze, L., Flechsig, E., Enari, M., & Weissmann, C. (2003). A quantitative, highly sensitive cell-based infectivity assay for mouse scrapie prions. *Proceedings of the National Academy of Sciences*, *100*(20), 11666–11671. https://doi.org/10.1073/pnas.1834432100

Köhling, R., Nischt, R., Vasudevan, A., Ho, M., Weiergräber, M., Schneider, T., & Smyth, N. (2006). Nidogen and nidogen-associated basement membrane proteins and neuronal plasticity. *Neurodegenerative Diseases, 3*(1-2). https://doi.org/10.1159/000092094

Kon, E., Filardo, G., Condello, V., Collarile, M., Di Martino, A., Zorzi, C., & Marcacci, M. (2011). Second-generation autologous chondrocyte implantation: Results in patients older than 40 years. *American Journal of Sports Medicine*, *39*(8). https://doi.org/10.1177/0363546511404675

Korvatska, O., Strand, N. S., Berndt, J. D., Strovas, T., Chen, D. H., Leverenz, J. B., Kiianitsa, K., Mata, I. F., Karakoc, E., Greenup, J. L., Bonkowski, E., Chuang, J., Moon, R. T., Eichler, E. E., Nickerson, D. A., Zabetian, C. P., Kraemer, B. C., Bird, T. D., & Raskind, W. H. (2013). Altered splicing of ATP6AP2 causes X-linked parkinsonism with spasticity (XPDS). *Human Molecular Genetics*, *22*(16). https://doi.org/10.1093/hmg/ddt180

Kovač, V., & Šerbec, V. Č. (2022). Prion Protein: The Molecule of Many Forms and Faces. *International Journal of Molecular Sciences, 23*(3). https://doi.org/10.3390/ijms23031232

Kovacs, G. G., Sanchez-Juan, P., Ströbel, T., Schuur, M., Poleggi, A., Nocentini, S., Giannattasio, C., Belay, G., Bishop, M., Capellari, S., Parchi, P., Gelpi, E., Gal, A., Bakos, A., Molnar, M. J., Heinemann, U., Zerr, I., Knight, R. S. G., Mitrova, E., … Budka, H. (2010). Cathepsin D (C224T) polymorphism in sporadic and genetic creutzfeldt-jakob disease. *Alzheimer Disease and Associated Disorders*, *24*(1). https://doi.org/10.1097/WAD.0b013e3181ad378c

Kovacs, G. G., Seguin, J., Quadrio, I., Höftberger, R., Kapás, I., Streichenberger, N., Biacabe, A. G., Meyronet, D., Sciot, R., Vandenberghe, R., Majtenyi, K., László, L., Ströbel, T., Budka, H., & Perret-Liaudet, A. (2011). Genetic Creutzfeldt-Jakob disease associated with the E200K mutation: Characterization of a complex proteinopathy. *Acta Neuropathologica*, *121*(1). https://doi.org/10.1007/s00401-010-0713-y

Kretzschmar, H. A., Stowring, L. E., Westaway, D., Stubblebine, W. H., Prusiner, S. B., & Dearmond, S. J. (1986). Molecular Cloning of a Human Prion Protein cDNA. *DNA*, *5*(4). https://doi.org/10.1089/dna.1986.5.315

Küffer, A., Lakkaraju, A. K. K., Mogha, A., Petersen, S. C., Airich, K., Doucerain, C., Marpakwar, R., Bakirci, P., Senatore, A., Monnard, A., Schiavi, C., Nuvolone, M., Grosshans, B., Hornemann, S., Bassilana, F., Monk, K. R., & Aguzzi, A. (2016). The prion protein is an agonistic ligand of the G protein-coupled receptor Adgrg6. *Nature*, *536*(7617). https://doi.org/10.1038/nature19312

Ladogana, A., Puopolo, M., Croes, E. A., Budka, H., Jarius, C., Collins, S., Klug, G. M., Sutcliffe, T., Giulivi, A., Alperovitch, A., Delasnerie-Laupretre, N., Brandel, J. P., Poser, S., Kretzschmar, H., Rietveld, I., Mitrova, E., Cuesta, J.deP., Martinez-Martin, P., Glatzel, M., Aguzzi, A., … Zerr, I. (2005). Mortality from Creutzfeldt-Jakob disease and related

disorders in Europe, Australia, and Canada. Neurology, 64(9), 1586–1591. https://doi.org/10.1212/01.WNL.0000160117.56690.B2

Lässer, C., Seyed Alikhani, V., Ekström, K., Eldh, M., Torregrosa Paredes, P., Bossios, A., Sjöstrand, M., Gabrielsson, S., Lötvall, J., & Valadi, H. (2011). Human saliva, plasma and breast milk exosomes contain RNA: Uptake by macrophages. *Journal of Translational Medicine*, *9,* 9. https://doi.org/10.1186/1479-5876-9-9

Lau, L. W., Cua, R., Keough, M. B., Haylock-Jacobs, S., & Yong, V. W. (2013). Pathophysiology of the brain extracellular matrix: A new target for remyelination. *Nature Reviews Neuroscience, 14*(10). https://doi.org/10.1038/nrn3550

Laurens, N., Koolwijk, P., & de Maat, M. P. (2006). Fibrin structure and wound healing. *Journal of thrombosis and haemostasis : JTH, 4*(5). https://doi.org/10.1111/j.1538-7836.2006.01861.x

Lee, H. J., Bae, E. J., & Lee, S. J. (2014). Extracellular α-synuclein-a novel and crucial factor in Lewy body diseases. *Nature Reviews Neurology, 10*(2). https://doi.org/10.1038/nrneurol.2013.275

Lemarchant, S., Pruvost, M., Hébert, M., Gauberti, M., Hommet, Y., Briens, A., Maubert, E., Gueye, Y., Féron, F., Petite, D., Mersel, M., Do Rego, J. C., Vaudry, H., Koistinaho, J., Ali, C., Agin, V., Emery, E., & Vivien, D. (2014). TPA promotes ADAMTS-4-induced CSPG degradation, thereby enhancing neuroplasticity following spinal cord injury. *Neurobiology of Disease*, *66*, 28-42. https://doi.org/10.1016/j.nbd.2014.02.005

Leonard, C. E., & Taneyhill, L. A. (2020). The road best traveled: Neural crest migration upon the extracellular matrix. In *Seminars in Cell and Developmental Biology, 100*, 177-185. https://doi.org/10.1016/j.semcdb.2019.10.013

Lepelletier, F. X., Mann, D. M. A., Robinson, A. C., Pinteaux, E., & Boutin, H. (2017). Early changes in extracellular matrix in Alzheimer's disease. *Neuropathology and Applied Neurobiology*, *43*(2). https://doi.org/10.1111/nan.12295

Lewis, P. A., Properzi, F., Prodromidou, K., Clarke, A. R., Collinge, J., & Jackson, G. S. (2006). Removal of the glycosylphosphatidylinositol anchor from PrPSc by cathepsin D does not reduce prion infectivity. *Biochemical Journal*, *395*(2). https://doi.org/10.1042/BJ20051677

Lewis, V., Johanssen, V. A., Crouch, P. J., Klug, G. M., Hooper, N. M., & Collins, S. J. (2016). Prion protein "gamma-cleavage": Characterizing a novel endoproteolytic processing event. *Cellular and Molecular Life Sciences*, *73*(3). https://doi.org/10.1007/s00018-015-2022-z

Li, W., Du, C., Wang, H., & Zhang, C. (2014). Increased serum ADAMTS-4 in knee osteoarthritis: A potential indicator for the diagnosis of

osteoarthritis in early stages. *Genetics and Molecular Research*, *13*(4). https://doi.org/10.4238/2014.November.14.9

Liao, Y. U. C. J., Lebo, R. V., Clawson, G. A., & Smuckler, E. A. (1986). Human prion protein cDNA: Molecular cloning, chromosomal mapping, and biological implications. *Science*, *233*(4761). https://doi.org/10.1126/science.3014653

Liberski, P. P. (2012). GERSTMANN-STRÄUSSLER-SCHEINKER DISEASE. *Advances in Experimental Medicine and Biology, 724*, 128–137. https://doi.org/10.1007/978-1-4614-0653-2_10

Lima, A. N., de Oliveira, R. J., Braz, A. S. K., de Souza Costa, M. G., Perahia, D., & Scott, L. P. B. (2018). Effects of pH and aggregation in the human prion conversion into scrapie form: a study using molecular dynamics with excited normal modes. *European Biophysics Journal*, *47*(5). https://doi.org/10.1007/s00249-018-1292-4

Linsenmeier, L., Altmeppen, H. C., Wetzel, S., Mohammadi, B., Saftig, P., & Glatzel, M. (2017). Diverse functions of the prion protein – Does proteolytic processing hold the key? *Biochimica et Biophysica Acta - Molecular Cell Research, 1864*(11). https://doi.org/10.1016/j.bbamcr.2017.06.022

Litwack, E. D., Stipp, C. S., Kumbasar, A., & Lander, A. D. (1994). Neuronal expression of glypican, a cell-surface glycosylphosphatidylinositol-anchored heparan sulfate proteoglycan, in the adult rat nervous system. *Journal of Neuroscience*, *14*(6). https://doi.org/10.1523/jneurosci.14-06-03713.1994

Lou, E., Fujisawa, S., Morozov, A., Barlas, A., Romin, Y., Dogan, Y., Gholami, S., Moreira, A. L., Manova-Todorova, K., & Moore, M. A. S. (2012). Tunneling nanotubes provide a unique conduit for intercellular transfer of cellular contents in human malignant pleural mesothelioma. *PLoS ONE*, *7*(3). https://doi.org/10.1371/journal.pone.0033093

Lu, P., Takai, K., Weaver, V. M., & Werb, Z. (2011). Extracellular Matrix degradation and remodeling in development and disease. *Cold Spring Harbor Perspectives in Biology*, *3*(12). https://doi.org/10.1101/cshperspect.a005058

Luhr, K. M., Nordström, E. K., Löw, P., & Kristensson, K. (2004). Cathepsin B and L are involved in degradation of prions in GT1-1 neuronal cells. *NeuroReport*, *15*(10). https://doi.org/10.1097/01.wnr.0000134931.81690.34

Mahal, S. P., Demczyk, C. A., Smith, E. W., Klohn, P. C., & Weissmann, C. (2008). Assaying prions in cell culture: The standard scrapie cell assay (SSCA) and the scrapie cell assay in end point format (SCEPA). *Methods in Molecular Biology*, *459*, 49-68. https://doi.org/10.1007/978-1-59745-234-2_4

Majumdar, M. K., Askew, R., Schelling, S., Stedman, N., Blanchet, T., Hopkins, B., Morris, E. A., & Glasson, S. S. (2007). Double-knockout of ADAMTS-4 and ADAMTS-5 in mice results in physiologically normal animals and prevents the progression of osteoarthritis. *Arthritis and Rheumatism*, *56*(11). https://doi.org/10.1002/art.23027

Mangé, A., Béranger, F., Peoc'h, K., Onodera, T., Frobert, Y., & Lehmann, S. (2004). Alpha- and beta- cleavages of the amino-terminus of the cellular prion protein. *Biology of the Cell*, *96*(2). https://doi.org/10.1016/j.biolcel.2003.11.007

Marbiah, M. M., Harvey, A., West, B. T., Louzolo, A., Banerjee, P., Alden, J., Grigoriadis, A., Hummerich, H., Kan, H.-M., Cai, Y., Bloom, G. S., Jat, P., Collinge, J., & Klohn, P.-C. (2014). Identification of a gene regulatory network associated with prion replication. *The EMBO Journal*, *33*(14), 1527–1547. https://doi.org/10.15252/embj.201387150

Marconi, G. D., Fonticoli, L., Rajan, T. S., Pierdomenico, S. D., Trubiani, O., Pizzicannella, J., & Diomede, F. (2021). Epithelial-mesenchymal transition (Emt): The type-2 emt in wound healing, tissue regeneration and organ fibrosis. *Cells, 10*(7). https://doi.org/10.3390/cells10071587

Marzo, L., Marijanovic, Z., Browman, D., Chamoun, Z., Caputo, A., & Zurzolo, C. (2013). 4-hydroxytamoxifen leads to prPSc clearance by conveying both prpC and prPSc to lysosomes independently of autophagy. *Journal of Cell Science*, *126*(6). https://doi.org/10.1242/jcs.114801

Masters, C. L., Bateman, R., Blennow, K., Rowe, C. C., Sperling, R. A., & Cummings, J. L. (2015). Alzheimer's disease. *Nature Reviews Disease Primers, 1*, 15056. https://doi.org/10.1038/nrdp.2015.56

Masyuk, A. I., Huang, B. Q., Ward, C. J., Gradilone, S. A., Banales, J. M., Masyuk, T. V., Radtke, B., Splinter, P. L., & LaRusso, N. F. (2010). Biliary exosomes influence cholangiocyte regulatory mechanisms and proliferation through interaction with primary cilia. *American Journal of Physiology - Gastrointestinal and Liver Physiology*, *299*(4). https://doi.org/10.1152/ajpgi.00093.2010

McBride, P. A., Wilson, M. I., Eikelenboom, P., Tunstall, A., & Bruce, M. E. (1998). Heparan sulfate proteoglycan is associated with amyloid plaques and neuroanatomically targeted PrP pathology throughout the incubation period of scrapie-infected mice. *Experimental Neurology*, *149*(2). https://doi.org/10.1006/exnr.1997.6740

McDonald, A. J., Dibble, J. P., Evans, E. G. B., & Millhauser, G. L. (2014). A new paradigm for enzymatic control of α-cleavage and β-cleavage of the prion protein. *Journal of Biological Chemistry*, *289*(2). https://doi.org/10.1074/jbc.M113.502351

McDonald, A. J., Leon, D. R., Markham, K. A., Wu, B., Heckendorf, C. F., Schilling, K., Showalter, H. D., Andrews, P. C., McComb, M. E., Pushie, M. J., Costello, C. E., Millhauser, G. L., & Harris, D. A. (2019). Altered Domain Structure of the Prion Protein Caused by Cu2+ Binding and Functionally Relevant Mutations: Analysis by Cross-Linking, MS/MS, and NMR. *Structure*, *27*(6). https://doi.org/10.1016/j.str.2019.03.008

McDonald, A. J., & Millhauser, G. L. (2014). PrP overdrive: Does inhibition of a-Cleavage contribute to PrPC toxicity and prion disease? *Prion*, *8*(2). https://doi.org/10.4161/pri.28796

McKenzie, A. J., Hicks, S. R., Svec, K. V., Naughton, H., Edmunds, Z. L., & Howe, A. K. (2018). The mechanical microenvironment regulates ovarian cancer cell morphology, migration, and spheroid disaggregation. *Scientific Reports*, *8*(1). https://doi.org/10.1038/s41598-018-25589-0

McKinley, M. P., Meyer, R. K., Kenaga, L., Rahbar, F., Cotter, R., Serban, A., & Prusiner, S. B. (1991). Scrapie prion rod formation in vitro requires both detergent extraction and limited proteolysis. *Journal of Virology*, *65*(3). https://doi.org/10.1128/jvi.65.3.1340-1351.1991

McLaurin, J., Franklin, T., Zhang, X., Deng, J., & Fraser, P. E. (1999). Interactions of Alzheimer amyloid-β peptides with glycosaminoglycans. *European Journal of Biochemistry*, *266*(3). https://doi.org/10.1046/j.1432-1327.1999.00957.x

Michael, A., Bajracharya, S. D., Yuen, P. S. T., Zhou, H., Star, R. A., Illei, G. G., & Alevizos, I. (2010). Exosomes from human saliva as a source of microRNA biomarkers. *Oral Diseases*, *16*(1). https://doi.org/10.1111/j.1601-0825.2009.01604.x

Mironov, A., Latawiec, D., Wille, H., Bouzamondo-Bernstein, E., Legname, G., Williamson, R. A., Burton, D., DeArmond, S. J., Prusiner, S. B., & Peters, P. J. (2003). Cytosolic prion protein in neurons. *Journal of Neuroscience*, *23*(18). https://doi.org/10.1523/jneurosci.23-18-07183.2003

Miyata, S., Nishimura, Y., & Nakashima, T. (2007). Perineuronal nets protect against amyloid β-protein neurotoxicity in cultured cortical neurons. *Brain Research*, *1150*(1). https://doi.org/10.1016/j.brainres.2007.02.066

Mohamed, M. M., & Sloane, B. F. (2006). Cysteine cathepsins: Multifunctional enzymes in cancer. *Nature Reviews Cancer*, *6*(10). https://doi.org/10.1038/nrc1949

Mok, T., Jaunmuktane, Z., Joiner, S., Campbell, T., Morgan, C., Wakerley, B., Golestani, F., Rudge, P., Mead, S., Jäger, H. R., Wadsworth, J. D. F., Brandner, S., & Collinge, J. (2017). Variant Creutzfeldt–Jakob Disease in a Patient with Heterozygosity at PRNP Codon 129. *New England Journal of Medicine*, *376*(3). https://doi.org/10.1056/nejmc1610003

Montagna, P., Gambetti, P., Cortelli, P., & Lugaresi, E. (2003). Familial and sporadic fatal insomnia. *Lancet Neurology, 2*(3). https://doi.org/10.1016/S1474-4422(03)00323-5

Moradi, B., Schönit, E., Nierhoff, C., Hagmann, S., Oberle, D., Gotterbarm, T., Schmitt, H., & Zeifang, F. (2012). First-generation autologous chondrocyte implantation in patients with cartilage defects of the knee: 7 to 14 years' clinical and magnetic resonance imaging follow-up evaluation. *Arthroscopy - Journal of Arthroscopic and Related Surgery*, *28*(12). https://doi.org/10.1016/j.arthro.2012.05.883

Morawski, M., Brückner, G., Jäger, C., Seeger, G., Matthews, R. T., & Arendt, T. (2012). Involvement of perineuronal and perisynaptic extracellular matrix in Alzheimer's disease neuropathology. *Brain Pathology*, *22*(4). https://doi.org/10.1111/j.1750-3639.2011.00557.x

Motamedi-Shad, N., Monsellier, E., & Chiti, F. (2009). Amyloid formation by the model protein muscle acylphosphatase is accelerated by heparin and heparan sulphate through a scaffolding-based mechanism. *Journal of Biochemistry*, *146*(6). https://doi.org/10.1093/jb/mvp128

Motamedi-Shad, N., Monsellier, E., Torrasa, S., Relini, A., & Chiti, F. (2009). Kinetic analysis of amyloid formation in the presence of heparan sulfate. Faster unfolding and change of pathway. *Journal of Biological Chemistry*, *284*(43). https://doi.org/10.1074/jbc.M109.018747

Moya, K. L., Hässig, R., Créminon, C., Laffont, I., & Di Giamberardino, L. (2004). Enhanced detection and retrograde axonal transport of PrPc in peripheral nerve. *Journal of Neurochemistry*, *88*(1). https://doi.org/10.1046/j.1471-4159.2003.02150.x

Murray, K., Ritchie, D. L., Bruce, M., Young, C. A., Doran, M., Ironside, J. W., & Will, R. G. (2008). Sporadic Creutzfeldt-Jakob disease in two adolescents. *Journal of Neurology, Neurosurgery and Psychiatry*, *79*(1). https://doi.org/10.1136/jnnp.2006.104570

Naiki, H., & Nagai, Y. (2009). Molecular pathogenesis of protein misfolding diseases: Pathological molecular environments versus quality control systems against misfolded proteins. *Journal of Biochemistry, 146*(6). https://doi.org/10.1093/jb/mvp119

Nakamura, H., Fujii, Y., Inoki, I., Sugimoto, K., Tanzawa, K., Matsuki, H., Miura, R., Yamaguchi, Y., & Okada, Y. (2000). Brevican is degraded by matrix metalloproteinases and aggrecanase-1 (ADAMTS4) at different sites. *Journal of Biological Chemistry*, *275*(49). https://doi.org/10.1074/jbc.M003875200

Nakanishi, H. (2020). Cathepsin regulation on microglial function. *Biochimica et Biophysica Acta - Proteins and Proteomics, 1868*(9) (Vol. 1868, Issue 9). https://doi.org/10.1016/j.bbapap.2020.140465

Nishi, T., & Forgac, M. (2002). The vacuolar (H+)-ATPases - Nature's most versatile proton pumps. *Nature Reviews Molecular Cell Biology, 3*(2). https://doi.org/10.1038/nrm729

Notari, S., Appleby, B. S., & Gambetti, P. (2018). Variably protease-sensitive prionopathy. *Handbook of Clinical Neurology*, *153*, 175-190. https://doi.org/10.1016/B978-0-444-63945-5.00010-6

Notari, S., Strammiello, R., Capellari, S., Giese, A., Cescatti, M., Grassi, J., Ghetti, B., Langeveld, J. P. M., Zou, W. Q., Gambetti, P., Kretzschmar, H. A., & Parchi, P. (2008). Characterization of truncated forms of abnormal prion protein in Creutzfeldt-Jakob disease. *Journal of Biological Chemistry*, *283*(45). https://doi.org/10.1074/jbc.M801877200

Novak, U., & Kaye, A. H. (2000). Extracellular matrix and the brain: Components and function. *Journal of Clinical Neuroscience, 7*(4). https://doi.org/10.1054/jocn.1999.0212

Oesch, B., Westaway, D., Wälchli, M., McKinley, M. P., Kent, S. B. H., Aebersold, R., Barry, R. A., Tempst, P., Teplow, D. B., Hood, L. E., Prusiner, S. B., & Weissmann, C. (1985). A cellular gene encodes scrapie PrP 27-30 protein. *Cell*, *40*(4). https://doi.org/10.1016/0092-8674(85)90333-2

Ogura, T., Mosier, B. A., Bryant, T., & Minas, T. (2017). A 20-Year Follow-up after First-Generation Autologous Chondrocyte Implantation. *American Journal of Sports Medicine*, *45*(12). https://doi.org/10.1177/0363546517716631

Okada, Y., & Nakanishi, I. (1989). Activation of matrix metalloproteinase 3 (stromelysin) and matrix metalloproteinase 2 ('gelatinase') by human neutrophil elastase and cathepsin G. *FEBS Letters*, *249*(2). https://doi.org/10.1016/0014-5793(89)80657-X

Omid, H., Abdollahi, S., Bonakdar, S., Haghighipour, N., Shokrgozar, M. A., & Mohammadi, J. (2023). Biomimetic vascular tissue engineering by decellularized scaffold and concurrent cyclic tensile and shear stresses. *Journal of Materials Science: Materials in Medicine*, *34*(3). https://doi.org/10.1007/s10856-023-06716-4

Önfelt, B., Nedvetzki, S., Benninger, R. K. P., Purbhoo, M. A., Sowinski, S., Hume, A. N., Seabra, M. C., Neil, M. A. A., French, P. M. W., & Davis, D. M. (2006). Structurally Distinct Membrane Nanotubes between Human Macrophages Support Long-Distance Vesicular Traffic or Surfing of Bacteria. *The Journal of Immunology*, *177*(12). https://doi.org/10.4049/jimmunol.177.12.8476

Palanisamy, V., Sharma, S., Deshpande, A., Zhou, H., Gimzewski, J., & Wong, D. T. (2010). Nanostructural and transcriptomic analyses of human saliva derived exosomes. *PLoS ONE*, *5*(1). https://doi.org/10.1371/journal.pone.0008577

Pan, B. T., Teng, K., Wu, C., Adam, M., & Johnstone, R. M. (1985). Electron microscopic evidence for externalization of the transferrin receptor in vesicular form in sheep reticulocytes. *Journal of Cell Biology*, *101*(3). https://doi.org/10.1083/jcb.101.3.942

Pan, K. M., Baldwin, M., Nguyen, J., Gasset, M., Serban, A., Groth, D., Mehlhorn, I., Huang, Z., Fletterick, R. J., Cohen, F. E., & Prusiner, S. B. (1993). Conversion of α-helices into β-sheets features in the formation of the scrapie prion proteins. *Proceedings of the National Academy of Sciences of the United States of America*, *90*(23). https://doi.org/10.1073/pnas.90.23.10962

Parchi, P., Capellari, S., & Gambetti, P. (2000). Intracerebral distribution of the abnormal isoform of the prion protein in sporadic Creutzfeldt-Jakob disease and fatal insomnia. *Microscopy Research and Technique*, *50*(1). https://doi.org/10.1002/1097-0029(20000701)50:1<16::AID-JEMT4>3.0.CO;2-Y

Parchi, P., Chen, S. G., Brown, P., Zou, W., Capellari, S., Budka, H., Hainfellner, J., Reyes, P. F., Golden, G. T., Hauw, J. J., Gajdusek, D. C., & Gambetti, P. (1998). Different patterns of truncated prion protein fragments correlate with distinct phenotypes in P102L Gerstmann-Sträussler-Scheinker disease. *Proceedings of the National Academy of Sciences of the United States of America*, *95*(14). https://doi.org/10.1073/pnas.95.14.8322

Peixoto, P., Etcheverry, A., Aubry, M., Missey, A., Lachat, C., Perrard, J., Hendrick, E., Delage-Mourroux, R., Mosser, J., Borg, C., Feugeas, J. P., Herfs, M., Boyer-Guittaut, M., & Hervouet, E. (2019). EMT is associated with an epigenetic signature of ECM remodeling genes. *Cell Death and Disease*, *10*(3). https://doi.org/10.1038/s41419-019-1397-4

Perlmutter, L. S., Barrón, E., Saperia, D., & Chui, H. C. (1991). Association between vascular basement membrane components and the lesions of Alzheimer's disease. *Journal of Neuroscience Research*, *30*(4). https://doi.org/10.1002/jnr.490300411

Perlmutter, L. S., & Helena Chang Chui. (1990). Microangiopathy, the vascular basement membrane and Alzheimer's disease: a review. *Brain Research Bulletin*, *24*(5). https://doi.org/10.1016/0361-9230(90)90007-M

Peters, P. J., Mironov, A., Peretz, D., Van Donselaar, E., Leclerc, E., Erpel, S., DeArmond, S. J., Burton, D. R., Williamson, R. A., Vey, M., & Prusiner, S. B. (2003). Trafficking of prion proteins through a caveolae-mediated endosomal pathway. *Journal of Cell Biology*, *162*(4). https://doi.org/10.1083/jcb.200304140

Phatnani, H., Kwan, J., Sareen, D., Broach, J. R., Simmons, Z., Arcila-Londono, X., Lee, E. B., Van Deerlin, V. M., Shneider, N. A., Fraenkel, E., Ostrow, L. W., Baas, F., Zaitlen, N., Berry, J. D., Malaspina, A.,

Fratta, P., Cox, G. A., Thompson, L. M., Finkbeiner, S., … Svendsen, C. N. (2021). An integrated multi-omic analysis of iPSC-derived motor neurons from C9ORF72 ALS patients. *IScience*, *24*(11). https://doi.org/10.1016/j.isci.2021.103221

Philiastides, A., Ribes, J. M., Yip, D. C. M., Schmidt, C., Benilova, I., & Klöhn, P. C. (2019). A new cell model for investigating prion strain selection and adaptation. *Viruses*, *11*(10). https://doi.org/10.3390/v11100888

Piccardo, P., Liepnieks, J. J., William, A., Dlouhy, S. R., Farlow, M. R., Young, K., Nochlin, D., Bird, T. D., Nixon, R. R., Ball, M. J., DeCarli, C., Bugiani, O., Tagliavini, F., Benson, M. D., & Ghetti, B. (2001). Prion proteins with different conformations accumulate in Gerstmann-Sträussler-Scheinker disease caused by A117V and F198S mutations. *American Journal of Pathology*, *158*(6). https://doi.org/10.1016/S0002-9440(10)64692-5

Pisitkun, T., Shen, R. F., & Knepper, M. A. (2004). Identification and proteomic profiling of exosomes in human urine. *Proceedings of the National Academy of Sciences of the United States of America*, *101*(36). https://doi.org/10.1073/pnas.0403453101

Poliakov, A., Spilman, M., Dokland, T., Amling, C. L., & Mobley, J. A. (2009). Structural heterogeneity and protein composition of exosome-like vesicles (prostasomes) in human semen. *Prostate*, *69*(2). https://doi.org/10.1002/pros.20860

Prusiner, S. B. (1982). Novel proteinaceous infectious particles cause scrapie. *Science*, *216*(4542). https://doi.org/10.1126/science.6801762

Pyrgaki, C., Trainor, P., Hadjantonakis, A. K., & Niswander, L. (2010). Dynamic imaging of mammalian neural tube closure. *Developmental Biology*, *344*(2). https://doi.org/10.1016/j.ydbio.2010.06.010

Qi, B., Newcomer, R., & Sang, Q.-X. (2009). ADAM19/Adamalysin 19 Structure, Function, and Role as a Putative Target in Tumors and Inflammatory Diseases. *Current Pharmaceutical Design*, *15*(20). https://doi.org/10.2174/138161209788682352

Quijano, L. M., Naranjo, J. D., El-Mossier, S. O., Turner, N. J., Molina, C. P., Bartolacci, J., Zhang, L., White, L., Li, H., & Badylak, S. F. (2020). Matrix-bound nanovesicles: The effects of isolation method upon yield, purity, and function. *Tissue Engineering - Part C: Methods*, *26*(10). https://doi.org/10.1089/ten.tec.2020.0243

Radovanovic, I., Braun, N., Giger, O. T., Mertz, K., Miele, G., Prinz, M., Navarro, B., & Aguzzi, A. (2005). Truncated prion protein and Doppel are myelinotoxic in the absence of oligodendrocytic PrPC. *Journal of Neuroscience*, *25*(19). https://doi.org/10.1523/JNEUROSCI.0328-05.2005

Rauch, U. (2007). Brain matrix: Structure, turnover and necessity. *Biochemical Society Transactions*, *35*(4). https://doi.org/10.1042/BST0350656

Rauti, R., Renous, N., & Maoz, B. M. (2019). Mimicking the Brain Extracellular Matrix in Vitro: A Review of Current Methodologies and Challenges. *Israel Journal of Chemistry*, *19*(20). https://doi.org/10.1002/ijch.201900052

Re, L., Rossini, F., Re, F., Bordicchia, M., Mercanti, A., Fernandez, O. S. L., & Barocci, S. (2006). Prion protein potentiates acetylcholine release at the neuromuscular junction. *Pharmacological Research*, *53*(1). https://doi.org/10.1016/j.phrs.2005.09.002

Reid, S. E., Kay, E. J., Neilson, L. J., Henze, A., Serneels, J., McGhee, E. J., Dhayade, S., Nixon, C., Mackey, J. B., Santi, A., Swaminathan, K., Athineos, D., Papalazarou, V., Patella, F., Román-Fernández, Á., ElMaghloob, Y., Hernandez-Fernaud, J. R., Adams, R. H., Ismail, S., … Zanivan, S. (2017). Tumor matrix stiffness promotes metastatic cancer cell interaction with the endothelium. *The EMBO Journal*, *36*(16). https://doi.org/10.15252/embj.201694912

Ren, H., Shi, X., Tao, L., Xiao, J., Han, B., Zhang, Y., Yuan, X., & Ding, Y. (2013). Evaluation of two decellularization methods in the development of a whole-organ decellularized rat liver scaffold. *Liver International*, *33*(3). https://doi.org/10.1111/liv.12088

Ren, H., Zhao, F., Zhang, Q., Huang, X., & Wang, Z. (2022). Autophagy and skin wound healing. In *Burns and Trauma, 10*, tkac003. https://doi.org/10.1093/burnst/tkac003

Repnik, U., Stoka, V., Turk, V., & Turk, B. (2012). Lysosomes and lysosomal cathepsins in cell death. *Biochimica et Biophysica Acta - Proteins and Proteomics, 1824*(1). https://doi.org/10.1016/j.bbapap.2011.08.016

Ribes, J., Patel, M., Halim, H., Tooze, S., & Kloehn, P. (2022). Prion protein conversion at two distinct cellular sites precedes fibrillisation [Preprint]. https://doi.org/10.21203/rs.3.rs-1622593/v1

Ricard-Blum, S. (2011). The Collagen Family. *Cold Spring Harbor Perspectives in Biology*, *3*(1). https://doi.org/10.1101/cshperspect.a004978

Rice, A. J., Cortes, E., Lachowski, D., Cheung, B. C. H., Karim, S. A., Morton, J. P., & Del Río Hernández, A. (2017). Matrix stiffness induces epithelial-mesenchymal transition and promotes chemoresistance in pancreatic cancer cells. *Oncogenesis*, *6*(7). https://doi.org/10.1038/oncsis.2017.54

Rieder, E., Kasimir, M. T., Silberhumer, G., Seebacher, G., Wolner, E., Simon, P., & Weigel, G. (2004). Decellularization protocols of porcine

heart valves differ importantly in efficiency of cell removal and susceptibility of the matrix to recellularization with human vascular cells. *Journal of Thoracic and Cardiovascular Surgery*, *127*(2). https://doi.org/10.1016/j.jtcvs.2003.06.017

Riek, R., Hornemann, S., Wider, G., Billeter, M., Glockshuber, R., & Wuthrich, K. (1996). NMR structure of the mouse prion protein domain PrP (121-231). *Nature*, *382*(6587). https://doi.org/10.1038/382180a0

Robakis, N. K., Devine-Gage, E. A., Jenkins, E. C., Kascsak, R. J., Brown, W. T., Krawczun, M. S., & Silverman, W. P. (1986). Localization of a human gene homologous to the PrP gene on the p ARM of chromosome 20 and detection of PrP-related antigens in normal human brain. *Biochemical and Biophysical Research Communications*, *140*(2). https://doi.org/10.1016/0006-291X(86)90796-5

Robbins, P. D., & Morelli, A. E. (2014). Regulation of immune responses by extracellular vesicles. *Nature Reviews Immunology, 14*(3). https://doi.org/10.1038/nri3622

Rodriguez, R. A., Chen, L. Y., Plascencia-Villa, G., & Perry, G. (2017). Elongation affinity, activation barrier, and stability of Aβ42 oligomers/fibrils in physiological saline. *Biochemical and Biophysical Research Communications*, *487*(2). https://doi.org/10.1016/j.bbrc.2017.04.084

Rogaeva, E., Zadikoff, C., Ponesse, J., Schmitt-Ulms, G., Kawarai, T., Sato, C., Salehi-Rad, S., St. George-Hyslop, P., & Lang, A. E. (2006). Childhood onset in familial prion disease with a novel mutation in the PRNP gene. *Archives of Neurology*, *63*(7). https://doi.org/10.1001/archneur.63.7.1016

Rose, K. W. J., Taye, N., Karoulias, S. Z., & Hubmacher, D. (2021). Regulation of ADAMTS Proteases. In *Frontiers in Molecular Biosciences, 8*, 701959. https://doi.org/10.3389/fmolb.2021.701959

Rossi, A., Deveraux, Q., Turk, B., & Sali, A. (2004). Comprehensive search for cysteine cathepsins in the human genome. *Biological Chemistry*, *385*(5). https://doi.org/10.1515/BC.2004.040

Rouvinski, A., Karniely, S., Kounin, M., Moussa, S., Goldberg, M. D., Warburg, G., Lyakhovetsky, R., Papy-Garcia, D., Kutzsche, J., Korth, C., Carlson, G. A., Godsave, S. F., Peters, P. J., Luhr, K., Kristensson, K., & Taraboulos, A. (2014). Live imaging of prions reveals nascent PrPSc in cell-surface, raft-associated amyloid strings and webs. *The Journal of Cell Biology*, *204*(3), 423–441. https://doi.org/10.1083/jcb.201308028

Rowlands, D., Lensjø, K. K., Dinh, T., Yang, S., Andrews, M. R., Hafting, T., Fyhn, M., Fawcett, J. W., & Dick, G. (2018). Aggrecan directs extracellular matrix-mediated neuronal plasticity. *Journal of*

Neuroscience, *38*(47). https://doi.org/10.1523/JNEUROSCI.1122-18.2018

Rupp, I., Sologub, L., Williamson, K. C., Scheuermayer, M., Reininger, L., Doerig, C., Eksi, S., Kombila, D. U., Frank, M., & Pradel, G. (2011). Malaria parasites form filamentous cell-to-cell connections during reproduction in the mosquito midgut. *Cell Research*, *21*(4). https://doi.org/10.1038/cr.2010.176

Rustom, A., Saffrich, R., Markovic, I., Walther, P., & Gerdes, H. H. (2004). Nanotubular Highways for Intercellular Organelle Transport. *Science*, *303*(5660). https://doi.org/10.1126/science.1093133

Saá, P., Castilla, J., & Soto, C. (2006). Ultra-efficient replication of infectious prions by automated protein misfolding cyclic amplification. *Journal of Biological Chemistry*, *281*(46). https://doi.org/10.1074/jbc.M603964200

Saborio, G. P., Permanne, B., & Soto, C. (2001). Sensitive detection of pathological prion protein by cyclic amplification of protein misfolding. *Nature*, *411*(6839). https://doi.org/10.1038/35081095

Safar, J. G. (2012). Molecular pathogenesis of sporadic prion diseases in man. *Prion*, *6*(2). https://doi.org/10.4161/pri.18666

Safar, J., Wille, H., Itri, V., Groth, D., Serban, H., Torchia, M., Cohen, F. E., & Prusiner, S. B. (1998). Eight prion strains have PrP(Sc) molecules with different conformations. *Nature Medicine*, *4*(10). https://doi.org/10.1038/2654

Salas-Vidal, E., & Lomelí, H. (2004). Imaging filopodia dynamics in the mouse blastocyst. *Developmental Biology*, *265*(1). https://doi.org/10.1016/j.ydbio.2003.09.012

Salès, N., Hässig, R., Rodolfo, K., Di Giamberardino, L., Traiffort, E., Ruat, M., Frétier, P., & Moya, K. L. (2002). Developmental expression of the cellular prion protein in elongating axons. *European Journal of Neuroscience*, *15*(7). https://doi.org/10.1046/j.1460-9568.2002.01953.x

Salès, N., Rodolfo, K., Hässig, R., Faucheux, B., Di Giamberardino, L., & Moya, K. L. (1998). Cellular prion protein localization in rodent and primate brain. *European Journal of Neuroscience*, *10*(7). https://doi.org/10.1046/j.1460-9568.1998.00258.x

Schiff, E., Gousset, K., Browman, D., Langevin, C., Marijanovic, Z., & Zurzolo, C. (2008). Prions hijack tunneling nanotubes for intercellular spread. *BMC Proceedings*, *2*(S1). https://doi.org/10.1186/1753-6561-2-s1-p63

Schneider, C., Lehmann, J., Van Osch, G. J. V. M., Hildner, F., Teuschl, A., Monforte, X., Miosga, D., Heimel, P., Priglinger, E., Redl, H., Wolbank, S., & Nürnberger, S. (2016). Systematic comparison of protocols for the preparation of human articular cartilage for use as scaffold material in

cartilage tissue engineering. *Tissue Engineering - Part C: Methods*, *22*(12). https://doi.org/10.1089/ten.tec.2016.0380

Schneider, L., Murray, P., Lévy, R., & Wilmshurst, P. (2022). Time to retract Lancet paper on tissue engineered trachea transplants. *BMJ (Clinical research ed.)*, *376,* o498. https://doi.org/10.1136/bmj.o498

Schonberger, O., Horonchik, L., Gabizon, R., Papy-Garcia, D., Barritault, D., & Taraboulos, A. (2003). Novel heparan mimetics potently inhibit the scrapie prion protein and its endocytosis. *Biochemical and Biophysical Research Communications*, *312*(2). https://doi.org/10.1016/j.bbrc.2003.10.150

Schultz, G. S., & Wysocki, A. (2009). Interactions between extracellular matrix and growth factors in wound healing. *Wound Repair and Regeneration, 17*(2). https://doi.org/10.1111/j.1524-475X.2009.00466.x

Schultz, V., Suflita, M., Liu, X., Zhang, X., Yu, Y., Li, L., Green, D. E., Xu, Y., Zhang, F., DeAngelis, P. L., Liu, J., & Linhardt, R. J. (2017). Heparan sulfate domains required for fibroblast growth factor 1 and 2 signaling through fibroblast growth factor receptor 1c. *Journal of Biological Chemistry*, *292*(6). https://doi.org/10.1074/jbc.M116.761585

Scott, L. E., Weinberg, S. H., & Lemmon, C. A. (2019). Mechanochemical Signaling of the Extracellular Matrix in Epithelial-Mesenchymal Transition. In *Frontiers in Cell and Developmental Biology*, *7*, 135. https://doi.org/10.3389/fcell.2019.00135

Sennoune, S. R., Bakunts, K., Martínez, G. M., Chua-Tuan, J. L., Kebir, Y., Attaya, M. N., & Martínez-Zaguilán, R. (2004). Vacuolar H+-ATPase in human breast cancer cells with distinct metastatic potential: Distribution and functional activity. *American Journal of Physiology - Cell Physiology*, *286*(6). https://doi.org/10.1152/ajpcell.00407.2003

Sennoune, S. R., Luo, D., & Martínez-Zaguilán, R. (2004). Plasmalemmal vacuolar-type H+-ATPase in cancer biology. *Cell Biochemistry and Biophysics, 40*(2). https://doi.org/10.1385/CBB:40:2:185

Serebriiskii, I., Castelló-Cros, R., Lamb, A., Golemis, E. A., & Cukierman, E. (2008). Fibroblast-derived 3D matrix differentially regulates the growth and drug-responsiveness of human cancer cells. *Matrix Biology*, *27*(6). https://doi.org/10.1016/j.matbio.2008.02.008

Serot, J. M., Béné, M. C., Foliguet, B., & Faure, G. C. (1997). Altered choroid plexus basement membrane and epithelium in late-onset Alzheimer's disease: An ultrastructural study. *Annals of the New York Academy of Sciences*, *826,* 507-509. https://doi.org/10.1111/j.1749-6632.1997.tb48514.x

Sharma, S., Mukherjee, M., Kedage, V., Muttigi, M. S., Rao, A., & Rao, S. (2009). Sporadic Creutzfeldt-Jakob disease-A review. *International*

Journal of Neuroscience, *119*(11). https://doi.org/10.1080/00207450903139762

Sholoqu, N., Szegezdi, E., Lowery, A., Kerin, M., Pandit, A., & Zeugolis, D. I. (2016). Recreating complex pathophysiologies in vitro with extracellular matrix surrogates for anticancer therapeutics screening. *Drug Discovery Today, 21*(9). https://doi.org/10.1016/j.drudis.2016.06.001

Sigurdsson, B. (1954). RIDA, A Chronic Encephalitis of Sheep with General Remarks on Infections Which Develop Slowly and Some of Their Special Characteristics. In *British Veterinary Journal, 110*(9). https://doi.org/10.1016/S0007-1935(17)50172-4

Singh, H., Purohit, S. D., Bhaskar, R., Yadav, I., Gupta, M. K., & Mishra, N. C. (2022). Development of decellularization protocol for caprine small intestine submucosa as a biomaterial. *Biomaterials and Biosystems*, *5,* 100035. https://doi.org/10.1016/j.bbiosy.2021.100035

Smith, G. A., Howell, G. J., Phillips, C., Muench, S. P., Ponnambalam, S., & Harrison, M. A. (2016). Extracellular and luminal pH regulation by vacuolar H+-ATPase isoform expression and targeting to the plasma membrane and endosomes. *Journal of Biological Chemistry*, *291*(16). https://doi.org/10.1074/jbc.M116.723395

Snow, A. D., Cummings, J. A., & Lake, T. (2021). The Unifying Hypothesis of Alzheimer's Disease: Heparan Sulfate Proteoglycans/Glycosaminoglycans Are Key as First Hypothesized Over 30 Years Ago. *Frontiers in Aging Neuroscience, 13*, 710683. https://doi.org/10.3389/fnagi.2021.710683

Snow, A. D., Sekiguchi, R., Nochlin, D., Fraser, P., Kimata, K., Mizutani, A., Arai, M., Schreier, W. A., & Morgan, D. G. (1994). An important role of heparan sulfate proteoglycan (perlecan) in a model system for the deposition and persistence of fibrillar aβ-amyloid in rat brain. *Neuron*, *12*(1). https://doi.org/10.1016/0896-6273(94)90165-1

Snow, A. D., Wight, T. N., Nochlin, D., Koike, Y., Kimata, K., DeArmond, S. J., & Prusiner, S. B. (1990). Immunolocalization of heparan sulfate proteoglycans to the prion protein amyloid plaques of Gerstmann-Straussler syndrome, Creutzfeldt-Jakob disease and scrapie. *Laboratory Investigation*, *63*(5). PMID: 1977959

Sobotič, B., Vizovišek, M., Vidmar, R., Van Damme, P., Gocheva, V., Joyce, J. A., Gevaert, K., Turk, V., Turk, B., & Fonović, M. (2015). Proteomic identification of cysteine cathepsin substrates shed from the surface of cancer cells. *Molecular and Cellular Proteomics*, *14*(8). https://doi.org/10.1074/mcp.M114.044628

Soldevila, M., Andrés, A. M., Ramírez-Soriano, A., Marquès-Bonet, T., Calafell, F., Navarro, A., & Bertranpetit, J. (2006). The prion protein

gene in humans revisited: Lessons from a worldwide resequencing study. *Genome Research*, *16*(2). https://doi.org/10.1101/gr.4345506

Son, E. D., Kim, H., Choi, H., Lee, S. H., Lee, J. Y., Kim, S., Closs, B., Lee, S., Chung, J. H., & Hwang, J. S. (2009). Cathepsin G increases MMP expression in normal human fibroblasts through fibronectin fragmentation, and induces the conversion of proMMP-1 to active MMP-1. *Journal of Dermatological Science, 53*(2). https://doi.org/10.1016/j.jdermsci.2008.08.006

Sorg, B. A., Berretta, S., Blacktop, J. M., Fawcett, J. W., Kitagawa, H., Kwok, J. C. F., & Miquel, M. (2016). Casting a wide net: Role of perineuronal nets in neural plasticity. *Journal of Neuroscience*, *36*(45). https://doi.org/10.1523/JNEUROSCI.2351-16.2016

Sowinski, S., Jolly, C., Berninghausen, O., Purbhoo, M. A., Chauveau, A., Köhler, K., Oddos, S., Eissmann, P., Brodsky, F. M., Hopkins, C., Önfelt, B., Sattentau, Q., & Davis, D. M. (2008). Membrane nanotubes physically connect T cells over long distances presenting a novel route for HIV-1 transmission. *Nature Cell Biology*, *10*(2). https://doi.org/10.1038/ncb1682

Stockman, S. (1913). Scrapie: An obsecure disease of sheep. *Journal of Comparative Pathology and Therapeutics*, *26*, 317-327. https://doi.org/10.1016/S0368-1742(13)80060-4

Sparkes, R. S., Simon, M., Cohn, V. H., Fournier, R. E., Lem, J., Klisak, I., Heinzmann, C., Blatt, C., Lucero, M., & Mohandas, T. (1986). Assignment of the human and mouse prion protein genes to homologous chromosomes. *Proceedings of the National Academy of Sciences of the United States of America*, *83*(19). https://doi.org/10.1073/pnas.83.19.7358

Stahl, N., Baldwin, M. A., Prusiner, S. B., Teplow, D. B., Hood, L., Gibson, B. W., & Burlingame, A. L. (1993). Structural Studies of the Scrapie Prion Protein Using Mass Spectrometry and Amino Acid Sequencing. *Biochemistry*, *32*(8). https://doi.org/10.1021/bi00059a016

Stahl, N., Borchelt, D. R., Hsiao, K., & Prusiner, S. B. (1987). Scrapie prion protein contains a phosphatidylinositol glycolipid. *Cell*, *51*(2). https://doi.org/10.1016/0092-8674(87)90150-4

Street, J. M., Barran, P. E., Mackay, C. L., Weidt, S., Balmforth, C., Walsh, T. S., Chalmers, R. T. A., Webb, D. J., & Dear, J. W. (2012). Identification and proteomic profiling of exosomes in human cerebrospinal fluid. *Journal of Translational Medicine*, *10*(1). https://doi.org/10.1186/1479-5876-10-5

Streuli, C. (1999). Extracellular matrix remodelling and cellular differentiation. In *Current Opinion in Cell Biology* (Vol. 11, Issue 5). https://doi.org/10.1016/S0955-0674(99)00026-5

Sun, Y., Xu, S., Jiang, M., Liu, X., Yang, L., Bai, Z., & Yang, Q. (2021). Role of the Extracellular Matrix in Alzheimer's Disease. *Frontiers in Aging Neuroscience, 13*, 707466. https://doi.org/10.3389/fnagi.2021.707466

Sykova, E., & Nicholson, C. (2008). Diffusion in Brain Extracellular Space. *Physiological Reviews*, *88*, 1277–1340. https://doi.org/10.1152/physrev.00027.2007.-Diffusion

Szepesi, Z., Bijata, M., Ruszczycki, B., Kaczmarek, L., & Wlodarczyk, J. (2013). Matrix Metalloproteinases Regulate the Formation of Dendritic Spine Head Protrusions during Chemically Induced Long-Term Potentiation. *PLoS ONE*, *8*(5). https://doi.org/10.1371/journal.pone.0063314

Tagliavini, F., Lievens, P. M. J., Tranchant, C., Warter, J. M., Mohr, M., Giaccone, G., Perini, F., Rossi, G., Salmona, M., Piccardo, P., Ghetti, B., Beavis, R. C., Bugiani, O., Frangione, B., & Prelli, F. (2001). A 7-kDa Prion Protein (PrP) Fragment, an Integral Component of the PrP Region Required for Infectivity, Is the Major Amyloid Protein in Gerstmann-Sträussler-Scheinker Disease A117V. *Journal of Biological Chemistry*, *276*(8). https://doi.org/10.1074/jbc.M007062200

Tagliavini, F., Prelli, F., Ghiso, J., Bugiani, O., Serban, D., Prusiner, S. B., Farlow, M. R., Ghetti, B., & Frangione, B. (1991). Amyloid protein of Gerstmann-Straussler-Scheinker disease (Indiana kindred) is an 11 kd fragment of prion protein with an N-terminal glycine at codon 58. *EMBO Journal*, *10*(3). https://doi.org/10.1002/j.1460-2075.1991.tb07977.x

Tan, Z. H., Dharmadhikari, S., Liu, L., Wolter, G., Shontz, K. M., Reynolds, S. D., Johnson, J., Breuer, C. K., & Chiang, T. (2022). Tracheal Macrophages During Regeneration and Repair of Long-Segment Airway Defects. *Laryngoscope*, *132*(4). https://doi.org/10.1002/lary.29698

Tanaka, M., Fujiwara, A., Suzuki, A., Yamasaki, T., Hasebe, R., Masujin, K., & Horiuchi, M. (2016). Comparison of abnormal isoform of prion protein in prion-infected cell lines and primary-cultured neurons by PrPSc-specific immunostaining. *Journal of General Virology*, *97*(8). https://doi.org/10.1099/jgv.0.000514

Tancini, B., Buratta, S., Delo, F., Sagini, K., Chiaradia, E., Pellegrino, R. M., Emiliani, C., & Urbanelli, L. (2020). Lysosomal exocytosis: The extracellular role of an intracellular organelle. *Membranes, 10*(12). https://doi.org/10.3390/membranes10120406

Taraboulos, A., Raeber, A. J., Borchelt, D. R., Serban, D., & Prusiner, S. B. (1992). Synthesis and trafficking of prion proteins in cultured cells. *Molecular Biology of the Cell*, *3*(8). https://doi.org/10.1091/mbc.3.8.851

Taraboulos, A., Serban, D., & Prusiner, S. B. (1990). Scrapie prion proteins accumulate in the cytoplasm of persistently infected cultured cells. *Journal of Cell Biology*, *110*(6). https://doi.org/10.1083/jcb.110.6.2117

Tardivel, M., Bégard, S., Bousset, L., Dujardin, S., Coens, A., Melki, R., Buée, L., & Colin, M. (2016). Tunneling nanotube (TNT)-mediated neuron-to neuron transfer of pathological Tau protein assemblies. *Acta Neuropathologica Communications*, *4*(1). https://doi.org/10.1186/s40478-016-0386-4

Tauchi, R., Imagama, S., Natori, T., Ohgomori, T., Muramoto, A., Shinjo, R., Matsuyama, Y., Ishiguro, N., & Kadomatsu, K. (2012). The endogenous proteoglycan-degrading enzyme ADAMTS-4 promotes functional recovery after spinal cord injury. *Journal of Neuroinflammation*, *9*, 53. https://doi.org/10.1186/1742-2094-9-53

Taylor, D. A., Lee, P. F., Barac, Y., Hochman-Mendez, C., & Sampaio, L. C. (2020). Chapter 15: Decellularization of whole hearts for cardiac regeneration. *Emerging Technologies for Heart Diseases: Volume 1: Treatments for Heart Failure and Valvular Disorders*. 291-310. https://doi.org/10.1016/B978-0-12-813706-2.00015-4

Taylor, D. R., Parkin, E. T., Cocklin, S. L., Ault, J. R., Aschcroft, A. E., Turner, A. J., & Hooper, N. M. (2009). Role of ADAMs in the ectodomain shedding and conformational conversion of the prion protein. *Journal of Biological Chemistry*, *284*(34). https://doi.org/10.1074/jbc.M109.032599

Tennant, J. M., Li, M., Henderson, D. M., Tyer, M. L., Denkers, N. D., Haley, N. J., Mathiason, C. K., & Hoover, E. A. (2020). Shedding and stability of CWD prion seeding activity in cervid feces. *PLoS ONE*, *15*(3). https://doi.org/10.1371/journal.pone.0227094

Théry, C., Witwer, K. W., Aikawa, E., Alcaraz, M. J., Anderson, J. D., Andriantsitohaina, R., Antoniou, A., Arab, T., Archer, F., Atkin-Smith, G. K., Ayre, D. C., Bach, J. M., Bachurski, D., Baharvand, H., Balaj, L., Baldacchino, S., Bauer, N. N., Baxter, A. A., Bebawy, M., … Zuba-Surma, E. K. (2018). Minimal information for studies of extracellular vesicles 2018 (MISEV2018): a position statement of the International Society for Extracellular Vesicles and update of the MISEV2014 guidelines. *Journal of Extracellular Vesicles*, *7*(1). https://doi.org/10.1080/20013078.2018.1535750

Thomsen, M. S., Routhe, L. J., & Moos, T. (2017). The vascular basement membrane in the healthy and pathological brain. *Journal of Cerebral Blood Flow and Metabolism 37*(10). https://doi.org/10.1177/0271678X17722436

Tohda, C., & Tohda, M. (2017). Extracellular cathepsin L stimulates axonal growth in neurons. *BMC Research Notes*, *10*(1). https://doi.org/10.1186/s13104-017-2940-y

Tonge, D. A., De Burgh, H. T., Docherty, R., Humphries, M. J., Craig, S. E., & Pizzey, J. (2012). Fibronectin supports neurite outgrowth and axonal

regeneration of adult brain neurons in vitro. *Brain Research*, *1453*, 8-16. https://doi.org/10.1016/j.brainres.2012.03.024

Tortorella, M. D., Burn, T. C., Pratta, M. A., Abbaszade, I., Hollis, J. M., Liu, R., Rosenfeld, S. A., Copeland, R. A., Decicco, C. P., Wynn, R., Rockwell, A., Yang, F., Duke, J. L., Solomon, K., George, H., Bruckner, R., Nagase, H., Itoh, Y., Ellis, D. M., … Arner, E. C. (1999). Purification and cloning of aggrecanase-1: A member of the ADAMTS family of proteins. *Science*, *284*(5420). https://doi.org/10.1126/science.284.5420.1664

Tran, A. P., Sundar, S., Yu, M., Lang, B. T., & Silver, J. (2018). Modulation of receptor protein tyrosine phosphatase sigma increases chondroitin sulfate proteoglycan degradation through cathepsin B secretion to enhance axon outgrowth. *Journal of Neuroscience*, *38*(23). https://doi.org/10.1523/JNEUROSCI.3214-17.2018

Turk, E., Teplow, D. B., Hood, L. E., & Prusiner, S. B. (1988). Purification and properties of the cellular and scrapie hamster prion proteins. *European Journal of Biochemistry*, *176*(1). https://doi.org/10.1111/j.1432-1033.1988.tb14246.x

Turk, V., Stoka, V., Vasiljeva, O., Renko, M., Sun, T., Turk, B., & Turk, D. (2012). Cysteine cathepsins: From structure, function and regulation to new frontiers. *Biochimica et Biophysica Acta - Proteins and Proteomics, 1824*(1). https://doi.org/10.1016/j.bbapap.2011.10.002

Valenzuela, J. C., Heise, C., Franken, G., Singh, J., Schweitzer, B., Seidenbecher, C. I., & Frischknecht, R. (2014). Hyaluronan-based extracellular matrix under conditions of homeostatic plasticity. *Philosophical Transactions of the Royal Society B: Biological Sciences*, *369*(1654). https://doi.org/10.1098/rstb.2013.0606

Van Der Kamp, M. W., & Daggett, V. (2010). Influence of pH on the human prion protein: Insights into the early steps of misfolding. *Biophysical Journal*, *99*(7). https://doi.org/10.1016/j.bpj.2010.07.063

Van Everbroeck, B., Dobbeleir, I., De Waele, M., De Leenheir, E., Lübke, U., Martin, J. J., & Cras, P. (2004). Extracellular protein deposition correlates with glial activation and oxidative stress in Creutzfeldt-Jakob and Alzheimer's disease. *Acta Neuropathologica*, *108*(3). https://doi.org/10.1007/s00401-004-0879-2

Veith, N. M., Plattner, H., Stuermer, C. A. O., Schulz-Schaeffer, W. J., & Bürkle, A. (2009). Immunolocalisation of PrPSc in scrapie-infected N2a mouse neuroblastoma cells by light and electron microscopy. *European Journal of Cell Biology*, *88*(1) https://doi.org/10.1016/j.ejcb.2008.08.001

Vella, L. J., Greenwood, D. L. V., Cappai, R., Scheerlinck, J. P. Y., & Hill, A. F. (2008). Enrichment of prion protein in exosomes derived from ovine

cerebral spinal fluid. *Veterinary Immunology and Immunopathology*, *124*(3–4). https://doi.org/10.1016/j.vetimm.2008.04.002

Vella, L. J., Sharples, R. A., Lawson, V. A., Masters, C. L., Cappai, R., & Hill, A. F. (2007). Packaging of prions into exosomes is associated with a novel pathway of PrP processing. *Journal of Pathology*, *211*(5). https://doi.org/10.1002/path.2145

Velnar, T., Bailey, T., & Smrkolj, V. (2009). The wound healing process: An overview of the cellular and molecular mechanisms. *Journal of International Medical Research 37*(5). https://doi.org/10.1177/147323000903700531

Verma, P., & Dalal, K. (2011). ADAMTS-4 and ADAMTS-5: Key enzymes in osteoarthritis. *Journal of Cellular Biochemistry*, *112*(12). https://doi.org/10.1002/jcb.23298

Victoria, G. S., Arkhipenko, A., Zhu, S., Syan, S., & Zurzolo, C. (2016). Astrocyte-to-neuron intercellular prion transfer is mediated by cell-cell contact. *Scientific Reports*, *6,* 20762. https://doi.org/10.1038/srep20762

Vidoni, C., Follo, C., Savino, M., Melone, M. A. B., & Isidoro, C. (2016). The Role of Cathepsin D in the Pathogenesis of Human Neurodegenerative Disorders. *Medicinal Research Reviews, 36*(5). https://doi.org/10.1002/med.21394

Vincenti, M. P., & Brinckerhoff, C. E. (2007). Signal transduction and cell-type specific regulation of matrix metalloproteinase gene expression: Can MMPs be good for you? *Journal of Cellular Physiology, 213*(2). https://doi.org/10.1002/jcp.21208

Wagner, C. A., Finberg, K. E., Breton, S., Marshansky, V., Brown, D., & Geibel, J. P. (2004). Renal vacuolar H+-ATPase. *Physiological Reviews, 84*(4). https://doi.org/10.1152/physrev.00045.2003

Wang, J., Gu, B. J., Masters, C. L., & Wang, Y. J. (2017). A systemic view of Alzheimer disease - Insights from amyloid-β metabolism beyond the brain. *Nature Reviews Neurology, 13*(10). https://doi.org/10.1038/nrneurol.2017.111

Wang, L., Wu, D., Robinson, C. V., Wu, H., & Fu, T. M. (2020). Structures of a Complete Human V-ATPase Reveal Mechanisms of Its Assembly. *Molecular Cell*, *80*(3). https://doi.org/10.1016/j.molcel.2020.09.029

Wang, R., Long, T., Hassan, A., Wang, J., Sun, Y., Xie, X. S., & Li, X. (2020). Cryo-EM structures of intact V-ATPase from bovine brain. *Nature Communications*, *11*(1). https://doi.org/10.1038/s41467-020-17762-9

Wang, R., Wang, J., Hassan, A., Lee, C. H., Xie, X. S., & Li, X. (2021). Molecular basis of V-ATPase inhibition by bafilomycin A1. *Nature Communications*, *12*(1). https://doi.org/10.1038/s41467-021-22111-5

Wang, X., Wang, E., Cao, J., Xiong, F., Yang, Y., & Liu, H. (2017). MiR-145 inhibits the epithelial-to-mesenchymal transition via targeting ADAM19 in human glioblastoma. *Oncotarget*, *8*(54). https://doi.org/10.18632/oncotarget.21442

Wenborn, A., Terry, C., Gros, N., Joiner, S., D'Castro, L., Panico, S., Sells, J., Cronier, S., Linehan, J. M., Brandner, S., Saibil, H. R., Collinge, J., & Wadsworth, J. D. F. (2015). A novel and rapid method for obtaining high titre intact prion strains from mammalian brain. *Scientific Reports*, *5*, 10062. https://doi.org/10.1038/srep10062

Wilgus, T. A. (2012). Growth Factor–Extracellular Matrix Interactions Regulate Wound Repair. *Advances in Wound Care*, *1*(6). https://doi.org/10.1089/wound.2011.0344

Will, R. G., Ironside, J. W., Zeidler, M., Cousens, S. N., Estibeiro, K., Alperovitch, A., Poser, S., Pocchiari, M., Hofmar, A., & Smith, P. G. (1996). A new variant of Creutzfeldt-Jakob disease in the UK. *Lancet*, *347*(9006). https://doi.org/10.1016/S0140-6736(96)91412-9

Wishart, A. L., Conner, S. J., Guarin, J. R., Fatherree, J. P., Peng, Y., McGinn, R. A., Crews, R., Naber, S. P., Hunter, M., Greenberg, A. S., & Oudin, M. J. (2020). Decellularized extracellular matrix scaffolds identify full-length collagen VI as a driver of breast cancer cell invasion in obesity and metastasis. *Science Advances*, *6*(43). https://doi.org/10.1126/sciadv.abc3175

Wolf, G. (2008). Retinoic acid as cause of cell proliferation or cell growth inhibition depending on activation of one of two different nuclear receptors. *Nutrition Reviews, 66*(1). https://doi.org/10.1111/j.1753-4887.2007.00006.x

Wolf, J. H., & Foley, P. (2005). Hans Gerhard Creutzfeldt (1885-1964): A life in neuropathology. *Journal of Neural Transmission*, *112*(8). https://doi.org/10.1007/s00702-005-0288-2

Woods, T., & Gratzer, P. F. (2005). Effectiveness of three extraction techniques in the development of a decellularized bone-anterior cruciate ligament-bone graft. *Biomaterials*, *26*(35). https://doi.org/10.1016/j.biomaterials.2005.05.066

Wopfner, F., Weidenhöfer, G., Schneider, R., Von Brunn, A., Gilch, S., Schwarz, T. F., Werner, T., & Schätzl, H. M. (1999). Analysis of 27 mammalian and 9 avian PrPs reveals high conservation of flexible regions of the prion protein. *Journal of Molecular Biology*, *289*(5). https://doi.org/10.1006/jmbi.1999.2831

Wroe, S. J., Pal, S., Siddique, D., Hyare, H., Macfarlane, R., Joiner, S., Linehan, J. M., Brandner, S., Wadsworth, J. D., Hewitt, P., & Collinge, J. (2006). Clinical presentation and pre-mortem diagnosis of variant Creutzfeldt-Jakob disease associated with blood transfusion: a case

report. *Lancet*, *368*(9552). https://doi.org/10.1016/S0140-6736(06)69835-8

Xu, D., & Esko, J. D. (2014). Demystifying heparan sulfate-protein interactions. *Annual Review of Biochemistry 83*, 129–157. https://doi.org/10.1146/annurev-biochem-060713-035314

Xu, L., Nirwane, A., & Yao, Y. (2019). Basement membrane and blood-brain barrier. *Stroke and Vascular Neurology, 4*(2). https://doi.org/10.1136/svn-2018-000198

Xue, J., Wang, J., Liu, Q., & Luo, A. (2013). Tumor necrosis factor-α induces ADAMTS-4 expression in human osteoarthritis chondrocytes. *Molecular Medicine Reports*, *8*(6). https://doi.org/10.3892/mmr.2013.1729

Yadati, T., Houben, T., Bitorina, A., & Shiri-Sverdlov, R. (2020). The Ins and Outs of Cathepsins: Physiological Function and Role in Disease Management. *Cells, 9*(7). https://doi.org/10.3390/cells9071679

Yaghoubi, A., Azarpira, N., Karbalay-Doust, S., Daneshi, S., Vojdani, Z., & Talaei-Khozani, T. (2022). Prednisolone and mesenchymal stem cell preloading protect liver cell migration and mitigate extracellular matrix modification in transplanted decellularized rat liver. *Stem Cell Research and Therapy*, *13*(1). https://doi.org/10.1186/s13287-022-02711-8

Yam, A. Y., Gao, C. M., Wang, X., Wu, P., & Peretz, D. (2010). The octarepeat region of the prion protein is conformationally altered in PrPSc. *PLoS ONE*, *5*(2). https://doi.org/10.1371/journal.pone.0009316

Yamamoto, A., Tagawa, Y., Yoshimori, T., Moriyama, Y., Masaki, R., & Tashiro, Y. (1998). Bafilomycin A1 prevents maturation of autophagic vacuoles by inhibiting fusion between autophagosomes and lysosomes in rat hepatoma cell line, H-4-II-E cells. *Cell Structure and Function*, *23*(1). https://doi.org/10.1247/csf.23.33

Yamasaki, T., Suzuki, A., Hasebe, R., & Horiuchi, M. (2014). Comparison of the anti-prion mechanism of four different anti-prion compounds, anti-PrP monoclonal antibody 44B1, pentosan polysulfate, chlorpromazine, and U18666A, in prion-infected mouse neuroblastoma cells. *PLoS ONE*, *9*(9). https://doi.org/10.1371/journal.pone.0106516

Yang, D. Q., Feng, S., Chen, W., Zhao, H., Paulson, C., & Li, Y. P. (2012). V-ATPase subunit ATP6AP1 (Ac45) regulates osteoclast differentiation, extracellular acidification, lysosomal trafficking, and protease exocytosis in osteoclast-mediated bone resorption. *Journal of Bone and Mineral Research*, *27*(8). https://doi.org/10.1002/jbmr.1623

Yim, Y. I., Park, B. C., Yadavalli, R., Zhao, X., Eisenberg, E., & Greene, L. E. (2015). The multivesicular body is the major internal site of prion conversion. *Journal of Cell Science*, *128*(7). https://doi.org/10.1242/jcs.165472

Yoshimori, T., Yamamoto, A., Moriyama, Y., Futai, M., & Tashiro, Y. (1991). Bafilomycin A1, a specific inhibitor of vacuolar-type H+-ATPase, inhibits acidification and protein degradation in lysosomes of cultured cells. *Journal of Biological Chemistry*, *266*(26). https://doi.org/10.1016/s0021-9258(19)47429-2

Zahn, R., Liu, A., Lührs, T., Riek, R., Von Schroetter, C., Garcia, F. L., Billeter, M., Calzolai, L., Wider, G., & Wüthrich, K. (2000). NMR solution structure of the human prion protein. *Proceedings of the National Academy of Sciences of the United States of America*, *97*(1). https://doi.org/10.1073/pnas.97.1.145

Zarow, C., Barron, E., Chui, H. C., & Perlmutter, L. S. (1997). Vascular basement membrane pathology and Alzheimer's disease. *Annals of the New York Academy of Sciences*, *826*, 147-160. https://doi.org/10.1111/j.1749-6632.1997.tb48467.x

Zhang, Y., Bi, J., Huang, J., Tang, Y., Du, S., & Li, P. (2020). Exosome: A review of its classification, isolation techniques, storage, diagnostic and targeted therapy applications. In *International Journal of Nanomedicine, 15,* 6917–6934. https://doi.org/10.2147/IJN.S264498

Zhang, Y., Spiess, E., Groschup, M. H., & Bürkle, A. (2003). Up-regulation of cathepsin B and cathepsin L activities in scrapie-infected mouse Neuro2a cells. In *Journal of General Virology, 84*(8). https://doi.org/10.1099/vir.0.19153-0

Zhao, P., Liu, D., Song, C., Li, D., Zhang, X., Horecny, I., Zhang, F., Yan, Y., Zhuang, L., Li, J., Liu, S., Mao, Y., Feng, J., Liu, J., & Tao, W. (2022). Discovery of Isoindoline Amide Derivatives as Potent and Orally Bioavailable ADAMTS-4/5 Inhibitors for the Treatment of Osteoarthritis. *ACS Pharmacology and Translational Science*, *5*(7). https://doi.org/10.1021/acsptsci.2c00023

Zhou, X.-H., Brakebusch, C., Matthies, H., Oohashi, T., Hirsch, E., Moser, M., Krug, M., Seidenbecher, C. I., Boeckers, T. M., Rauch, U., Buettner, R., Gundelfinger, E. D., & Fässler, R. (2001). Neurocan Is Dispensable for Brain Development. *Molecular and Cellular Biology*, *21*(17). https://doi.org/10.1128/mcb.21.17.5970-5978.2001

Zhu, S., Victoria, G. S., Marzo, L., Ghosh, R., & Zurzolo, C. (2015). Prion aggregates transfer through tunneling nanotubes in endocytic vesicles. *Prion*, *9*(2). https://doi.org/10.1080/19336896.2015.1025189

Zlotnik, I. (1958). The histopathology of the brain stem of sheep affected with experimental scrapie. *Journal of Comparative Pathology*, *68*(4). https://doi.org/10.1016/s0368-1742(58)80048-x

Zou, W. Q., Puoti, G., Xiao, X., Yuan, J., Qing, L., Cali, I., Shimoji, M., Langeveld, J. P. M., Castellani, R., Notari, S., Crain, B., Schmidt, R. E., Geschwind, M., DeArmond, S. J., Cairns, N. J., Dickson, D., Honig, L.,

Torres, J. M., Mastrianni, J., … Gambetti, P. (2010). Variably protease-sensitive prionopathy: A new sporadic disease of the prion protein. *Annals of Neurology*, *68*(2). https://doi.org/10.1002/ana.22094